



LOMA LINDA UNIVERSITY

Loma Linda University
TheScholarsRepository@LLU: Digital
Archive of Research, Scholarship &
Creative Works

Loma Linda University Electronic Theses, Dissertations & Projects

12-2019

Effects of Gestational Corticosteroids and Caloric Restriction on the Neonatal Cerebrovasculature

Naomi Franco

Follow this and additional works at: <https://scholarsrepository.llu.edu/etd>



Part of the [Physiology Commons](#)

Recommended Citation

Franco, Naomi, "Effects of Gestational Corticosteroids and Caloric Restriction on the Neonatal Cerebrovasculature" (2019). *Loma Linda University Electronic Theses, Dissertations & Projects*. 1895. <https://scholarsrepository.llu.edu/etd/1895>

This Dissertation is brought to you for free and open access by TheScholarsRepository@LLU: Digital Archive of Research, Scholarship & Creative Works. It has been accepted for inclusion in Loma Linda University Electronic Theses, Dissertations & Projects by an authorized administrator of TheScholarsRepository@LLU: Digital Archive of Research, Scholarship & Creative Works. For more information, please contact scholarsrepository@llu.edu.

LOMA LINDA UNIVERSITY
School of Medicine
in conjunction with the
Faculty of Graduate Studies

Effects of Gestational Corticosteroids and Caloric Restriction on the Neonatal
Cerebrovasculature

by

Naomi Franco

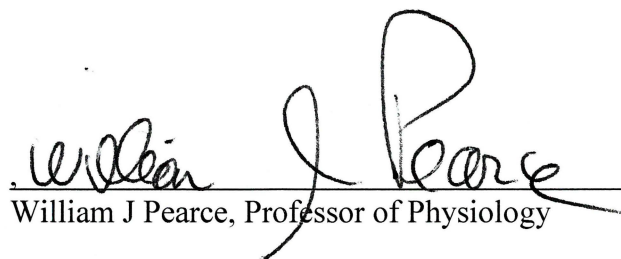
A Dissertation submitted in partial satisfaction of
the requirements for the degree
Doctor of Philosophy in Physiology

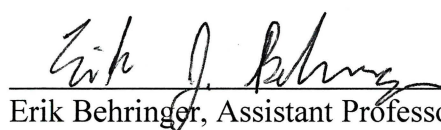
December 2019

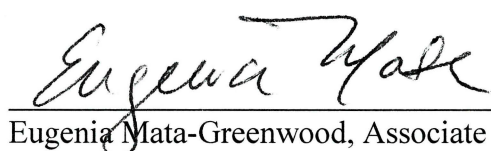
© 2019

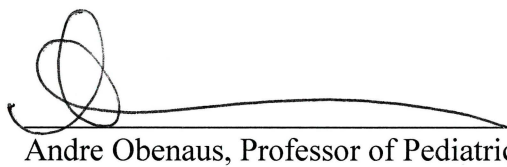
Patsy Naomi Franco
All Rights Reserved

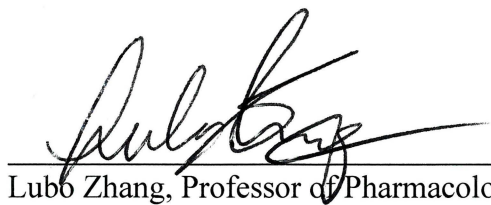
Each person whose signature appears below certifies that this dissertation in his/her opinion is adequate, in scope and quality, as a dissertation for the degree Doctor of Philosophy.


Chairperson
William J Pearce, Professor of Physiology


Erik Behringer, Assistant Professor of Pharmacology


Eugenia Mata-Greenwood, Associate Professor of Pharmacology


Andre Obenaus, Professor of Pediatrics, University of California, Irvine


Lubo Zhang, Professor of Pharmacology

ACKNOWLEDGEMENTS

“It was the best of times, it was the worst of times, it was the age of wisdom, it was the age of foolishness, it was the epoch of belief, it was the epoch of incredulity, it was the season of Light, it was the season of Darkness, it was the spring of hope, it was the winter of despair, we had everything before us, we had nothing before us, we were all going direct to Heaven, we were all going direct the other way.” ~ Charles Dickens

First, I would like to thank my thesis advisor, Dr. William Pearce, for his guidance and mentorship throughout this journey that have shaped the person I now am. His abundant knowledge (in all things!), tremendous kindness, and patience created the spring of hope I needed to succeed. I would also like to thank my undergraduate professor, Dr. Benjamin Thornton, who opened my eyes to the world of research and for the early investment he made in me. I would also like to acknowledge all the Lab A members who each took me in as part of the family, especially Lara Durrant. I also had great pleasure working with the Obenaus Lab, whose collaborative spirit made the completion of this dissertation possible. In addition, the support and community within the Perinatal Department, along with the guidance of each of my committee members is also greatly appreciated.

I am deeply grateful for my amazing parents and family members, especially my dearest sister, and their encouragement and support on this journey. My late grandmother, Julia Maldonado, was also an integral part of my PhD journey. Her incurable disease lit a spark in me to fight for the vulnerable and search for answers that would bring hope and life. Finally, I would like to thank my best friend and husband, Nefty Franco, for keeping me sane, cooking me dinners, accompanying me during late nights in the lab, and loving me unconditionally in the best and worst of times. To God be the glory!

CONTENT

Approval Page.....	iii
Acknowledgements.....	iv
List of Figures	viii
List of Tables	x
List of Abbreviations	xi
Abstract.....	xiii
Chapter	
1. Introduction.....	1
Fetal Programming.....	1
Maternal Food Restriction and Programming.....	1
Fetal Programming Mechanisms	3
Glucocorticoids and the Hypothalamic-Pituitary-Adrenal Axis.....	4
Epigenetics: microRNA	5
Metyrapone	6
Cerebrovasculature	8
Vascular Smooth Muscle Cells.....	9
HI Model.....	11
Clinical Significance.....	11
Purpose and Central Hypothesis	12
References.....	14
2. Prenatal Metyrapone Treatment Modulates Neonatal Cerebrovascular Structure, Function and Vulnerability to Mild Hypoxic-Ischemic Injury	20
Abstract.....	21
Introduction.....	23
Methods.....	26
General Preparation	26
Blood Collection and Corticosterone Analysis.....	27
Carotid Ligation and Hypoxic Exposure: A Model of Mild HI.....	28
Neurobehavior.....	28
Perfusion Fixation.....	29
Post-mortem MRI	30
Histological Quantification of Ischemic Injury	31

Confocal Microscopy.....	32
Vessel Myography	34
Statistics	34
Results.....	35
General Findings.....	35
Blood Collection and Corticosterone Analysis.....	38
MRI.....	41
Brain Histology.....	43
Confocal Microscopy.....	46
Passive Diameter and Compliance.....	50
Vessel Myography	53
Neurobehavior	56
Discussion.....	57
Perspectives and Significance.....	67
Acknowledgments.....	68
Supplemental Figures and Table.....	70
References.....	73
3. Maternal Food Restriction Modulates Cerebrovasculature Structure, Function and Vulnerability to Mild Hypoxic-Ischemic Injury: Effects of Metyrapone.....	80
Abstract.....	81
Introduction.....	83
Methods.....	84
General Preparation	84
Blood Collection and Corticosterone Analysis.....	87
Carotid Ligation and Hypoxic Exposure: A Model of Mild HI.....	88
Neurobehavior.....	88
Perfusion Fixation.....	89
Vessel Myography	90
Statistics	90
Result	91
General Findings.....	91
Blood Collection and Corticosterone Analysis.....	92
Passive Diameter and Arterial Compliance	99
Vessel Myography	101
Neurobehavior.....	104
Discussion.....	107

The Effects of MFR Programming on Neonatal Plasma GC Levels	108
The Effects of Gestational MET on Neonatal Plasma GC Levels within MFR Pups	109
The Effects of MFR Programming on Passive Diameters and Arterial Compliance	111
The Effects of MFR Programming on Contractile Function	112
The Effects of MFR Programming on Neurobehavior	114
Conclusion	116
References	118
4. Optimization of Confocal Colocalization of Contractile Proteins in Neonatal Middle Cerebral Arteries	122
Abstract	123
Introduction	125
Methods	126
Images	126
Masking	128
Minimal Pixel Intensity	128
Segmentation	128
Statistics	129
Results and Discussion	129
Optimization of Minimum Pixel Intensity	129
Optimization of Masking	132
Optimization of Segmentation	134
Conclusion	136
References	138
5. Conclusions and Future Directions	140

FIGURES

Figures	Page
Chapter 1	
1. Schematic diagram of corticosteroid synthesis.....	7
Chapter 2	
1. Experimental Overview of Embryonic and Postnatal Events.....	37
2. Effects of metyrapone-induced fetal transformation on the time course of plasma corticosterone in a neonatal model of mild hypoxic-ischemic encephalopathy	40
3. Effects of metyrapone-induced fetal transformation on brain injury in HI and Sham P11 pups.....	42
4. Effects of metyrapone-induced fetal transformation on HI-induced brain tissue injury.....	45
5. Effects of metyrapone-induced fetal transformation on confocal colocalization of smooth muscle contractile proteins in MCA from Sham and HI pups.....	49
6. Effects of metyrapone-induced fetal transformation on passive arterial diameter and compliance in MCAs from Sham and HI pups	52
7. Effects of metyrapone-induced fetal transformation on changes in diameter, wall calcium, and calcium sensitivity induced by pressure and K^+ in MCA of Sham and HI pups.....	55
8. Supplemental: Effects of metyrapone-induced fetal transformation on brain injury in HI and Sham P11 pups.....	70
9. Supplemental: Effects of metyrapone-induced fetal transformation on HI-induced brain tissue injury	71
Chapter 3	
1. Experimental Overview of Embryonic and Postnatal Events: MFR	86
2. Effects of maternal food restriction and metyrapone-induced fetal programming on baseline (pre-surgical) plasma corticosterone in neonatal pups.....	94

3. Effects of maternal food restriction and metyrapone-induced fetal programming on the time course of plasma corticosterone in a neonatal model of mild hypoxic-ischemic encephalopathy	95
4. Effects of maternal food restriction, metyrapone-induced fetal programming, and sex on the time course of plasma corticosterone in a neonatal model of mild hypoxic-ischemic encephalopathy	98
5. Effects of maternal food restriction and metyrapone-induced fetal programming on passive diameter and compliance in MCAs from Sham and HI pups	100
6. Effects of maternal food restriction and metyrapone-induced fetal programming on changes in diameter, wall calcium, and calcium sensitivity induced by pressure and K ⁺ in MCA of Sham and HI pups.....	103
7. Effects of maternal food restriction and metyrapone-induced fetal programming on neurobehavior in Sham and HI pups.....	105
Chapter 4	
1. The Effects of Baseline Correction Method on Colocalization Coefficients	131
2. The Effects of Masking Method on Colocalization Coefficients	133
3. The Effects of Segmentation Method on Colocalization Coefficients	135
Chapter 5	
1. Transcriptomic changes in miRNAs, ECM, Cytoskeleton, and Myosin Families 24h following mild HI injury in a P11 SF rat	142

TABLES

Tables	Page
Chapter 2	
1. Male-female Analysis	72
Chapter 3	
1. The Relative Changes of Gestational Diet and Postnatal Mild Hypoxic-Ischemia in Neonatal Rats.	106
Chapter 5	
1. Predicted target miRs that are most affected by mild HI in an SF neonate.	143

ABBREVIATIONS

ACTH	Adrenocorticotropic Hormone
ADC	Apparent Diffusion Coefficient
BBB	Blood-Brain Barrier
CD	Control Diet
CRH	Corticotrophin-releasing Hormone
DWI	Diffusion Weighted Imaging
ECM	Extracellular Matrix
EGTA	Ethylene Glycol-bis (β -aminoethyl ether)-N, N, N', N'- Tetra acetic Acid
FJ	FIJI
FJC	FluoroJade-C
GC	Glucocorticoid
GFAP	Glial Fibrillary Acidic Protein
HI	Hypoxic-Ischemia
HPA	Hypothalamic Pituitary Axis
IBA1	Ionized Calcium-binding Adapter Molecule 1
LOX	Lysyl Oxidase
MCA	Middle Cerebral Artery
MET	Metyrapone
MFR	Maternal Food Restriction
MIR	microRNA, miRNA
MMP	Matrix Metalloproteinase
MRI	Magnetic Resonance Imaging
NM-MHC	Non-Muscle Myosin Heavy Chain
P#	Postnatal Day #
PSS	Physiological Saline Solution
SM-MHC	Smooth Muscle Myosin Heavy Chain

T2	T2-weighted Imaging
VEGF	Vascular Endothelial Growth Factor
VSMC	Vascular Smooth Muscle Cell

ABSTRACT OF THE DISSERTATION

Effects of Gestational Corticosteroids and Caloric Restriction on the Neonatal Cerebrovasculature

by

Patsy Naomi Franco

Doctor of Philosophy, Graduate Program in Physiology

Loma Linda University, December 2019

Dr. William Pearce, Chairperson

The prenatal environment plays a major role in influencing the health of adult offspring. Maternal food restriction (MFR) during pregnancy is a common stressor that correlates to long-term consequences, including increased risk of cardiovascular and metabolic diseases in adult offspring. Numerous studies report persistent changes following MFR, with an emphasis on the heart and kidney. These consequences are thought to occur via programming, in which a stressor, during critical developmental windows, permanently alters the structure and function of selective fetal tissues. Furthermore, the elevation of maternal glucocorticoids associated with intrauterine stressors is a proposed mechanism of several programming events, including MFR. Although cerebral blood vessels in the context of MFR and glucocorticoids are understudied, our group recently showed that adult rat cerebrovasculature is negatively altered by MFR. The existence of comorbidities, such as obesity and hypertension, in MFR adult rats led us to develop a mild hypoxic-ischemia (HI) injury model to test cerebrovasculature responses in non-obese and normotensive MFR neonates. Our first study examined the role of gestational glucocorticoids alone on neonatal cerebrovasculature and HI vulnerability. Four groups of Sprague-Dawley neonates were included: 1) Untreated-Sham; 2) MET-Sham; 3) Untreated-HI; 4) MET-HI. Metyrapone

(MET), a corticosteroid synthesis inhibitor, was administered via drinking water from gestational day 11 to term in rats fed an ad libitum diet. The second study examined the role of MFR and gestational glucocorticoids on neonatal cerebrovasculature and HI vulnerability. Four groups of Sprague-Dawley MFR neonates were studied: 1) Untreated-Sham; 2) MET-Sham; 3) Untreated-HI; 4) MET-HI. At day 10 of gestation, MFR rats, in a pair-fed model, underwent 50% caloric restriction. MET was administered via drinking water from gestational day 11 to term. These studies demonstrate that both changes to nutrition and glucocorticoid levels during gestation differentially impact basal physiology and responses to HI injury in neonates. Future studies will further investigate the role of MFR on cerebral and cerebrovasculature structure as well as probe into the role of epigenetic regulation on cerebrovasculature function.

CHAPTER ONE

INTRODUCTION

Fetal Programming

The epidemiologist David James Barker pioneered the idea that an adverse early life environment led to chronic diseases later in life. The term fetal programming was developed from Barker's epidemiological studies in England and Wales which showed that low birth weight was correlated with hypertension, diabetes, and cardiovascular disease (3). By definition, fetal programming is a persistent adaptation which results from increased stress during critical developmental windows. While the adaptation is important for survival in the suboptimal environment, tissues are permanently remodeled in a way that predisposes the offspring to disease later in life. Barker's work with the concept of fetal programming was further corroborated by epidemiological studies around the world (19, 72). Birth characteristics, such as birth weight, placental weight, and body size ratios, were correlated with increased disease risk factors, such as elevated blood pressure and glucose intolerance in children (45). However, persistent changes in molecular structure, biological systems, and disease risk driven by intrauterine stressors could be present without change in birth weight, giving rise to the possibility of subtle yet significant programming changes.

Maternal Food Restriction and Programming

Maternal food restriction (MFR) during pregnancy, one of many possible in utero stressors and of great interest to my lab, creates a suboptimal environment for the

developing fetus by reducing nutrient availability through maternal caloric restriction and thus limiting fetal growth. Numerous epidemiological and animal studies have shown how perturbations that decrease nutritional status have adverse consequences that persist into adulthood (26, 59, 76) and increase susceptibility to different diseases, such as hypertension and heart disease (46). Other long-lasting effects of MFR include increased risk of insulin resistance and type 2 diabetes, behavioral alterations, and immune system dysfunction. However, the timing, severity, and species in which malnutrition occurs during gestation determine the nature of the long-term effects in the offspring (57).

Unfortunately, conditions that may lead to MFR are not a phenomenon of the past. The Food and Agriculture Organization of the United Nations states that in 2017, more than 700 million people across the globe experienced severe levels of food insecurity, implying reduced food consumption and probable hunger. In some regions, such as Africa and Latin America, the incidence has risen in recent years. In addition, according to the United States Department of Agriculture, in 2018 over three million households in the US suffered from very low food security, defined as decreased food intake and disrupted eating patterns. Women are more likely to experience food insecurity and within this vulnerable population are woman of reproductive age. Providing these at-risk populations with adequate nutrition during pregnancy is ideal but remains a present challenge. This underscores the importance of understanding the mechanisms of food restriction during pregnancy in hopes of reverting or diminishing adverse developmental effects post-partum.

One of the key challenges of studying MFR involves the need to consider the contribution of various factors to disease outcome. Species selection, the particular

nutrient restriction (protein, carbohydrate, fat, vitamin), timing and duration of restriction, and the severity of the diet collectively play a role in defining MFR models and influencing the measured outcomes. Overall, the MFR model produces offspring with reduced birth weight and adult hypertension (25).

Fetal Programming Mechanisms

A number of mechanisms by which a gestational perturbation, such as MFR, imparts its long-lasting effects have been reported. These include placental dysfunction, intrauterine growth restriction, epigenetic modifications, and, recently, microbiome alterations (6, 13, 28, 35, 44). Another popular mechanism of how maternal food restriction may mediate its effects is through elevated maternal glucocorticoids (GCs), which belong to the class of molecules that produce long-term effects: hormones (54). This theory stems from research demonstrating that increased maternal stress (i.e. hunger) leads to excess levels of circulating maternal GCs that cross the placenta (64). The placenta has enzymatic (11β -hydroxysteroid dehydrogenase 2) (24) and transport barriers (P-glycoprotein) that inhibit GC overexposure in the fetus as GC levels are generally higher in the mother; this protection, however, is compromised during food restricted pregnancies (54, 75). 11β -hydroxysteroid dehydrogenase 2, through oxidation, catalyzes the conversion of active corticosterone into its inactive form, dehydrocorticosterone. In addition, reports demonstrate that this enzyme can be reduced in the placentas of food-restricted mothers (14). The portion of GCs that are not inactivated by the placenta then bind to ubiquitously-expressed GC and mineralocorticoid

receptors (27) affecting the transcription of various genes, ultimately altering the structure and function of several organs during specific windows of development.

In addition, there are reports that exposure to high levels of synthetic glucocorticoids during gestation result in intrauterine growth restriction, a common feature of MFR, in animals and humans (53, 62, 69), and may lead to adult hypertension in rat offspring (70). However, some of these results are controversial and may vary as a result of dosing frequency, glucocorticoid type (endogenous or exogenous), timing of the dosing, and species (40).

Glucocorticoids and the Hypothalamic-Pituitary-Adrenal Axis

The actions of glucocorticoid (GCs) hormones are manifold. GCs are primary stress hormones, possess potent anti-inflammatory actions, and play crucial roles in pregnancy and development (5, 64, 67). GC deficiency leads to death, while long-term overexposure in adults may result in increased risk of disease, including Cushing's syndrome, hypertension, and osteoporosis (65). The hypothalamic-pituitary-adrenal axis controls the secretion of GCs in both a circadian and stress-induced manner through the hypothalamic release of corticotropin-releasing hormone (CRH) that stimulates the release of adrenocorticotrophic hormone (ACTH) from the pituitary gland, which triggers the production of GC hormones by the adrenal cortex (50, 56). Various stressors, both physiological and psychological, trigger an increase in GC release (16, 50, 60). Through binding with mineralocorticoid and glucocorticoid receptors, glucocorticoids exert their wide-ranging actions and regulate their own release through inhibition of CRH and ACTH in classical negative feedback loops (52, 71).

Additionally, there is evidence that in utero dietary restriction alters the hypothalamic-pituitary-adrenal axis (HPA) during fetal and postnatal periods (33, 47, 49). To further corroborate this, in the model of MFR used in our studies (50% caloric restriction during the latter half of gestation), corticosterone levels were elevated before birth and depressed postnatally (42). The fetal hypothalamic pituitary adrenal axis is also activated in response to stress producing fetal-derived GCs and thus contributes to the GC excess (15). While the literature shows that GC levels are altered by prenatal stress and that synthetic GC maternal administration produces effects similar to MFR and other stress models, there is much controversy surrounding this theory (36). The role of GCs in programming may be secondary to a more key player. However, because adequate levels of GCs are necessary for normal fetal development (i.e. cell differentiation and organ maturation), understanding the mediators in the mechanism of GC signaling in the context of MFR will be important.

Epigenetics: microRNA

GCs have been implicated in epigenetic modification such as DNA methylation and histone modification which act on the DNA structure. One emerging form of epigenetic regulation is microRNAs (miRNAs), which are short, non-coding RNA molecules that function to either degrade mRNAs or repress protein translation. miRNAs play an important role in normal and pathological physiology. Furthermore, up to 30% of protein-coding genes are thought to be regulated by miRNA (61).

While the role of miRNAs in fetal programming is understudied, our group has shown that MFR alters the miRNA profile of offspring. Among the miRNAs altered by

MFR, miR-29c drew our interest as it was downregulated in animal models of MFR, influenced by increasing GCs levels, and reduced the expression of Col3A1, Col4A5, ELN, and MMP2, all integral components of the extracellular matrix (ECM) (10). The miR-29c-induced downregulation of these ECM proteins associated with the vasculature, suggests that vascular structure and function may be altered by both GCs and miR-29c.

Metyrapone

Studying the effects of glucocorticoids can be done via the introduction or withdrawal of the hormone. Glucocorticoid withdrawal can be accomplished via adrenalectomy or mifepristone (a glucocorticoid receptor antagonist), both of which are not without complications during pregnancy (8, 9). Metyrapone (MET), a corticosteroid synthesis inhibitor, plays a key role in the elucidation of glucocorticoid-dependent effects. Other names by which MET has been referred to include SU-4885 and metopirone. MET acts by inhibiting 11- β hydroxylase and aldosterone synthase activity, which are important for the conversion of 11-deoxycorticosterone in corticosterone in rodents, or cortisol in humans, and in the conversion of corticosterone to aldosterone (Figure 1). Blockage of these steroidogenic activities creates an effective reduction in corticosterone (37, 41) and aldosterone activity (30) but may increase the activity of precursors, such as 11-deoxycorticosterone and progesterone. MET also readily crosses the placenta (73). In light of these effects, MET has also been used in a model of congenital adrenal hyperplasia (29).

In addition, MET is used clinically to diagnose adrenal insufficiency and treat Cushing's syndrome (17, 31). Like many other drugs, MET also produces off-target

effects that are independent of glucocorticoids, such as altered temperature regulation (22) and neuronal protection (38). Importantly, several animal studies have employed metyrapone to examine the effects of glucocorticoids in various stress pathologies (11, 39, 42, 48, 55).

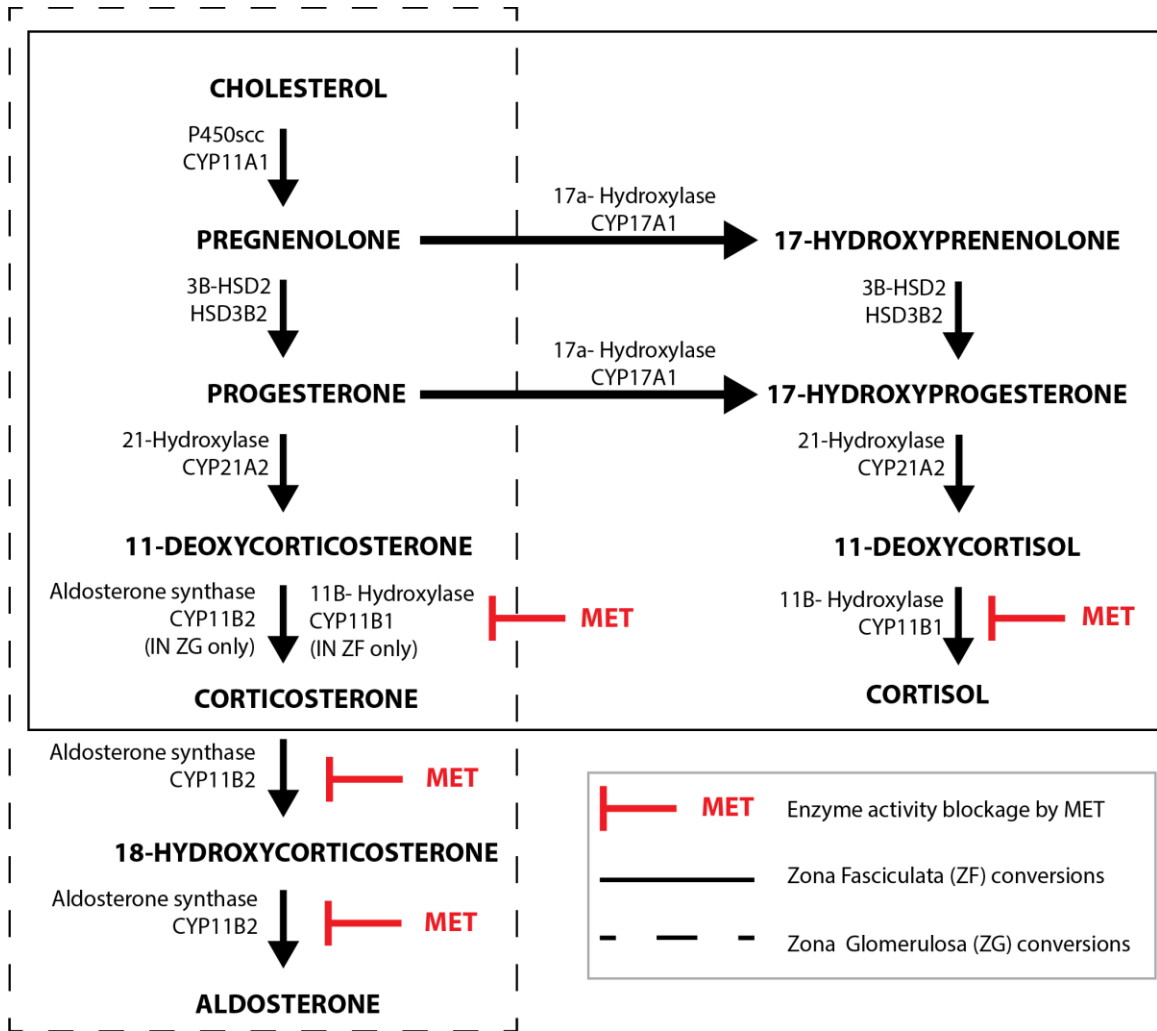


Figure 1. Schematic diagram of corticosteroid synthesis. Metyrapone (MET) blocks the enzymatic activities of CYP11B1 and CYP11B2 in the adrenal glands thus reducing the synthesis of the corticosteroids: corticosterone, cortisol, and aldosterone.

Cerebrovasculature

One of the effects of maternal food restriction is vascular remodeling in the offspring. Impairments in the vascular function of the kidneys, heart and skeletal muscle have been well-documented but cerebrovasculature alterations in relation to fetal nutritional programming is understudied. Additionally, the cerebrovasculature merits further study within the field of perinatal cerebrovascular disease research which has given much attention to neurons, glia and astrocytes. The cerebral vessels may be a main player in perinatal cerebrovascular disease given that the cerebrovasculature plays an important role in the perfusion of brain tissue and maintenance of normal brain function (78).

In young rats, in other mammals, and in preterm human babies the cerebrovasculature continues developing post-partum and is thus immature and sensitive to fluctuations in blood pressure. Furthermore, throughout the early postnatal period the cerebral microvascular bed (arterioles, venules, and capillaries) is actively under remodeling and changes in the neonatal brain microenvironment may alter the establishment of adequate metabolic-vascular coupling (32). It is possible that fetal stress, such as caloric restriction, program an altered postnatal brain microenvironment, including changes in the expression of vascular endothelial growth factor (43), and thus modulate neonatal cerebrovascular structure and function under normal and stressed conditions (4).

Additionally, corticosteroids, such as corticosterone and aldosterone, are known to modulate arterial function (68, 74, 77). Glucocorticoids have been known to increase vascular stiffness and reduce angiogenesis; however, the developmental stage in which

glucocorticoids are manipulated, along with the duration and severity of the manipulation, may produce differing results. Aldosterone has been documented to reduce cerebral vessel dilation and increase vascular remodeling (21). The receptor that aldosterone preferentially binds, the mineralocorticoid receptor, appears later in development than the more ubiquitous glucocorticoid receptor (20). This may imply that corticosterone, relative to aldosterone, has a more pronounced role in the fetal developmental period. How MFR may influence aldosterone expression and activity may be important in fully understanding vascular function.

Our group also found that MFR decreased cerebral vessel compliance in adult rats, thus increasing arterial stiffness and reducing vessel contractility and that some of these effects were ablated by MET (23). These changes suggest heightened vascular ischemic vulnerability, which may be influenced by corticosteroids. Studies involving the neonatal brain blood vessels may be pivotal in developing therapies for perinatal cerebrovascular disease.

Vascular Smooth Muscle Cells

Vascular smooth muscle cells (vSMCs) are an important part of the cerebrovasculature. They exist in a variety of phenotypes (i.e. contractile, synthetic, proliferative, migratory) (63). SMC phenotypic modulation, the ability to change phenotype based on tissue demand, is an important part of SMC function. For instance, tissue injury induces a phenotypic shift toward synthetic vSMCs which produce extracellular matrix proteins to aid in tissue restoration. Importantly, a shift from contractile to non-contractile phenotype is usually indicative of a diseased state (51).

Furthermore, biological factors, such as age, environmental factors and epigenetics (12) play a role in determining the phenotypic distribution of SMCs. For example, immature vSMCs, which predominate at a younger age, have a large synthetic population and smaller contractile population than the profile of vSMCs found in adults. This age-related difference contributes to variances in regulation of contraction (7).

The contractile function is mediated mainly through calcium-dependent pathways via regulation of intracellular calcium and myofilament calcium sensitivity (18). The phosphorylation and dephosphorylation of the contractile protein, myosin light chain, controls the level of contraction, which in turn, along with vSMC profile, affects the myogenic response in the cerebrovasculature. The myogenic response allows SMCs to react to changing arterial pressures. As blood pressure increases, blood vessels constrict; as blood pressure drops, blood vessels dilate. This occurs to maintain a constant flow of blood to the brain. This is inherent to smooth muscle cells and occurs independently of neuronal, hormonal, or metabolic influence. The myogenic response is a key indicator of vascular health and can thus be studied, especially in the context of ischemia. The cerebrovascular response to fluctuations in cerebral blood flow and metabolic demand following the ischemic insult determines the extent of damage. In neonatal infants, particularly those born prematurely, myogenic response can be compromised due to a lower proportion of contractile vSMCs performing the contractile work (7). The mechanisms by which maternal food restriction may alter both myogenic response and vSMC phenotype of the cerebrovasculature merits further study to advance the outcome of perinatal vascular diseases, such as stroke and hypoxic-ischemic encephalopathy (HI).

HI Model

In order to test vascular programming effects of MFR and MET, we developed a novel mild model of HI injury, understanding that vessel function and structure are altered in response to HI (34, 51, 58). Modified from the Rice-Vannucci protocol (66), our new model requires the performance of unilateral carotid ligation in P9 or P10 pups, and after a 24-hour recovery period, exposure to 8% oxygen for 90 minutes. This differs from the traditional Rice-Vannucci protocols in both the recovery time following carotid ligation (4-8 hours) and the exposure length to hypoxic gases (3.5 hours).

Our mild model allows for quantifying injury in the most susceptible regions while a more severe model would produce injury in several regions. Through this milder model we hope to identify the proverbial “canary in the coal mine,” to gauge the most sensitive responders for P11 rats. Currently, various animal models are used to study neonatal hypoxic-ischemia. They involve different species (rat, mouse), different ages (P7 and P10), and different lengths of hypoxic exposure (1.5-3 hours). While these models produce differing levels of ischemic damage (2), the basic characteristics of brain injury are present, such as damage to the hippocampal area. Understanding that each species undergoes age-sensitive developmental events is also very important in understanding normal cerebral physiology and vulnerability to HI injury (1).

Clinical Significance

Through better understanding of how in utero stress and gestational alterations of corticosteroid levels influence the neonatal vasculature, especially through identification of the most vulnerable cells, new approaches can be developed to treat perinatal

cerebrovasculature diseases. Additionally, world hunger is on the rise and about one in every nine people in the world suffer from hunger. By answering the questions of how maternal food restriction affects the offspring and what role corticosteroids play in development, these studies may aid in identifying modifiable perinatal mechanisms whereby food restriction modulates the cerebrovasculature and other cerebral targets, and thus offer targets for the development of future treatment options in neonates affected by food insecurity.

Purpose and Central Hypothesis

The following studies tested the hypothesis that in utero stress via maternal food restriction alters cerebrovasculature structure and function thus altering neonatal ischemic vulnerability. We propose that the programming effects occur in part through glucocorticoid-dependent and independent pathways, highlighting the importance of corticosteroids in vascular and non-vascular development. Metyrapone, a corticosteroid synthesis inhibitor, was used to assess the effects of corticosteroids.

Chapter Two, entitled, “Prenatal metyrapone treatment modulates neonatal cerebrovascular structure, function and vulnerability to mild hypoxic-ischemic injury,” focused primarily on the sole effects of gestational corticosteroid reduction on HI-induced vulnerability in the cerebrovasculature, as well other cerebral tissues. The results of that study demonstrated that corticosteroids during gestation play a key role in normal cerebrovascular development and glial activation, induce persistent changes that in neonates manifest beneficially as preservation of post-ischemic contractile

differentiation, but worsen cerebrovascular compliance following ischemia, and increase ischemic neuronal injury, and compromise neurobehavior.

Chapter Three, entitled, “Maternal food restriction modulates neonatal cerebrovascular structure, function and vulnerability to mild hypoxic-ischemic injury: effects of metyrapone,” focused on examining the role of maternal food restriction on the cerebrovascular, neurobehavioral, HPA axis responses to mild HI injury in neonatal rats. The role of corticosteroids, such as glucocorticoids, in MFR was also examined through gestational MET dosing. These studies will be expanded to examine cerebral histology and vSMC phenotype.

Chapter Four, entitled, “Optimization of confocal colocalization of contractile proteins in neonatal middle cerebral arteries,” primarily focused on refining a heavily-employed method of determining protein proximity from confocal imaging. The goal of this study was to standardize the methods used to determine colocalization to increase statistical sensitivity and efficiency.

Chapter Five, entitled, “Conclusions and Future Directions,” included a foundation for future studies as well as concluding remarks. Overall, this dissertation should advance studies on fetal programming and the neonatal cerebrovasculature.

References

1. **Semple B, Blomgren K, Gimlin K, Ferriero D, Noble-Haeusslein Linda.** Brain development in rodents and humans: Identifying benchmarks of maturation and vulnerability to injury across species. *Progress in neurobiology* 106-107: 1-16, 2013.
2. **Ashwal S, Tone B, Tian HR, Chong S, and Obenaus A.** Comparison of two neonatal ischemic injury models using magnetic resonance imaging. *Pediatr Res* 61: 9-14, 2007.
3. **Barker DJ.** The fetal and infant origins of disease. *European journal of clinical investigation* 25: 457-463, 1995.
4. **Bogorad MI, DeStefano JG, Linville RM, Wong AD, and Searson PC.** Cerebrovascular plasticity: Processes that lead to changes in the architecture of brain microvessels. *J Cereb Blood Flow Metab* 39: 1413-1432, 2019.
5. **Busada JT, and Cidlowski JA.** Mechanisms of Glucocorticoid Action During Development. *Current topics in developmental biology* 125: 147-170, 2017.
6. **Calatayud M, Koren O, and Collado MC.** Maternal Microbiome and Metabolic Health Program Microbiome Development and Health of the Offspring. *Trends in endocrinology and metabolism: TEM* 30: 735-744, 2019.
7. **Charles SM, Zhang L, Cipolla MJ, Buchholz JN, and Pearce WJ.** Roles of cytosolic Ca²⁺ concentration and myofilament Ca²⁺ sensitization in age-dependent cerebrovascular myogenic tone. *Am J Physiol Heart Circ Physiol* 299: H1034-1044, 2010.
8. **Chatelain A, Dupouy JP, and Allaume P.** Fetal-maternal adrenocorticotropin and corticosterone relationships in the rat: effects of maternal adrenalectomy. *Endocrinology* 106: 1297-1303, 1980.
9. **Chen J, Wang J, Shao J, Gao Y, Xu J, Yu S, Liu Z, and Jia L.** The unique pharmacological characteristics of mifepristone (RU486): from terminating pregnancy to preventing cancer metastasis. *Medicinal research reviews* 34: 979-1000, 2014.
10. **Chuang TD, Pearce WJ, and Khorram O.** miR-29c induction contributes to downregulation of vascular extracellular matrix proteins by glucocorticoids. *Am J Physiol Cell Physiol* 309: C117-125, 2015.
11. **Chuang TD, Sakurai R, Gong M, Khorram O, and Rehan VK.** Role of miR-29 in Mediating Offspring Lung Phenotype in a Rodent Model of Intrauterine Growth Restriction. *Am J Physiol Regul Integr Comp Physiol* 2018.
12. **Clifford RL, Singer CA, and John AE.** Epigenetics and miRNA emerge as key regulators of smooth muscle cell phenotype and function. *Pulmonary pharmacology & therapeutics* 26: 75-85, 2013.
13. **Conradt E, Adkins DE, Crowell SE, Raby KL, Diamond LM, and Ellis B.** Incorporating epigenetic mechanisms to advance fetal programming theories. *Development and psychopathology* 30: 807-824, 2018.

14. **Correia-Branco A, Keating E, and Martel F.** Maternal undernutrition and fetal developmental programming of obesity: the glucocorticoid connection. *Reprod Sci* 22: 138-145, 2015.
15. **Cottrell EC, Holmes MC, Livingstone DE, Kenyon CJ, and Seckl JR.** Reconciling the nutritional and glucocorticoid hypotheses of fetal programming. *FASEB J* 26: 1866-1874, 2012.
16. **Craft TK, and Devries AC.** Vulnerability to stroke: implications of perinatal programming of the hypothalamic-pituitary-adrenal axis. *Front Behav Neurosci* 3: 54, 2009.
17. **Daniel E, Aylwin S, Mustafa O, Ball S, Munir A, Boelaert K, Chortis V, Cuthbertson DJ, Daousi C, Rajeev SP, Davis J, Cheer K, Drake W, Gunganah K, Grossman A, Gurnell M, Powlson AS, Karavitaki N, Huguet I, Kearney T, Mohit K, Meeran K, Hill N, Rees A, Lansdown AJ, Trainer PJ, Minder AE, and Newell-Price J.** Effectiveness of Metyrapone in Treating Cushing's Syndrome: A Retrospective Multicenter Study in 195 Patients. *The Journal of clinical endocrinology and metabolism* 100: 4146-4154, 2015.
18. **Davis MJ, and Hill MA.** Signaling mechanisms underlying the vascular myogenic response. *Physiological reviews* 79: 387-423, 1999.
19. **de Boo HA, and Harding JE.** The developmental origins of adult disease (Barker) hypothesis. *The Australian & New Zealand journal of obstetrics & gynaecology* 46: 4-14, 2006.
20. **Diaz R, Brown RW, and Seckl JR.** Distinct ontogeny of glucocorticoid and mineralocorticoid receptor and 11beta-hydroxysteroid dehydrogenase types I and II mRNAs in the fetal rat brain suggest a complex control of glucocorticoid actions. *J Neurosci* 18: 2570-2580, 1998.
21. **Dinh QN, Arumugam TV, Young MJ, Drummond GR, Sobey CG, and Chrissobolis S.** Aldosterone and the mineralocorticoid receptor in the cerebral circulation and stroke. *Exp Transl Stroke Med* 4: 21, 2012.
22. **Drouet JB, Michel V, Peinnequin A, Alonso A, Fidler N, Maury R, Buguet A, Cespuglio R, and Canini F.** Metyrapone blunts stress-induced hyperthermia and increased locomotor activity independently of glucocorticoids and neurosteroids. *Psychoneuroendocrinology* 35: 1299-1310, 2010.
23. **Durrant LM, Khorram O, Buchholz JN, and Pearce WJ.** Maternal food restriction modulates cerebrovascular structure and contractility in adult rat offspring: effects of metyrapone. *Am J Physiol Regul Integr Comp Physiol* 306: R401-410, 2014.
24. **Edwards CR, Benediktsson R, Lindsay RS, and Seckl JR.** Dysfunction of placental glucocorticoid barrier: link between fetal environment and adult hypertension? *Lancet* 341: 355-357, 1993.
25. **Edwards LJ, Coulter CL, Symonds ME, and McMillen IC.** Prenatal undernutrition, glucocorticoids and the programming of adult hypertension. *Clin Exp Pharmacol Physiol* 28: 938-941, 2001.

26. **El Hajj N, Schneider E, Lehnen H, and Haaf T.** Epigenetics and life-long consequences of an adverse nutritional and diabetic intrauterine environment. *Reproduction* 148: R111-120, 2014.
27. **Funder JW.** Glucocorticoid and mineralocorticoid receptors: biology and clinical relevance. *Annual review of medicine* 48: 231-240, 1997.
28. **Galjaard S, Devlieger R, and Van Assche FA.** Fetal growth and developmental programming. *J Perinat Med* 41: 101-105, 2013.
29. **Goldman AS.** Experimental model of congenital adrenal cortical hyperplasia produced in utero with an inhibitor of 11-beta-steroid hydroxylase. *The Journal of clinical endocrinology and metabolism* 27: 1390-1394, 1967.
30. **Gomez-Sanchez CE, Zhou MY, Cozza EN, Morita H, Foecking MF, and Gomez-Sanchez EP.** Aldosterone biosynthesis in the rat brain. *Endocrinology* 138: 3369-3373, 1997.
31. **Hana V, Dokoupilova M, Marek J, and Plavka R.** Recurrent ACTH-independent Cushing's syndrome in multiple pregnancies and its treatment with metyrapone. *Clinical endocrinology* 54: 277-281, 2001.
32. **Harb R, Whiteus C, Freitas C, and Grutzendler J.** In vivo imaging of cerebral microvascular plasticity from birth to death. *J Cereb Blood Flow Metab* 33: 146-156, 2013.
33. **Hawkins P, Steyn C, McGarrigle HH, Calder NA, Saito T, Stratford LL, Noakes DE, and Hansona MA.** Cardiovascular and hypothalamic-pituitary-adrenal axis development in late gestation fetal sheep and young lambs following modest maternal nutrient restriction in early gestation. *Reprod Fertil Dev* 12: 443-456, 2000.
34. **Hu X, De Silva TM, Chen J, and Faraci FM.** Cerebral Vascular Disease and Neurovascular Injury in Ischemic Stroke. *Circ Res* 120: 449-471, 2017.
35. **Jansson T, and Powell TL.** Role of the placenta in fetal programming: underlying mechanisms and potential interventional approaches. *Clin Sci (Lond)* 113: 1-13, 2007.
36. **Jaquiere AL, Oliver MH, Bloomfield FH, Connor KL, Challis JR, and Harding JE.** Fetal exposure to excess glucocorticoid is unlikely to explain the effects of periconceptual undernutrition in sheep. *J Physiol* 572: 109-118, 2006.
37. **Jenkins JS, Meakin JW, Nelson DH, and Thorn GW.** Inhibition of adrenal steroid 11-oxygenation in the dog. *Science* 128: 478-480, 1958.
38. **Kaminski RM, and Rogawski MA.** 11beta-Hydroxylase inhibitors protect against seizures in mice by increasing endogenous neurosteroid synthesis. *Neuropharmacology* 61: 133-137, 2011.
39. **Keller CM, Breaux KN, and Goeders NE.** Effects of the combination of metyrapone and oxazepam on cocaine-induced increases in corticosterone in the medial prefrontal cortex and nucleus accumbens. *Psychoneuroendocrinology* 77: 75-83, 2017.

40. **Kemp MW, Newnham JP, Challis JG, Jobe AH, and Stock SJ.** The clinical use of corticosteroids in pregnancy. *Hum Reprod Update* 22: 240-259, 2016.
41. **Kennedy JA, Hartman N, Sbriglio R, Khuri E, and Kreek MJ.** Metyrapone-induced withdrawal symptoms. *British journal of addiction* 85: 1133-1140, 1990.
42. **Khorram O, Ghazi R, Chuang TD, Han G, Naghi J, Ni Y, and Pearce WJ.** Excess Maternal Glucocorticoids in Response to In Utero Undernutrition Inhibit Offspring Angiogenesis. *Reprod Sci* 2013.
43. **Khorram O, Ghazi R, Chuang TD, Han G, Naghi J, Ni Y, and Pearce WJ.** Excess maternal glucocorticoids in response to in utero undernutrition inhibit offspring angiogenesis. *Reprod Sci* 21: 601-611, 2014.
44. **Kwon EJ, and Kim YJ.** What is fetal programming?: a lifetime health is under the control of in utero health. *Obstetrics & gynecology science* 60: 506-519, 2017.
45. **Langley-Evans SC.** Intrauterine programming of hypertension by glucocorticoids. *Life Sci* 60: 1213-1221, 1997.
46. **Langley-Evans SC, Langley-Evans AJ, and Marchand MC.** Nutritional programming of blood pressure and renal morphology. *Archives of physiology and biochemistry* 111: 8-16, 2003.
47. **Lesage J, Blondeau B, Grino M, Breant B, and Dupouy JP.** Maternal undernutrition during late gestation induces fetal overexposure to glucocorticoids and intrauterine growth retardation, and disturbs the hypothalamo-pituitary adrenal axis in the newborn rat. *Endocrinology* 142: 1692-1702, 2001.
48. **Lim R, Fedulov AV, and Kobzik L.** Maternal stress during pregnancy increases neonatal allergy susceptibility: role of glucocorticoids. *Am J Physiol Lung Cell Mol Physiol* 307: L141-148, 2014.
49. **Lingas R, Dean F, and Matthews SG.** Maternal nutrient restriction (48 h) modifies brain corticosteroid receptor expression and endocrine function in the fetal guinea pig. *Brain Res* 846: 236-242, 1999.
50. **Lupien SJ, McEwen BS, Gunnar MR, and Heim C.** Effects of stress throughout the lifespan on the brain, behaviour and cognition. *Nature reviews Neuroscience* 10: 434-445, 2009.
51. **Matchkov VV, Kudryavtseva O, and Aalkjaer C.** Intracellular Ca²⁺ Signalling and Phenotype of Vascular Smooth Muscle Cells. *Basic & Clinical Pharmacology & Toxicology* 110: 42-48, 2012.
52. **McEwen BS.** Central effects of stress hormones in health and disease: Understanding the protective and damaging effects of stress and stress mediators. *Eur J Pharmacol* 583: 174-185, 2008.
53. **Miller SL, Sutherland AE, Supramaniam VG, Walker DW, Jenkin G, and Wallace EM.** Antenatal glucocorticoids reduce growth in appropriately grown and growth-restricted

- ovine fetuses in a sex-specific manner. *Reproduction, fertility, and development* 24: 753-758, 2012.
54. **Moisiadis VG, and Matthews SG.** Glucocorticoids and fetal programming part 2: Mechanisms. *Nature reviews Endocrinology* 10: 403-411, 2014.
 55. **Murata H, Higuchi T, and Otagiri M.** Oral pharmacokinetics and in-vitro metabolism of metyrapone in male rats. *The Journal of pharmacy and pharmacology* 68: 970-979, 2016.
 56. **Oakley RH, and Cidlowski JA.** The biology of the glucocorticoid receptor: new signaling mechanisms in health and disease. *J Allergy Clin Immunol* 132: 1033-1044, 2013.
 57. **Painter RC, Roseboom TJ, and Bleker OP.** Prenatal exposure to the Dutch famine and disease in later life: an overview. *Reproductive toxicology (Elmsford, NY)* 20: 345-352, 2005.
 58. **Poittevin M, Lozeron P, Hilal R, Levy BI, Merkulova-Rainon T, and Kubis N.** Smooth muscle cell phenotypic switching in stroke. *Translational stroke research* 5: 377-384, 2014.
 59. **Pruis MG, Lendvai A, Bloks VW, Zwier MV, Baller JF, de Bruin A, Groen AK, and Plosch T.** Maternal western diet primes non-alcoholic fatty liver disease in adult mouse offspring. *Acta Physiol (Oxf)* 210: 215-227, 2014.
 60. **Radak D, Resanovic I, and Isenovic ER.** Changes in hypothalamus-pituitary-adrenal axis following transient ischemic attack. *Angiology* 65: 723-732, 2014.
 61. **Rajewsky N.** microRNA target predictions in animals. *Nature genetics* 38 Suppl: S8-13, 2006.
 62. **Reinisch JM, Simon NG, Karow WG, and Gandelman R.** Prenatal exposure to prednisone in humans and animals retards intrauterine growth. *Science* 202: 436-438, 1978.
 63. **Rensen SS, Doevendans PA, and van Eys GJ.** Regulation and characteristics of vascular smooth muscle cell phenotypic diversity. *Netherlands heart journal : monthly journal of the Netherlands Society of Cardiology and the Netherlands Heart Foundation* 15: 100-108, 2007.
 64. **Reynolds RM.** Glucocorticoid excess and the developmental origins of disease: two decades of testing the hypothesis--2012 Curt Richter Award Winner. *Psychoneuroendocrinology* 38: 1-11, 2013.
 65. **Rhen T, and Cidlowski JA.** Antiinflammatory action of glucocorticoids--new mechanisms for old drugs. *N Engl J Med* 353: 1711-1723, 2005.
 66. **Rice JE, Vannucci RC, and Brierley JB.** The influence of immaturity on hypoxic-ischemic brain damage in the rat. *Annals of neurology* 9: 131-141, 1981.
 67. **Rog-Zielinska EA, Craig MA, Manning JR, Richardson RV, Gowans GJ, Dunbar DR, Gharbi K, Kenyon CJ, Holmes MC, Hardie DG, Smith GL, and Chapman KE.** Glucocorticoids promote structural and functional maturation of foetal cardiomyocytes: a role for PGC-1alpha. *Cell death and differentiation* 22: 1106-1116, 2015.

68. **Roghair RD, Segar JL, Sharma RV, Zimmerman MC, Jagadeesha DK, Segar EM, Scholz TD, and Lamb FS.** Newborn lamb coronary artery reactivity is programmed by early gestation dexamethasone before the onset of systemic hypertension. *Am J Physiol Regul Integr Comp Physiol* 289: R1169-1176, 2005.
69. **Seckl JR.** Glucocorticoids and small babies. *The Quarterly journal of medicine* 87: 259-262, 1994.
70. **Seckl JR.** Glucocorticoids, feto-placental 11 beta-hydroxysteroid dehydrogenase type 2, and the early life origins of adult disease. *Steroids* 62: 89-94, 1997.
71. **Tsigos C, and Chrousos GP.** Hypothalamic-pituitary-adrenal axis, neuroendocrine factors and stress. *Journal of psychosomatic research* 53: 865-871, 2002.
72. **Victora CG, Adair L, Fall C, Hallal PC, Martorell R, Richter L, and Sachdev HS.** Maternal and child undernutrition: consequences for adult health and human capital. *Lancet* 371: 340-357, 2008.
73. **Vidyasagar D, and Chernick V.** Placental transfer of metopirone. *Biol Neonate* 21: 471-474, 1972.
74. **Vinukonda G, Dummula K, Malik S, Hu F, Thompson CI, Csiszar A, Ungvari Z, and Ballabh P.** Effect of prenatal glucocorticoids on cerebral vasculature of the developing brain. *Stroke* 41: 1766-1773, 2010.
75. **Whorwood CB, Firth KM, Budge H, and Symonds ME.** Maternal undernutrition during early to midgestation programs tissue-specific alterations in the expression of the glucocorticoid receptor, 11beta-hydroxysteroid dehydrogenase isoforms, and type 1 angiotensin ii receptor in neonatal sheep. *Endocrinology* 142: 2854-2864, 2001.
76. **Wood-Bradley RJ, Henry SL, Vrselja A, Newman V, and Armitage JA.** Maternal dietary intake during pregnancy has longstanding consequences for the health of her offspring. *Can J Physiol Pharmacol* 91: 412-420, 2013.
77. **Young MJ, and Adler GK.** Aldosterone, the Mineralocorticoid Receptor and Mechanisms of Cardiovascular Disease. *Vitam Horm* 109: 361-385, 2019.
78. **Zhang JH, Badaut J, Tang J, Obenaus A, Hartman R, and Pearce WJ.** The vascular neural network--a new paradigm in stroke pathophysiology. *Nat Rev Neurol* 8: 711-716, 2012.

CHAPTER TWO

PRENATAL METYRAPONE TREATMENT MODULATES NEONATAL CEREBROVASCULAR STRUCTURE, FUNCTION AND VULNERABILITY TO MILD HYPOXIC-ISCHEMIC INJURY

By

Naomi Franco, Lara M. Durrant, Desirelys Carreon, Elizabeth Haddad, Adam Vergara,
Catherine Cascavita, Andre Obenaus, William J. Pearce

This chapter has been published by the American Journal of Physiology-Regulatory,
Integrative, and Comparative Physiology

Abstract

This study explored the hypothesis that late gestational reduction of corticosteroids transforms the cerebrovasculature, and modulates postnatal vulnerability to mild hypoxic-ischemic (HI) injury. Four groups of Sprague-Dawley neonates were studied: 1) Untreated-Sham; 2) MET-Sham; 3) Untreated-HI; 4) MET-HI. Metyrapone (MET), a corticosteroid synthesis inhibitor, was administered via drinking water from gestational day 11 to term. In Shams, MET administration: 1) decreased reactivity of the Hypothalamic-Pituitary-Adrenal (HPA) axis to surgical trauma in P9 pups by 37%; 2) promoted cerebrovascular contractile differentiation in middle cerebral arteries (MCA); 3) decreased compliance up to 46%, and increased depolarization-induced calcium mobilization in MCAs by 28%; 4) mildly increased hemispheric cerebral edema by 5%, decreased neuronal degeneration by 66% and increased astroglial and microglial activation by 10-fold and 4-fold, respectively; and 5) increased righting reflex times by 29%. Regarding HI, metyrapone-induced fetal transformation: 1) diminished reactivity of the HPA axis to HI-induced stress in P9/P10 pups; 2) enhanced HI-induced contractile de-differentiation in MCAs; 3) lessened the effects of HI on MCA compliance and calcium mobilization; 4) decreased HI-induced neuronal injury but unmasked regional HI-induced depression of microglial activation; and 5) attenuated the negative effects of HI on open field exploration, but enhanced the detrimental effects of HI on negative geotaxis responses by 79%. Overall, corticosteroids during gestation appear essential for normal cerebrovascular development and glial quiescence, but induce persistent changes that in neonates manifest beneficially as preservation of post-ischemic contractile

differentiation, but detrimentally as worsened ischemic cerebrovascular compliance, increased ischemic neuronal injury, and compromised neurobehavior.

Introduction

Vital for life corticosteroids influence diverse physiological functions by binding to ubiquitous mineralocorticoid and glucocorticoid (GC) receptors to exert their wide-ranging effects. Corticosteroid levels are regulated by hypothalamic release of corticotropin-releasing hormone (CRH) that stimulates release of pituitary adrenocorticotrophic hormone (ACTH), which triggers the production and secretion of corticosteroid hormones by the adrenal cortex. Corticosteroid release increases in response to physiological circadian rhythms as well as stresses such as those caused by food deprivation or fear. Corticosteroid release is also regulated through feedback inhibition of hypothalamic CRH and pituitary ACTH release (43). Whereas glucocorticoid release is regulated primarily through ACTH levels, the major mineralocorticoid, aldosterone, is principally regulated by the renin-angiotensin system. Careful regulation of aldosterone is important to maintain fluid homeostasis, blood pressure control (34), and arterial stiffness (4, 49). GCs are potent inhibitors of inflammation, and thus are used clinically to treat autoimmune diseases (44). and to accelerate lung development in fetuses at high risk for premature birth (16). GC therapy, however, is not without risks; sustained supra-physiological levels of GCs, whether endogenous or exogenous, can lead to adverse health consequences including hypertension, osteoporosis, and metabolic syndrome (44).

Owing to their anti-inflammatory and anti-proliferative effects, GCs are also employed to treat multiple vascular pathologies, including those that involve altered patterns of angiogenesis (65), contractile reactivity (16), wall stiffness (50), and arterial restenosis, particularly following stent implantation (14). Many of the vascular effects of

GCs are attributable to their ability to modulate smooth muscle phenotype, which is highly dynamic and readily transitions among migratory, proliferative, synthetic, and contractile characteristics (37). These transitions typically culminate in altered vascular structure, compliance and contractile reactivity (24, 37).

Given the significant vascular effects of corticosteroids, the present study investigated the sustained effects of altered corticosteroid levels during gestation, on postnatal cerebrovascular structure and function as a model of fetal cerebrovascular transformation (43), defined here as the consequences of adverse intrauterine events that influence fetal vascular development and persist after birth. As such, this fetal vascular transformation includes the effects of both genomic and non-genomic fetal vascular programming. Abundant experimental evidence supports the hypothesis that late gestation is a critical developmental window, during which increased GC exposure modulates developmental trajectories that lead to altered reactivity to stress and compromised cardiovascular, metabolic, and psychological fitness in adult life (35). Conversely, decreased levels of GCs during gestation promote impaired growth (52), disruption in cerebral neurotransmitter synthesis (31), alterations in Hypothalamic-Pituitary-Adrenal (HPA) axis function and reactivity to stress (69). Decreased levels of corticosteroids during gestation also impact cerebrovasculature structure and function in adult offspring (13).

Corticosteroid levels can be decreased by adrenalectomy which creates complications during pregnancy (7, 8). Corticosteroid levels also can be decreased by metyrapone (MET), an agent commonly used to treat Cushing's syndrome (21). MET blocks the production of cortisol in humans, and corticosterone in rodents, as well as

mineralocorticoids, by inhibiting 11 β -hydroxylase (27, 46) with few detrimental side effects, and has been useful in elucidating the effects of corticosteroids in multiple stress pathologies (10, 13, 29). Like many other drugs, MET can produce multiple diverse effects attributable to elevated levels of corticosteroid precursors, such as progesterone, and downstream consequences of reduced glucocorticoid and aldosterone availability including altered temperature regulation (12) and enhanced inflammation (44). In light of this spectrum of effects, MET has been employed to induce symptoms of congenital adrenal hyperplasia (17). The work presented here uses a well-tolerated gestational MET dosing regimen (daily oral administration of 0.5 mg/ml from gestational day 11 to term) previously shown to alter plasma corticosterone levels in rat offspring, and to reduce corticosteroid-induced effects in lung and vascular tissues (10, 13).

To probe the early consequences of fetal transformation caused by corticosteroid reduction, the present study employs a novel model of cerebral injury caused by mild hypoxic-ischemia (HI). Whereas severe models of HI rapidly and extensively injure multiple cerebral cell types (11), these models also can obscure identification of the cell types most vulnerable to even mild ischemic insults (3), including cell types of the cerebrovasculature (42). The model of mild HI injury developed for the present study was modified from the Rice-Vannucci model (45) to enhance detection of ischemia-induced injury to the cerebrovasculature (70). The hypothesis tested is that attenuation of corticosteroid levels during the second half of gestation transforms the cerebrovasculature, modulates the structure and function of cerebral arteries, and alters their vulnerability to mild postnatal HI insults.

Methods

General Preparation

The Loma Linda University Institutional Animal Care and Use Committee approved all experimental procedures used in these studies. The Animal Care Facility housed first-time pregnant Sprague-Dawley rats (Charles River Laboratories, Hollister, CA; Envigo Laboratories, Placentia, CA) at constant temperature and humidity with a 12:12-h:light-dark cycle with food and water ad libitum. From day 11 of gestation until term (21 days), approximately half of the rats' drinking water contained MET (cat# 14994 Cayman Chemical Company, Ann Arbor, MI), freshly dissolved each day at a final concentration of 0.5 mg/ml (**Figure 1**). Previous studies have demonstrated this concentration of MET to block maternal corticosterone synthesis and significantly reduce plasma corticosterone levels in both fetal and neonatal blood (29). Daily water consumption did not differ between Untreated (standard filtered water) and MET treated dams. All rats delivered spontaneously, and pups remained with their dams until the day of surgery. The overall study design included four groups of Sprague-Dawley rats: 1) Sham-operated animals (Untreated-Sham), 2) Animals that underwent unilateral carotid ligation surgery followed by hypoxia 24 hours later (Untreated-HI), 3) Sham animals that were administered MET during gestation (MET-Sham), and 4) HI animals that received MET during gestation (MET-HI).

Blood Collection and Corticosterone Analysis

A time course study of corticosterone levels relative to the timing of the hypoxic insult quantified changes in corticosterone levels in each of the experimental groups (**Figure 1**). The collection of whole trunk blood into Lithium Heparin blood collection tubes (Greiner Bio-One, Kremsmunster, Austria) occurred at the time of sacrifice, according to four time course endpoints: immediately before surgery (pre-treatment baseline; **GC Endpoint 1**), 2 hours after unilateral carotid ligation (post-surgical baseline; **GC Endpoint 2**); 2 hours after HI injury (early ischemic endpoint; **GC Endpoint 3**); and 24 hours after HI injury (late ischemic endpoint; **GC Endpoint 4**). To reduce variability due to circadian oscillations in corticosterone levels, blood collection always occurred during a 4-hour block in the morning. Plasma samples then underwent centrifugation at 2000 RPM at 4 °C for 15 minutes to yield aliquots frozen at -20 °C.

In preparation for ELISA assays, the sample extraction procedure included treatment with perchloric acid followed by potassium hydroxide, which released any corticosterone bound by protein in thawed plasma samples. Twice repeated additions of ethyl acetate followed by centrifugation extracted corticosterone in the samples into the supernatant. A Savant SpeedVac Concentrator (ThermoFisher Scientific, Waltham, MA), then evaporated the supernatants. This step of the extraction concluded with capping and freezing the dried samples at -80 °C until the time of assay.

Corticosterone quantification employed an ELISA kit (cat#: ADI-900-097, ENZO Life Sciences, Farmingdale, NY) and a Gen5 1.11 BioTek microplate reader to read the samples (run in duplicate) at 405 nm. Known standards, provided and run with each kit, enabled construction of standard curves that determined the quantity of corticosterone in

each sample in picograms per milliliter. The kits detected a minimum concentration of 27 pg/ml and provided intra-assay variations no greater than 4%.

Carotid Ligation and Hypoxic Exposure: A Model of Mild Hypoxic-Ischemia

On postnatal days 9 and 10 (P9, P10), which correspond to the brain development of a full-term human infant (39), randomly selected pup littermates received surgical treatment (**Figure 1**). Following the induction of anesthesia with 3% isoflurane inhalation, the pups underwent right carotid ligation using 5-0 surgical silk (Ischemia surgery) or dissection without ligation (Shams). All surgeries typically lasted less than 15 minutes, which minimized the potential neuroprotective effects of isoflurane exposure (5). Post-surgical pups recovered with their dam for 24 hours, after which pups designated for hypoxia experienced exposure to a commercially prepared mixture containing 8% oxygen with balance nitrogen for 90 minutes in a sealed, humidified chamber maintained at 37 °C. An oxygen monitor continuously displayed oxygen levels in the chamber to assure consistency of the hypoxic exposure. After hypoxic exposure, the pups recovered 15 minutes under normoxic conditions (room air) in the chamber, and then continued recovery with their dam. Sham pups, which had no carotid ligation, were exposed to normoxia (room air) for 90 minutes at 37 °C.

Neurobehavior

Three neurobehavioral assessments (righting reflex, open field, and the negative geotaxis reflex) quantified behavioral responses 24 hours after hypoxic exposure in P11/P12 pups from each of the experimental groups. Each test consisted of two trials that

were averaged for analysis. To eliminate time of day differences in behavior, testing always occurred within the same 3-hour block in the morning. A heating pad set at 37 °C prevented loss of body heat and pups rested between trials on the heating pad. The time each pup was separated from its dam did not exceed 20 minutes. Wiping down all surfaces of the behavioral apparatus with 70% ethanol between trials helped remove pup scent and reduce bacterial transfer.

The righting reflex examined the ability of each pup to return to its four paws after being placed in a supine position. Observations of exploratory activity in the open field test enabled quantification of the number of times a rat's head (specifically, the point between the ears) moved into a new 2 cm by 2 cm square in an enclosed acrylic arena (38x40x40cm) during a 45-second interval. The negative geotaxis reflex tested the amount of time, up to 60 seconds, required for a pup placed head-downward on a 25° mesh incline to turn 180° (indicated by position of its head and front paws).

Perfusion-Fixation

Following behavioral testing, transcardial perfusion-fixation enabled subsequent measurement of HI injury via MRI and histology. After the induction of anesthesia with 3% isoflurane inhalation, the perfusion procedure began with exposure of the heart followed by the passage of a 25-gauge butterfly needle through the left ventricle and into the aorta. A peristaltic pump (Model EP-1 Econo Pump; Bio Rad, Hercules, CA) connected to the needle infused phosphate-buffered saline into the vasculature for the removal of blood through an incision in the right atrium. After this, perfusion with a solution containing 4% paraformaldehyde at 8 ml/min fixed the brain. The entire

procedure, not including induction time, lasted approximately 15 minutes. Following perfusion fixation, post-fixation of the extracted brains was accomplished overnight in 4% PFA in PBS at 4 °C.

Post-mortem MRI

An 11.7T Bruker Avance instrument (Bruker Biospin, Billerica, MA, USA.) generated images from whole perfusion-fixed brains. Two imaging sequences (T2-weighted (T2WI) and diffusion weighted imaging (DWI)) assessed HI injury for changes in water content and water mobility, respectively. Each sequence collected 20 coronal slices with a slice thickness of 0.75 mm. The T2 sequence used the following parameters: TR/TE = 3000/10 ms, matrix = 192 × 192 zero-filled to 256 x 256 at reconstruction, field of view (FOV) = 1.5 cm, and a total of 2 averages. The DWI sequence employed these parameters: TR/TE = 5000/31.2 ms, b-value = 200 s/mm², matrix = 64 × 64 zero-filled to 128 x 128 at reconstruction, FOV = 1.5 cm, and a total of 2 averages. MATLAB, along with in-house processing software utilizing Hierarchical Region Splitting (HRS), generated T2 maps, and JIM, a medical imaging analysis software (Xinapse Systems Ltd; West Bergholt, Essex; United Kingdom) processed the DWIs to produce ADC maps. Manually drawn regions of interest (R) sampled quantitative values in right (ipsilateral), left (contralateral to the side of carotid ligation), cortical (R2-4, 6-8 in **Figure 4A**), and striatal (R1 and 5 in **Figure 4A**) hemispheres for each slice of all ADC and T2 maps. **Figure 3** depicts R2 and R6 of the middle cerebral artery territory and the average of each region by hemisphere. Complete regional analysis data is included in **Supplemental Figure 1**. For comparisons across groups, posterior/anterior analyses utilized the R

averages from 10 coronal slices per animal for each group, starting from where the hippocampal formation is prominent to where the olfactory bulbs begin to appear.

Histological Quantification of Ischemic Injury

After MRI, saturation of whole brains in PBS with 30% sucrose provided cryoprotection prior to the embedding of 2-mm thick slices in OCT compound (Fischer Scientific, Waltham, MA) at -80 °C. Coronal sections cut into 25 µm brain sections enabled analysis of brain injury in the same regions (R1-8; see **Figure 4**) used in MRI measurements. **Figure 4C-E** depicts R2 and R6 representative data from the middle cerebral artery territory and the averages of each region by hemisphere. Full regional analysis data is included in **Supplemental Figure 2**. All staining runs included a slide cut from a standard block of brain tissue, and the same standard block was used for all runs for a given stain. At the beginning of each imaging session, the standard section was imaged first, and used to set the key parameters for imaging, selected to provide between 1% and 5% saturation, as confirmed off-line. All slides in the same staining run were imaged using exactly the same imaging parameters. The software analysis routines used to analyze images from stained brain sections quantified areas beneath the distributions of pixel numbers versus pixel intensity. The routines automatically varied minimum intensity thresholds for inclusion to maximize the statistical sensitivity for each marker in group-wise comparisons. The markers analyzed included FluoroJade C (FJC, Histo-Chem, 0.0001% in 0.1% acetic acid at 22 °C for 10 minutes), c-Fos (EMD Millipore, PC05-100UG @ 1:20 in PBS containing 2% normal goat serum (NGS)), Glial Fibrillary Acidic Protein (GFAP, EMD Millipore, MAB3402 @ 1:1000 in PBS containing 0.5%

BSA and 0.5% Triton-X at 4 °C for 19 hours) and Iba1 (Wako Pure Chemical Industries, 019-1974 @ 1:400 in PBS containing 2% BSA at 4 °C for 18 hours).

Validation of the titers for each of the antibodies used to quantify brain tissue markers relied on the results of immunoblots of PAGE gels performed with at least 5 different titers to probe standards prepared from adult brain homogenates. By definition, optimum primary titers identified only one major band. Optimum secondary antibody titers, by definition, produced a blank image after IHC staining in the presence of secondary but not primary antibodies.

Confocal Microscopy

The confocal microscopy protocol used MCAs from separate cohorts of P11/12 pups in the four treatment groups. Overnight fixation of these MCA segments in 4% PFA preceded the embedding of arteries in paraffin and subsequent cutting into 5 µm coronal sections. All IHC staining runs included a slide cut from a standard block of an adult cerebral artery, and the same standard block was used for all runs for a given stain. Double-staining the sections with antibodies against smooth muscle α Actin (Sigma-Aldrich, A5228 @ 1:300 in PBS containing 2% NGS, 1% BSA at 4 °C for 18 hours) and either smooth muscle myosin heavy chain (Abcam, Ab53219 @ 1:400 in PBS containing 2% NGS, 1% BSA at 4 °C for 18 hours) or non-muscle myosin heavy chain (BioLegend, Poly19099 @ 1:300 in PBS containing 2% NGS, 1% BSA at 4 °C for 18 hours) allowed for identification of smooth muscle phenotype. The visualization procedure used secondary antibodies (Dylight-488 and Dylight-633 @ 1:300) in PBS containing 2% NGS, 1% BSA incubated at 22 °C for 2 hours. An Olympus FV1000 confocal microscope

produced coronal images using a lens with a numerical aperture of 1.4 to yield lateral resolutions between 146 and 185 nm, and axial resolutions between 545 and 693 nm, depending on the wavelengths of illumination. For imaging, the standard section was imaged first, and used to set the key parameters for imaging including scan time, gain, illumination intensity, and photomultiplier voltage, as appropriate to provide between 1% and 5% saturation, which was confirmed off-line. All images were captured on the same day under identical conditions. Analyses of the confocal images of the artery sections employed CoLocalizer Pro (Version 2.6.1, CoLocalization Research Software) to calculate the extent of colocalization between the markers in each pair. Each pixel (above a set threshold) in each double-stained image fell into one of three categories: Low Marker#1 and Low Marker #2, Low Marker #1 and High Marker #2, and High Marker #1 and High Marker #2 (Marker 1 represented one of the two myosin heavy chain isoforms and Marker 2 represented smooth muscle α Actin). The analysis involved calculation of the number of colocalized pixels in each category as a percentage of the total number of colocalized pixels for both markers across all 3 categories (defined as 100%). Previous publications include detailed descriptions of all these methods (13, 40) and validation by comparison to other established methods for quantitation of protein colocalization via confocal microscopy (63).

Validation of the titers for each of the antibodies used to image cerebrovascular contractile proteins relied on the results of immunoblots of PAGE gels performed with at least 5 different titers to probe standards prepared from homogenates of adult cerebral arteries. By definition, optimum primary titers identified only one major band. Optimum secondary antibody titers, by definition, produced a blank image after IHC staining in the

presence of secondary but not primary antibodies. These approaches have been standard practice for many years (1, 41).

Vessel Myography

To determine the contractile characteristics of MCAs, experiments with adjacent MCA artery segments included serial recordings of arterial diameter, first in physiological saline solution (PSS) and then in 120 mM K⁺ solution to determine maximum contractile capacity. Fura-2-AM (ThermoFisher Scientific) loaded at 1 μM, enabled simultaneous measurement of smooth muscle calcium concentration. The protocol included measurements in PSS and then 120 mM K⁺ at 20, 40, 60 and 80 mm Hg. After the final pressure step, addition of a zero calcium, 3 mM EGTA solution quenched cytosolic calcium to enable measurement of passive diameters at each pressure level used for contractility measurements. Previous publications detail all methods employed in these measurements (6, 13, 40).

Statistics

In all cases, N refers to the number of animals studied. For measurements of plasma corticosterone and all neurobehavioral assessments, Behren's-Fischer analyses with pooled variance compared values between groups. One-way ANOVA analyses with post-hoc comparisons using the Fisher Paired Least Significant Difference tested significance among the MRI endpoints, among all four brain histology markers, and for vessel myography by using area under the curve for each myography parameter (artery diameter, wall calcium, and calcium sensitivity). Behren's-Fischer analysis with pooled

variance compared values for the colocalization coefficient and detected group-wise differences in the percentages of total pixels in each of the three categories for each marker pair. A D'Agostino-Pearson K2 test confirmed normal distributions of all data sets, and within ANOVA analyses, Levene's test of equality verified homogeneity of variance.

Results

General findings

These protocols used 112 animals divided into three cohorts: 1) corticosterone time course (57 pups from 8 litters); 2) behavior, MRI and histology (31 pups from 5 litters); and 3) myography and confocal colocalization (24 pups from 10 litters). Each cohort included four experimental groups: 18 Untreated-Sham and 25 Untreated-HI pups from 10 litters whose mothers received normal drinking water during gestation, as well as 15 MET-Sham and 16 MET-HI pups from seven litters that had undergone MET-induced fetal transformation produced by administration of MET in maternal drinking water during the latter half of gestation (**Figure 1**). In addition, the corticosterone time course cohort involved 10 additional groups from six litters: four Untreated Pre-Surgery (GC Endpoint 1), four Untreated Sham-Ligated (GC Endpoint 2), four Untreated Ligated (GC Endpoint 2), four Untreated 2-hour Post Normoxia (GC Endpoint 3), and four Untreated 2-hour Post Hypoxia pups (GC Endpoint 3), as well as three MET Pre-Surgery (GC Endpoint 1), three MET Sham-Ligated (GC Endpoint 2), four MET Ligated (GC Endpoint 2), four MET 2-hour Post Normoxia (GC Endpoint 3), and four MET 2-hour

Post Hypoxia pups (GC Endpoint 3). On average, each rat mother gave birth to 12 pups whose sex was determined by urogenital distance. Across all pups, approximately 50% were male and 50% were female. Pups were randomly selected for all experiments. For the 14 endpoints reported in this study, and an additional 10 endpoints with larger rat pup populations than reported in this study, ANOVA revealed no sexually dimorphic differences, consistent with other studies of the neonatal cerebrovasculature (33). Supplemental Table 1 summarizes these statistical results.

Birth weight was significantly less (11%) in pups transformed by gestational MET (5.7 ± 0.1 g) when compared to Untreated pups (6.4 ± 0.2 g). At P11/P12, the weights of Untreated-Sham and MET-Sham pups did not differ significantly. At 24-hours following the hypoxic insult, Untreated-HI pups (17.6 ± 0.7 g) weighed significantly less (10%) than Untreated-Sham pups (19.6 ± 0.5 g). Gestational MET ablated this difference; pup weights in the MET-Sham (20.3 ± 1.2 g) and MET-HI groups (19.8 ± 0.9 g) did not differ significantly.

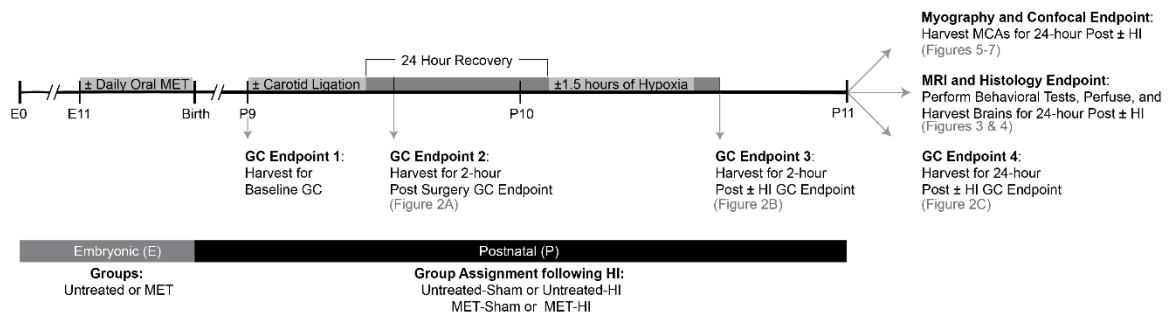


Figure 1. Experimental Overview of Embryonic and Postnatal Events. As indicated in the above diagram (not to scale), half of the pregnant Sprague-Dawley rats received a daily oral dose of 0.5 mg/ml of metyrapone (MET) in the drinking water beginning at E11 through term, yielding two groups: the Untreated group (untreated water), and the MET group (MET-treated water). After birth, designated pups were euthanized at four specific timepoints after which trunk blood was collected to determine the plasma glucocorticoid (GC) levels. At P11, one cohort of rats was harvested for the final GC endpoint, a second was harvested to obtain arteries for myography and confocal measurements, and a third cohort underwent behavioral testing followed by perfusion fixation, ex vivo MRI evaluation, and histological analysis.

Blood Collection and Corticosterone Analysis

The ELISA assay used in these studies could detect a difference of 42.9% with a power ≥ 0.8 for the number of pups used ($n=57$). In P9 pups prior to surgery (see **Figure 1, GC Endpoint 1**), baseline plasma corticosterone did not differ significantly between Untreated pups (5.3 ± 2.7 ng/ml), and those transformed by gestational MET (3.4 ± 1.6 ng/ml) given this absence of effect, the experimental design excluded corticosterone sampling at any time points earlier than P9. Two hours after surgery but 22 hours prior to hypoxic exposure in Untreated pups (see **Figure 1, GC Endpoint 2**), unilateral carotid ligation significantly elevated plasma corticosterone to approximately 2-fold greater than in Sham-Ligated Untreated pups (**Figure 2A**). However, in pups transformed by gestational MET, plasma corticosterone did not differ significantly between pups that underwent carotid ligation and Sham surgeries (**Figure 2A**). At this time point (post-surgery, pre-hypoxia), MET-induced fetal transformation significantly decreased neonatal plasma corticosterone in both Sham (Untreated: 7.0 ± 0.6 ng/ml; MET: 4.4 ± 1.3 ng/ml) and carotid ligated (Untreated: 13.9 ± 5.3 ng/ml; MET: 5.5 ± 0.7 ng/ml) pups (**Figure 2A**).

At 2 hours post-hypoxia in Untreated pups (see **Figure 1, GC Endpoint 3**), plasma corticosterone averaged to values significantly less in Carotid-Ligated (1.5 ± 0.5 ng/ml) than in Sham (3.4 ± 0.9 ng/ml) pups (**Figure 2B**). Again, in pups transformed by gestational MET, plasma corticosterone did not differ significantly between pups that underwent carotid ligation (3.6 ± 1.9 ng/ml) and Sham (2.7 ± 1.4 ng/ml) surgeries. At this time point (2 hours post-hypoxia, or 26 hours post-surgery), values in Untreated and

MET-transformed Sham animals did not differ significantly, nor did values in Untreated and MET-transformed pups with carotid ligation (**Figure 2B**).

At 24 hours post-hypoxia (see **Figure 1, GC Endpoint 4**), plasma corticosterone did not differ significantly among any of the groups (**Figure 2C**). Over the time course of all measurements, plasma corticosterone decreased progressively in all experimental groups. Superimposed on this trend, plasma corticosterone differed significantly between Sham and ligated, pre-hypoxic Untreated pups, but not between Sham and ligated, pre-hypoxic pups transformed with gestational MET. This pattern infers that transformation with MET during the last half of gestation depressed neonatal reactivity to stress.

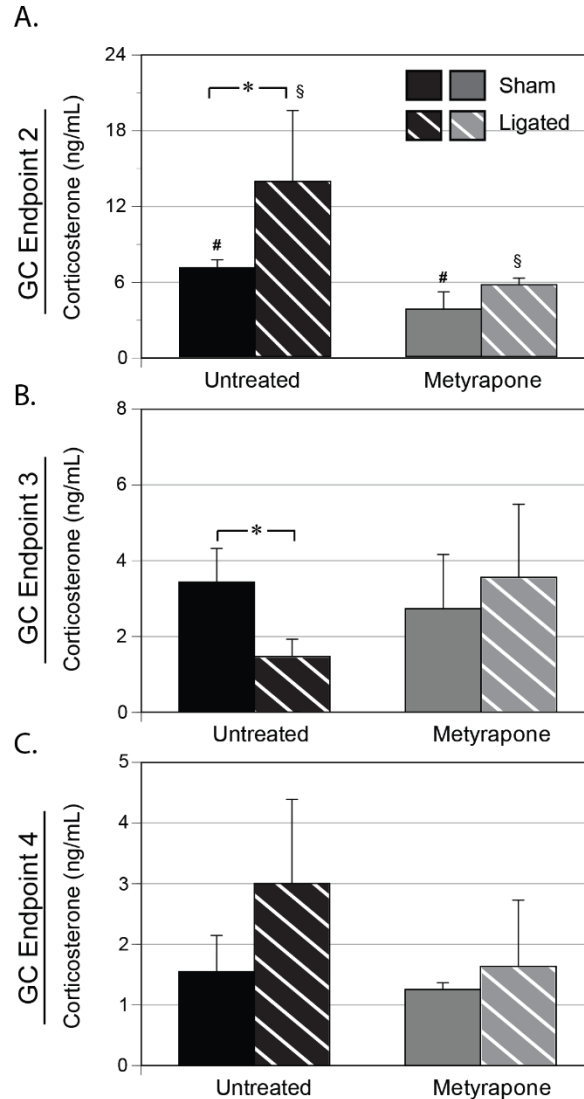


Figure 2. Effects of metyrapone-induced fetal transformation on the time course of plasma corticosterone in a neonatal model of mild hypoxic-ischemic encephalopathy. Plasma corticosterone measurements were collected at the time of sacrifice in the four treatment groups at three time points (see Figure 1). **Figure 2A:** Corticosterone concentrations were measured at 2 hours post-carotid ligation or Sham-surgery, which was also 24 hours pre-hypoxia. N=4 animals per group except in the MET-HI group where N=3. **Figure 2B:** Corticosterone levels were assessed 2 hours post-hypoxia or normoxia in animals that were ligated or Sham-operated 24 hours prior, respectively. N=4 per group. **Figure 2C:** Plasma corticosterone was measured 24 hours post-hypoxia or normoxia in Ligated or Sham-operated pups. N=4 per group except in the Untreated-HI group where N=7. Note that the vertical scale for each time point is different due to decreasing corticosterone levels with advancing age. Data are presented as mean \pm SEM. Statistically significant differences determined via Behren's-Fischer with pooled variance are indicated by: * = Sham vs Ligated.; # = Sham vs. MET-Sham; § = Ligated vs. MET-Ligated.

MRI

T2 and ADC results demonstrated the mild effects of the HI model introduced in this paper, as well as the influence of MET-induced fetal transformation on neonatal cerebral tissue integrity under both basal conditions and after a mild HI insult (**Figure 3A**). The methods used to measure these results could detect a difference of 1.8% (T2) and 4.5% (ADC) with a power ≥ 0.8 for the number of pups used (n=19). A total of 8 regions (see **Figure 4A**) were analyzed (**Supplemental Figure 1**), but emphasis was given to regions 2 and 6 which represent the MCA territory. T2 values, which generally identify cerebral edema, exhibited significantly greater values between Untreated-Sham and MET-Sham pups, particularly on the right side of the brain (ipsilateral to the side of carotid ligation) but not individually within regions 2 or 6. T2 values did not differ significantly between Untreated-Sham and Untreated-HI pups, or between MET-Sham and MET-HI pups, in any region examined (**Figure 3B**).

ADC values, which typically indicate changes in water mobility and cell swelling, did not differ significantly between Untreated-Sham and MET-Sham pups. ADC values also did not differ significantly between Untreated-Sham and Untreated-HI pups, or between MET-Sham and MET-HI pups, in any region examined (**Figure 3B**). In aggregate, the imaging results revealed that MET-induced fetal transformation increased neonatal T2 values, but not ADC values.

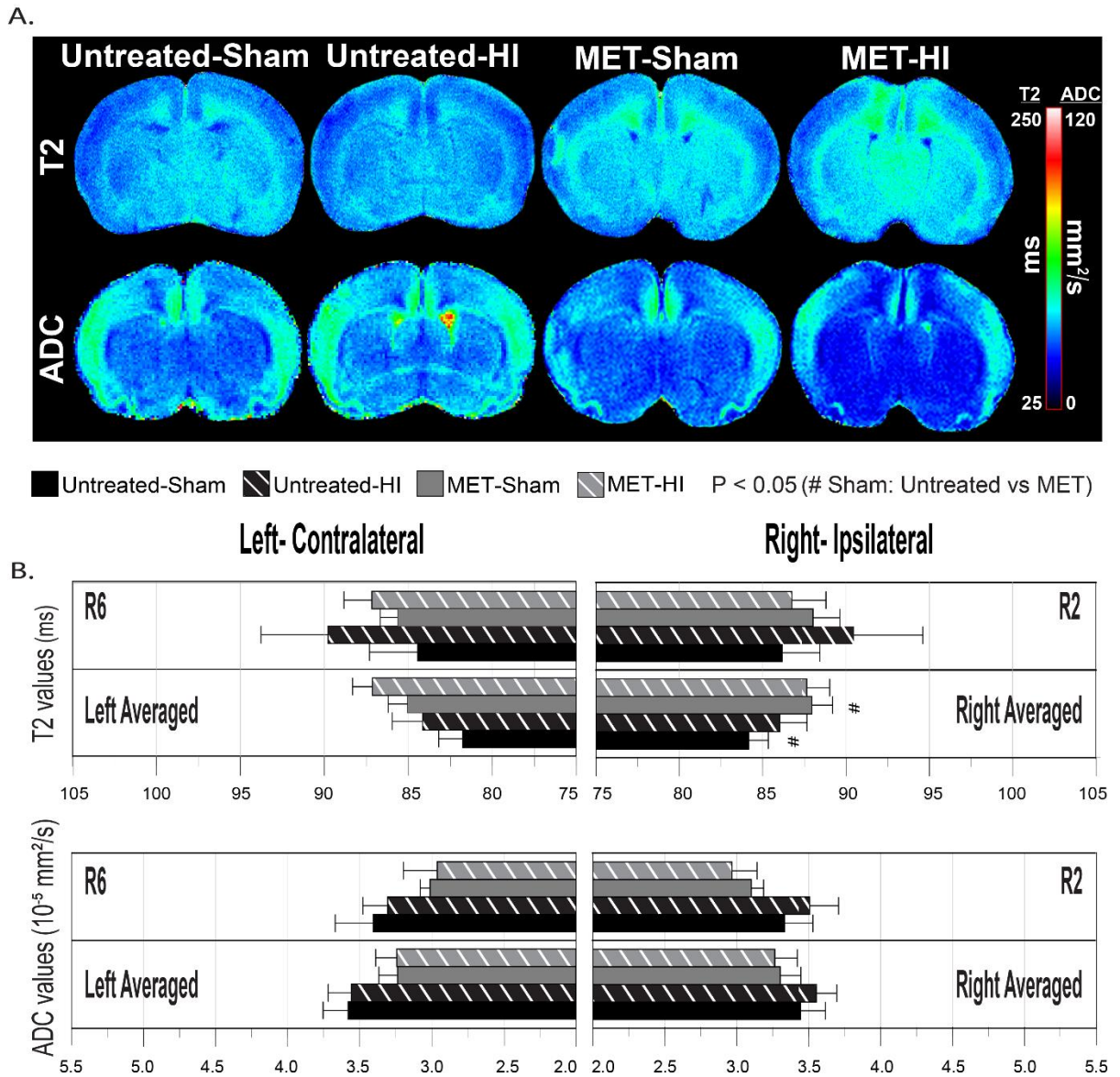


Figure 3. Effects of metyrapone-induced fetal transformation on brain injury in HI and Sham P11 pups. Figure 3A: The images shown indicate representative T2-weighted imaging (T2) and apparent diffusion coefficient (ADC) maps from post mortem pups euthanized 24 hours post HI injury or Sham surgery. Figure 3B: Region of interest sampling of the MR images produced 8 separate values, designated with the letter R and corresponding region number as shown in Figure 4A. The upper halves of the T2 and ADC panels labelled R2 and R6, summarize the regional results, whereas the lower halves of these panels represent hemispheric averages (Left Averaged, Right Averaged). Supplemental Figure 1 includes complete results for all regions. Hashmarks (#, P<0.05) denote significant group-group differences, as determined via ANOVA with a post-hoc-Fischer's LSD analysis for Untreated-Sham vs. MET-Sham; no other group-group comparisons yielded significant differences. The columns and error bars indicate the mean \pm SEM for N=4 in Untreated-Sham and N=5 in all other groups.

Brain Histology

A panel of marker stains (FJC, GFAP, Iba1, c-Fos) revealed cerebral structural changes induced by MET-induced fetal transformation and HI in multiple regions of serial, neonatal coronal sections, with emphasis on regions 2 and 6 that represent the MCA territory (**Figure 4A**). The supplementary data includes a full regional analysis data of all four markers (**Supplemental Figure 2**). The methods used to measure these changes in FJC, GFAP, Iba1, and c-Fos, could detect differences of 29.9%, 46.8%, 21.3% and 35.4%, respectively with a power ≥ 0.8 for the number of pups used (n=21). FJC staining, which typically indicates neuronal degeneration (51), was not significantly different in Untreated-Sham and MET-Sham brains in R2 or R6; however, the FJC signal of the combined average of all right regions was significantly higher in Untreated-Sham than in MET-Sham. Regional FJC staining intensity was significantly less in Untreated-Sham brains than in Untreated-HI brains (R2, R6), but not between MET-Sham and MET-HI brains (**Figure 4B & 4C**).

GFAP, which stains intermediate filaments in activated astrocytes (22), was significantly less in Untreated-Sham than in MET-Sham brains on the side of injury (right side) when all regions were combined (**Figure 4D**). GFAP values did not differ between Sham and HI pups in Untreated or gestational MET-transformed dams in R2 and R6, or in the left or right hemispheric averages. Overall, MET-induced fetal transformation increased the neonatal GFAP signal independent of the HI insult across all brain regions. Iba1 levels, a marker of activated microglia (26), were generally less in Untreated-Sham than in MET-Sham brains, at both the regional and hemispheric levels (**Figure 4E**). Iba1 levels varied little between Untreated-Sham and Untreated-HI groups

at both the regional and hemispheric levels. However, local but not hemispheric Iba1 levels in R2 were significantly greater in MET-Sham than in MET-HI brains.

Levels of c-Fos, an early marker of cellular stress across many cell types (53), varied highly and did not provide consistent discrimination between groups. Data for this marker is only shown in the supplementary data section (**Supplemental Figure 2**).

Across all markers, HI induced significant changes only in FJC staining of Untreated pup brains, and gestational MET inhibited these neonatal differences. In addition, gestational MET significantly increased neonatal astrocyte activation and microglial activation throughout the brain. These results emphasize the cell-type specificity of the effects of gestational MET and mild HI injury in neonatal rat pup brains.

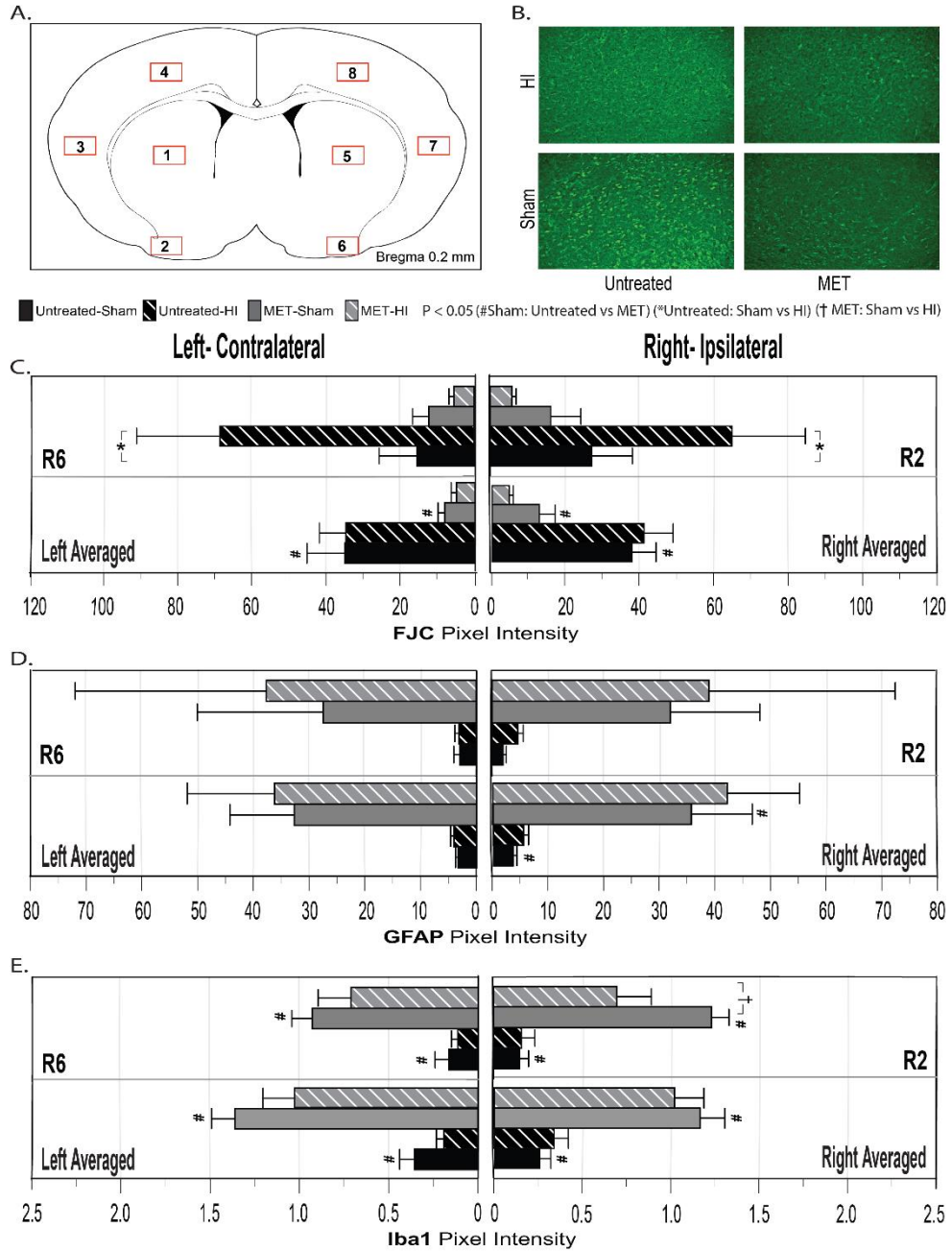


Figure 4. Effects of metyrapone-induced fetal transformation on HI-induced brain tissue injury. Figure 4A represents the location of the region of interest (R) examined, marked by a numbered red box. Figure 4B shows representative images of FJC for each of the four experimental groups in R6. The remaining panels depict signal intensities for FJC (Figure 4C), GFAP (Figure 4D), and Iba1 (Figure 4E)) for the four experimental groups in R2 and R6. Supplemental Figure 2 includes complete results for all regions. For all groups, N=5 except the Untreated-HI group where N=6. The following symbols indicate statistically significant differences (P<0.05) determined via ANOVA with a post-hoc-Fischer's LSD analysis: #=Untreated-Sham vs. MET-Sham; *=Untreated-Sham vs. Untreated-HI; †=MET-Sham vs. MET-HI.

Confocal Microscopy

The experimental approach included confocal microscopy to assess contractile protein organization of Smooth Muscle α Actin (α Actin) with two different myosin heavy chain isoforms: a) Smooth Muscle Myosin Heavy Chain (SM-MHC), and b) Non-Muscle Myosin Heavy Chain (NM-MHC) (**Figure 5**). In relation to smooth muscle phenotype, a leftward shift in pixel counts (e.g. decrease in High-High and increase in Low-Low) for colocalization of α Actin with MHC, suggests contractile **de**-differentiation. The methods used to measure α Actin -SM-MHC colocalization values could detect differences of 6.0% (Low-Low), 12.4% (Low-High), and 35.9% (High-High) with a power ≥ 0.8 for the number of pups in each quadrant (n=24). In comparison with Untreated-Sham values, MET-Sham values were significantly less in the Low-Low category and were significantly greater in Low-High and High-High categories, indicating gestational MET produced a rightward shift in pixel distributions, and correspondingly greater contractile differentiation in neonatal Sham arteries (**Figure 5B**). In comparison with Untreated-Sham arteries, Untreated-HI arteries exhibited no significant differences in α Actin -SM-MHC colocalization. In contrast, in neonatal arteries transformed by gestational MET, HI induced a leftward shift in pixel distributions that implied contractile **de**-differentiation, intimating that gestational MET unmasked a mild **de**-differentiating effect of HI in neonates.

The methods used to measure α Actin -NM-MHC colocalization values could detect differences of 5.6% (Low-Low), 12.0% (Low-High), and 41.9% (High-High) with a power ≥ 0.8 for the number of pups in each quadrant (n=24). As revealed by comparison of Untreated-Sham and MET-Sham values of colocalization of NM-MHC

with α Actin, gestational MET significantly decreased neonatal colocalization in the High-High category indicating a leftward shift in pixel distributions and contractile **de**-differentiation (**Figure 5C**). Similarly, comparison of values for colocalization of NM-MHC with α Actin in Untreated-Shams and Untreated-HIs indicated that HI caused a significant loss of colocalization in the High-High category and a leftward shift in pixel distributions consistent with contractile **de**-differentiation. However, in arteries from animals transformed with gestational MET animals, HI had no significant effect on neonatal colocalization of NM-MHC with α Actin in the High-High category, but reduced colocalization in the Low-High category and increased colocalization in the Low-Low category, revealing a leftward shift in pixel distributions and contractile **de**-differentiation in moderately differentiated smooth muscle.

During the early stages of smooth muscle differentiation, NM-MHC (also referred to as SMemb) is the first isoform of myosin heavy chain to be expressed (25, 38). As vascular maturation proceeds, NM-MHC is gradually replaced by SM-MHC, which has approximately twice the contractile efficiency as reflected by the higher rate of its phosphorylation by myosin light chain kinase (2). Correspondingly, changes in contractile phenotype can involve simultaneous changes in the colocalization of both SM-MHC and NM-MHC with α Actin, particularly in immature arteries. From this perspective, in Sham arteries MET-induced fetal transformation induced greater contractile differentiation for SM-MHC, but contractile **de**-differentiation for NM-MHC, consistent with enhanced functional maturation. In Untreated arteries, HI was without effect for SM-MHC differentiation, but caused contractile **de**-differentiation for NM-MHC, consistent with moderately reduced contractile function. In arteries transformed by

gestational MET, HI produced contractile **de**-differentiation for both SM-MHC and NM-MHC, revealing marked contractile **de**-differentiation. Overall, the colocalization results emphasized that gestational MET and HI had opposing but non-additive effects on neonatal contractile differentiation, as indicated by colocalization of SM-MHC and NM-MHC with α Actin.

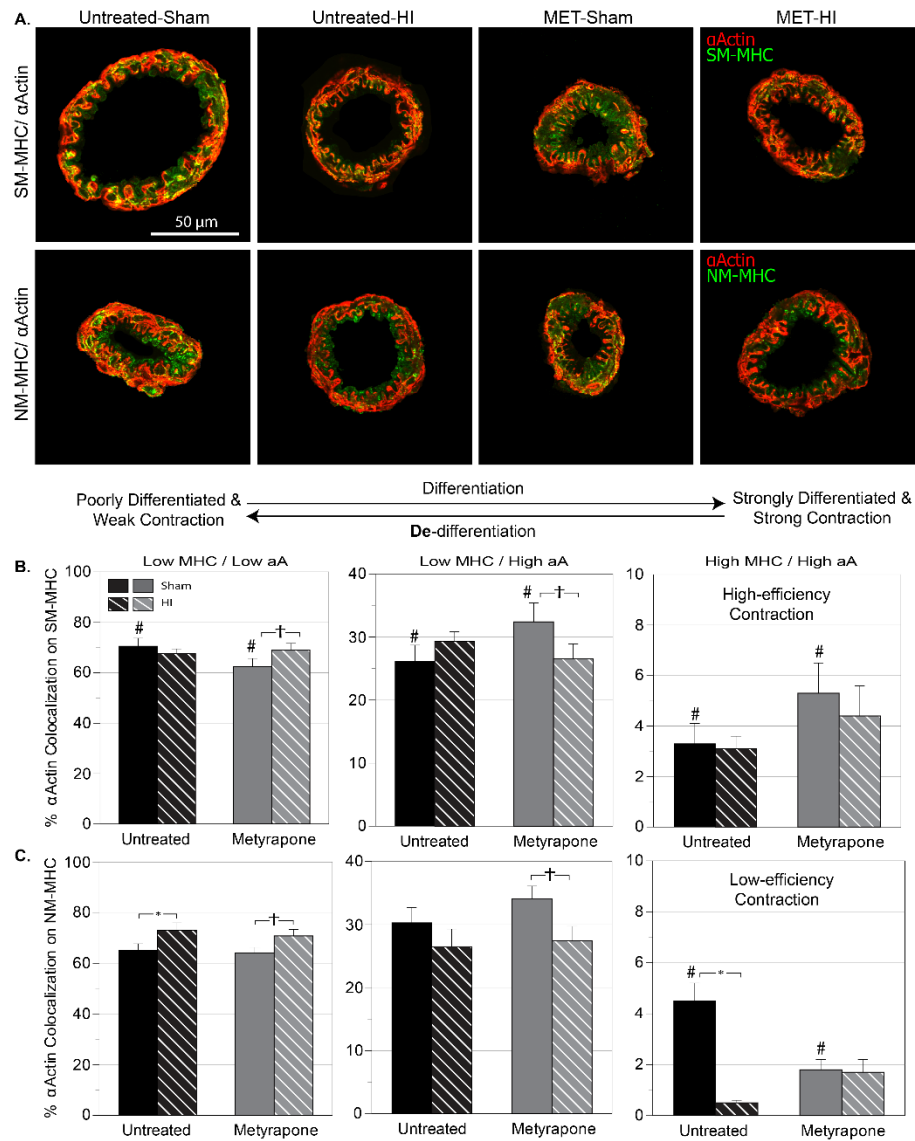


Figure 5. Effects of metyrapone-induced fetal transformation on confocal colocalization of smooth muscle contractile proteins in MCA from Sham and HI pups. Figure 5A: The images shown originated from middle cerebral arteries stained for Smooth Muscle α -Actin (α Actin) and Smooth-Muscle Myosin Heavy Chain (SM-MHC) (topmost row) or for α Actin and Non-Muscle Myosin Heavy Chain (NM-MHC) from each of the four treatment groups. Figures 5B and 5C: Confocal coefficients of colocalization for both marker pairs sorted into three distribution groups: Low MHC/Low α Actin, Low MHC/High α Actin, High MHC/High α Actin. Within each experimental group, all subgroups totaled to 100%. Note that the vertical scale for each of the three distribution groups differ (100% vs. 40% vs. 10%). In relation to smooth muscle phenotype, a leftward shift in pixel counts (e.g. decrease in High-High and increase in Low-Low) suggests contractile de-differentiation, and vice versa. Error bars indicate SEM with N=6 animals in all groups. The following symbols indicate statistical significance ($P < 0.05$) determined via Behren's-Fischer analyses with pooled variance: # = Untreated-Sham vs. MET-Sham; * = Untreated-Sham vs. Untreated-HI; † = MET-Sham vs. MET-HI.

Passive Diameter and Compliance

Across all groups, the average passive outer MCA diameter ranged from 165 ± 5 μm at 20 mm Hg to 207 ± 7 μm at 80 mm Hg (**Figure 6A, 6B**). For passive diameter measurements, these methods could detect a difference of 2.8% with a power ≥ 0.8 for the total number of pups used ($n=24$). Passive diameters between 20 and 60 mm Hg averaged to values that were significantly greater in MET-Sham compared to Untreated-Sham arteries, and in Untreated-HI compared to Untreated-Sham arteries. Conversely, passive diameters did not vary significantly between MET-Sham and MET-HI arteries, except at high pressures. Overall, both MET-induced fetal transformation and mild HI independently increased neonatal passive diameters and this effect was additive only at the highest pressures.

Average values of arterial compliance (**Figure 6C, 6D**) calculated from the slopes of normalized pressure-diameter curves, significantly decreased for all arteries with increasing pressure and ranged from $0.19 \pm .03\%$ diameter/mm Hg at 20 mm Hg to $0.04 \pm .01\%$ diameter/mm Hg at 80 mm Hg. For compliance measurements, these methods could detect a difference of 21.3% with a power ≥ 0.8 for the total number of pups used ($n=24$). Compliance in Untreated-Sham and MET-Sham arteries were similar at low and intermediate pressures, but at high pressures MET-Sham values were significantly less than Untreated-Sham values; MET depressed compliance at high pressure in sham arteries. HI also depressed compliance at high pressure, given that compliance was significantly less in Untreated-HI than in Untreated-Sham arteries at intermediate and high pressures. In contrast, in arteries transformed by gestational MET, HI had no significant effect on neonatal compliance at low and intermediate pressures,

but significantly increased compliance relative to MET-Sham arteries at high pressures. Thus, at high pressure only, both gestational MET and mild HI alone independently decreased neonatal arterial compliance. However, when these effects were combined, compliance in MET-HI arteries was significantly greater than in MET-Sham arteries.

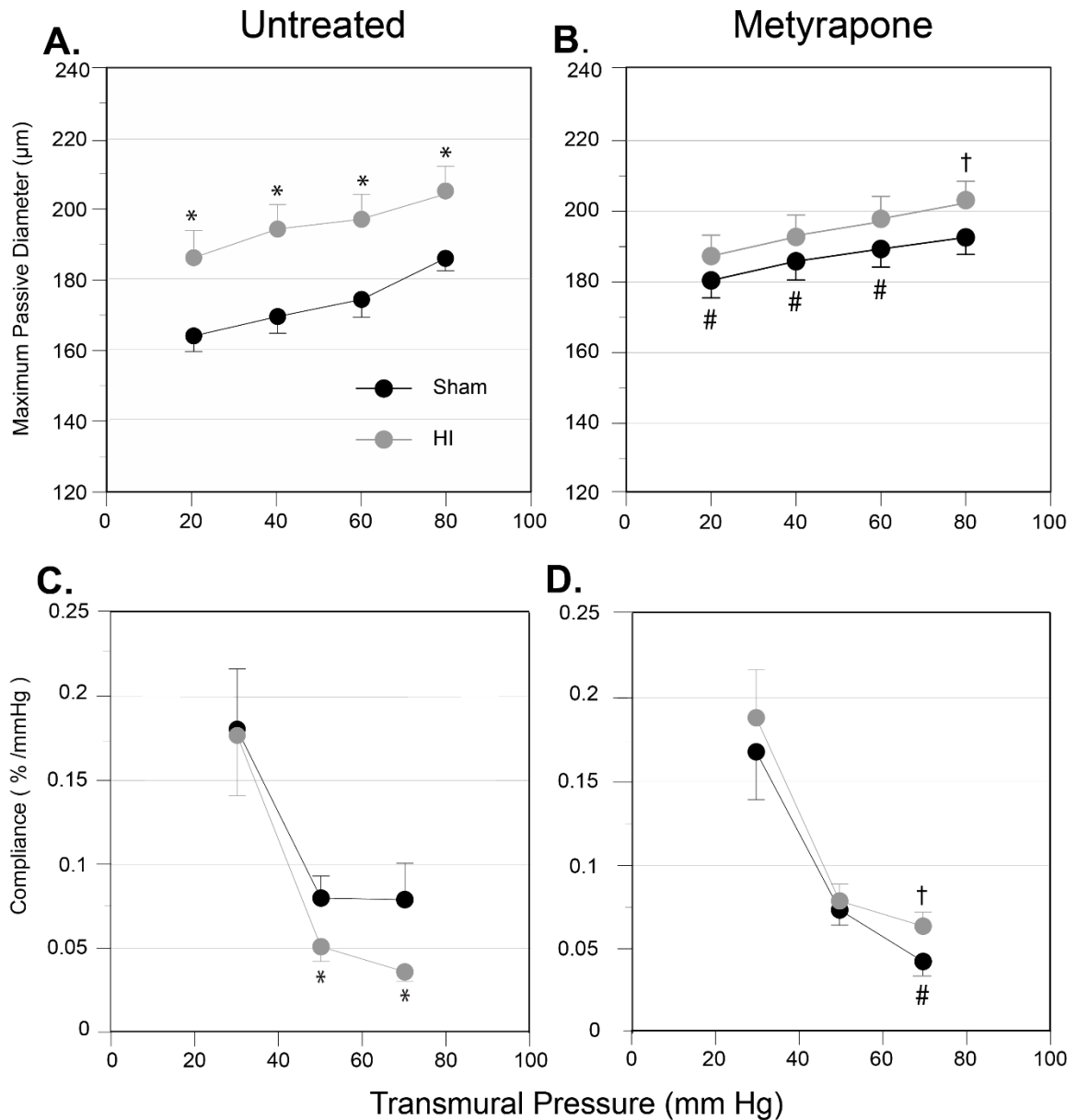


Figure 6. Effects of metyrapone-induced fetal transformation on passive arterial diameter and compliance in MCAs from Sham and HI pups. Figure 6A and 6B: For middle cerebral arteries from P11 pups, incubation in 3 mM EGTA buffer eliminated all active tone, and enabled measurement of passive vessel diameters as a function of transmural pressure. Figure 6C and 6D: Calculations from the slopes of passive diameter-pressure plots allowed for the determination of arterial compliance. Error bars indicate SEM for N = 6 in all groups. The following symbols indicate statistical significance ($P < 0.05$) determined via Behren's-Fischer analyses with pooled variance: # = Untreated-Sham vs. MET-Sham; * = Untreated-Sham vs. Untreated-HI; † = MET-Sham vs. MET-HI.

Vessel Myography

Measurements of pressure-induced active changes in artery diameter (ΔD) enabled assessment of myogenic reactivity from 20 to 80 mm Hg. Plots of these changes against intraluminal pressure allowed calculation of the areas beneath the ΔD -pressure curves (AUC), which in turn facilitated group-wise comparisons. For diameter measurements, these methods could detect a difference of 17.0% with a power ≥ 0.8 for the total number of pups used (n=24). Values of pressure-induced ΔD did not differ significantly among any of the groups (**Figure 7A**).

The methods used to measure intracellular wall calcium could detect a difference of 7.7% with a power ≥ 0.8 for areas beneath the Δ Wall Calcium-pressure curves (AUC) for the number of pups used (n=24). For pressure-induced changes in wall calcium concentration (Δ Wall Calcium), MET-Sham values did not significantly differ from Untreated-Sham arteries (**Figure 7B**). In contrast, compared to Untreated-Sham values of Δ Wall Calcium, Untreated-HI values were significantly greater (12.1%). In arteries from animals transformed with gestational MET, HI had no significant effect on neonatal Δ Wall Calcium. In parallel, estimates of myofilament calcium sensitivity did not vary significantly across the groups as a function of transmural pressure (**Figure 7C**). The methods used to estimate of myofilament calcium sensitivity, calculated as the ratios of $\Delta D/\Delta$ Wall Calcium could detect a difference of 19.6% with a power ≥ 0.8 for the number of pups used (n=24).

To complement measurements of myogenic reactivity, which largely reflect physiological activation of smooth muscle contraction, the experimental approach included assessments of depolarization-induced contractile reactivity produced by 120

mM potassium, to indicate maximum receptor-independent contractile capacity. As for measurements of myogenic reactivity, AUC calculations facilitated statistical comparisons across groups (**Figure 7D-F**). For potassium-induced contractions, group-wise comparisons yielded no significant differences in potassium-induced ΔD values. Regarding potassium-induced values of Δ Wall Calcium, the values were significantly greater in MET-Sham arteries than in Untreated-Sham arteries (28.1%). Relative to Untreated-Sham arteries, Untreated-HI arteries also exhibited significantly greater values of potassium-induced Δ Wall Calcium (29.3%), but calcium values did not differ between MET-Sham arteries and MET-HI arteries. For estimates of myofilament calcium sensitivity, values did not differ significantly between Untreated-Sham and MET-Sham arteries. In addition, Sham and HI arteries were not significantly different in arteries from either Untreated pups or those transformed with gestational MET.

In aggregate, mild HI did not induce changes in ΔD or calcium sensitivity responses to either physiological changes in transmural pressure or potassium depolarization in either Untreated or MET-transformed animals (**Figure 7A, 7C, 7D, 7F**). Conversely, mild HI significantly increased Δ Wall Calcium in response to either physiological changes in transmural pressure or potassium depolarization in Untreated but not MET-transformed arteries (**Figure 7B, 7E**). For potassium-induced contractions, gestational MET also increased neonatal Δ Wall Calcium in Sham arteries (**Figure 7E**).

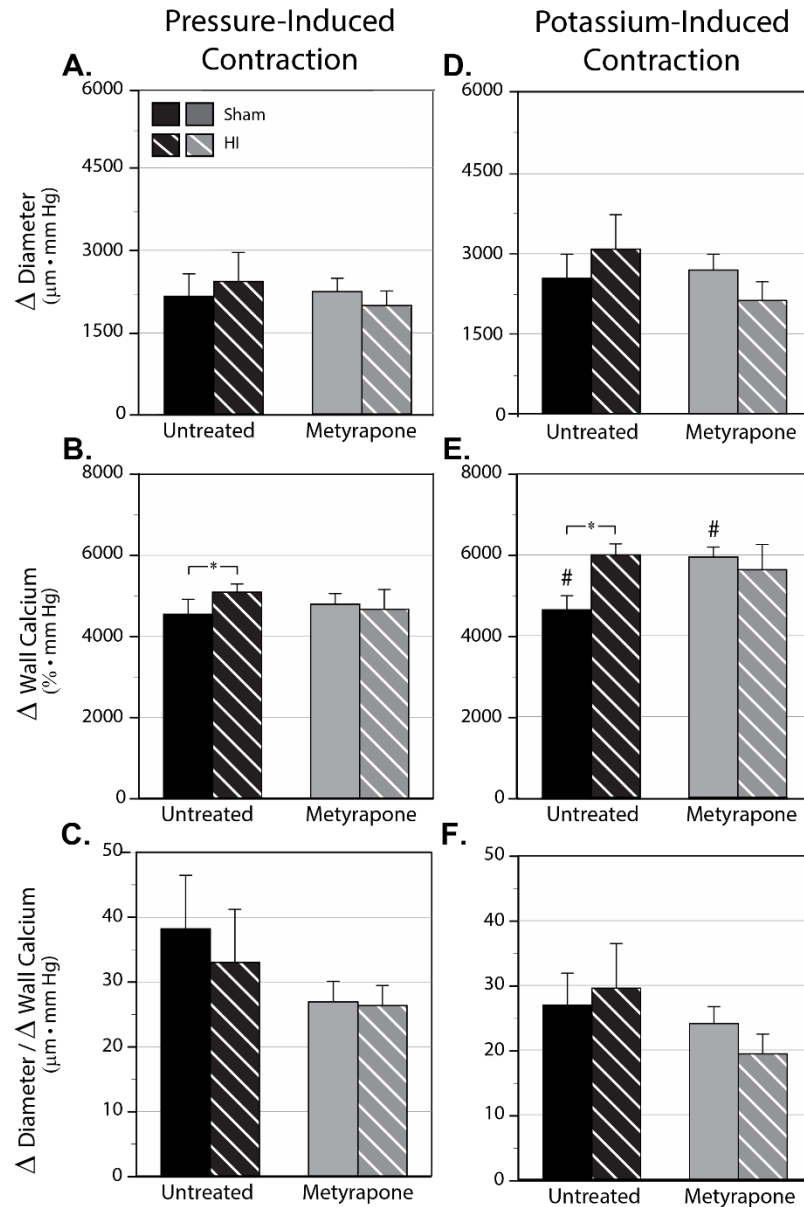


Figure 7. Effects of metyrapone-induced fetal transformation on changes in diameter, wall calcium, and calcium sensitivity induced by pressure and K^+ in MCA of Sham and HI pups. Middle cerebral artery measurements of contractile responses to changes in intraluminal pressure enabled assessment of responses in PSS alone (Figure 7A-C) and in PSS with 120 mM K^+ (Figure 7D-F). Plots of these changes against intraluminal pressure on the abscissa allowed calculation of the areas beneath the curves for three different parameters on the ordinate: outside diameter (Δ Diameter), wall calcium concentration (Δ Wall Calcium), and calcium sensitivity (Δ Diameter / Δ Wall Calcium). Error bars indicate SEM for $N = 6$ animals in all groups. The following symbols indicate statistical significance ($P < 0.05$) determined via Behren's-Fischer analyses with pooled variance: # = Untreated-Sham vs. MET-Sham; * = Untreated-Sham vs. Untreated-HI; † = MET-Sham vs. MET-HI.

Neurobehavior

Across the neurobehavioral assessments used in P11/P12 pups, the statistical sensitivity of the righting reflex test was 19.6% with a power ≥ 0.8 for the number of pups used (n=31). Righting reflex results revealed that MET-Sham pups took significantly longer than Untreated-Sham pups to return to an upright position. Significant differences for the righting reflex were not evident for any other comparisons. The open field assessment could detect differences of 12.6% with a power ≥ 0.8 for the number of pups used (n=31). Untreated-HI pups explored significantly fewer boxes (31.4 ± 1.9) than Untreated-Sham pups (39.8 ± 4.0). Field exploration values did not differ significantly for any other group-wise comparisons. Our negative geotaxis measurements could detect a significant difference of 27.9% with a power ≥ 0.8 for the number of pups used (n=31). For the negative geotaxis tests, MET-HI pups (17.0 ± 4.1 s) took significantly longer to turn 180° than MET-Sham pups (9.5 ± 2 s). Negative geotaxis values did not differ significantly for any other group-wise comparisons.

Discussion

The present study explores the hypothesis that late gestational reduction of corticosteroids transforms the long-term structure and function of the cerebrovasculature. A main corollary of this hypothesis is that this MET-induced fetal transformation modulates HI vulnerability during postnatal life. The present results demonstrate in unstressed neonates that MET during late gestation: 1) promoted cerebrovascular contractile differentiation through selective changes in the organization of myosin heavy chain isoforms; 2) increased passive diameters, selectively decreased compliance, and increased depolarization-induced mobilization of contractile calcium in middle cerebral arteries; 3) mildly increased hemispheric cerebral edema with decreased basal neuronal degeneration and increased astroglial and microglial activation; and 4) increased the time required to complete the righting reflex. The results also demonstrate in stressed (HI treated) neonates that gestational MET: 1) decreased reactivity of the HPA axis to stressful stimuli in P9/P10 rats; 2) enhanced the myosin isoform-specific contractile **de**-differentiation induced by HI; 3) reduced the effects of HI on passive diameter, compliance and calcium mobilization in middle cerebral arteries; 4) diminished the effects of HI on neuronal injury and unmasked regional HI depression of microglial activation; and 5) attenuated the negative effects of HI on open field exploration but enhanced the detrimental effects of HI on negative geotaxis responses. Together, these results argue that a deficit in gestational corticosteroid availability causes a mixture of beneficial effects on ischemic neuronal injury and cerebrovascular contractility, but detrimental effects on edema formation, glial and microglial activation, cerebrovascular compliance, and neurobehavior.

Given that alterations in prenatal GC levels can induce long-term changes to HPA function (35, 69), the present experiments first determined if fetal transformation induced by gestational reduction of GCs had a lasting impact on postnatal HPA axis function. Whereas baseline GC levels did not differ significantly in Untreated and MET-transformed P9 pups prior to surgery, carotid ligation and hypoxia produced significant GC transients that were absent in pups that experienced MET-induced fetal transformation (**Figure 2A and 2B**). This elimination of postnatal GC transients may have resulted from alterations in glucocorticoid feedback, or alternatively, increased degradation or decreased release of GC secondary to decreased release of, or sensitivity to, ACTH or CRF (35). At the molecular level, this attenuation could reflect decreased ACTH receptor levels, or depressed coupling of ACTH receptors to GC release; such mechanisms are highly dynamic (35, 36, 47). However, GC levels at 24 hours following hypoxia did not differ among any of the groups, revealing that both the transient effects of acute hypoxia, and the persistent effects of gestational MET, on the neonatal HPA axis primarily influenced reactivity to stress (**Figure 2C**). Additional measurements of acute responses to stress at later postnatal ages would be required to confirm any lasting effects of gestational MET on GC reactivity. Equally important, basal GC levels at 24 hours after exposure to either normoxia or hypoxia did not differ significantly among any of the four experimental groups, which emphasizes that all differences observed between groups (**Figures 3-7**, including behavior) cannot be explained by differences in basal postnatal levels of circulating GC.

The present experiments also explored the effects of gestational MET on neonatal cerebral tissue using MRI. Gestational MET in Sham animals led to increased T2 values

suggesting increased water content and presumably cerebral edema (**Figure 3B**: Untreated-Sham vs MET-Sham), implying that corticosteroid reduction during late gestation may compromise blood-brain-barrier (BBB) development, and thereby postnatal function (60). In support of this interpretation, glucocorticoids can inhibit the synthesis of extracellular matrix proteins, including matrix metalloproteinases that can influence vascular permeability (9). Corticosteroids can also influence expression of cerebral aquaporins, which in turn can influence BBB function and edema formation (64). In contrast to gestational MET, acute mild HI had no significant effect on neonatal brain edema.

To complement the MRI results, additional measurements quantified cell-type specific histological changes in three distinct brain markers: FJC for degenerating neurons (51), GFAP for activated astrocytes (22), and Iba1 for activated microglia (26) (**Figure 4**). Across the whole brain, MET-induced fetal transformation mitigated the number of FJC positive neurons in Sham animals (**Figure 4C**), despite the finding that GC levels were similar in Untreated-Sham and MET-Sham pups (**Figure 2C**). Gestational MET also increased activation of astrocytes (GFAP, **Figure 4D**) and microglia (Iba1, **Figure 4E**) in Sham animals. One possible explanation for these findings is that gestational MET included epigenetic changes that influenced postnatal expression of genes such as VEGF that influence cerebral capillary density and tissue perfusion (65). In turn, long-term changes in capillary density and tissue perfusion could influence cellular metabolism and turnover. Increased astrocyte activation could also contribute to the effects of gestational MET on edema, as observed in Sham animals (**Figure 3A, 3B**) (59). These possible effects of gestational MET-on the cerebral

parenchyma appear worthy of further examination, particularly in the context of epigenetic changes in the expression of genes that influence the activation and turnover of neurons, astrocytes, and microglia in the postnatal brain.

Across all brain regions, mild HI had no significant effect on the activation of either astrocytes (**Figure 4D**) or microglia (**Figure 4E**) in either Untreated pups, or those transformed by gestational MET. In contrast, HI markedly increased FJC staining in Regions 2 and 6 of Untreated pups, but not in pups transformed by gestational MET (**Figure 4C**). These findings reinforce the view that gestational corticosteroids, or their precursors such as progesterone (18), can influence postnatal vulnerability to HI (20, 48, 58). More specifically, these novel results support the view that gestational MET can be neuroprotective in neonates. Because these effects were independent of postnatal GC levels, the neuroprotection observed was probably a consequence of epigenetic changes in genes that remain to be identified, but probably influence neuronal growth and metabolism.

Another cell-type strongly affected by gestational MET was the vascular smooth muscle of middle cerebral arteries, which is a critical component of cerebrovascular structure and function (37). To explore the effects of gestational MET, the present study assessed phenotypic modulation of neonatal cerebral artery smooth muscle via confocal colocalization of two protein marker pairs: (1) α Actin and SM-MHC, indicative of a high-efficiency contractile phenotype, and (2) α Actin with NM-MHC, indicative of a low-efficiency contractile phenotype (2, 13, 25) (**Figure 5**). Comparisons of colocalization values in MET-Sham and Untreated-Sham arteries revealed that gestational MET enhanced neonatal α Actin colocalization with SM-MHC, but reduced

α Actin colocalization with NM-MHC, indicating that gestational MET promoted differentiation into a more mature, high-efficiency contractile phenotype in postnatal pups. This finding infers that normal gestational levels of corticosteroids retard contractile maturation in middle cerebral arteries. Whereas this observation corroborates previous findings (13, 66), other reports communicate that antenatal dexamethasone also can accelerate vascular differentiation in the short-term for some fetal smooth muscle (19). These inconsistencies may reflect the differences between short-term and long-term effects of corticosteroids on vascular smooth muscle, but other factors such as age, species and artery type probably also play some role.

In the context of mild HI, gestational MET unmasked an HI-induced **de**-differentiation of high-efficiency contractile smooth muscle (**Figure 5B**), and promoted **de**-differentiation of low-efficiency smooth muscle (**Figure 5C**), as indicated by a leftward shift in pixel distributions for both protein marker pairs in neonatal arteries. These changes in vascular smooth muscle phenotype argue that the lasting effects of gestational MET result in a greater level of contractile differentiation that is more vulnerable to the **de**-differentiating effects of HI in postnatal pups. At the genomic level, these effects may reflect interactions between gestational corticosteroids and epigenetic changes that influence postnatal responses to hypoxia inducible factors and transcription of genes encoding contractile proteins (56, 71). Functionally, this pattern of effects implies that gestational MET-alone would yield greater cerebrovascular contractility, and possibly improved contractile function such as that necessary for the autoregulation of cerebral blood flow (37). Conversely, gestational MET also could enhance HI-induced compromise of cerebrovascular contractile function in neonates.

To assess the functional consequences of altered smooth muscle phenotype, the experimental design included measurements of passive arterial diameter as a function of increasing transmural pressure to enable calculation of arterial compliance ($\Delta\text{volume}/\Delta\text{pressure}$), a risk factor for cardiovascular disease (32, 72). Structurally, passive arterial compliance is dominated by the net contributions of: (1) compliance-decreasing extracellular matrix (ECM) proteins, including collagens and the collagen crosslinking enzyme, lysyl oxidase (LOX); and (2) compliance-increasing ECM proteins, such as elastin and collagenolytic matrix metalloproteinases (MMPs) (67, 72). Increased fetal GC levels induced by maternal food-restriction can depress cerebral artery compliance, due at least in part to increased expression of collagens in the ECM (13, 28, 29). Importantly, these effects of maternal food-restriction on cerebral artery compliance were markedly dampened by MET during the last half of gestation, as in the present studies.

In light of findings that chronically elevated GCs during gestation can depress cerebrovascular compliance in adult offspring, the present study examined the transformative effects of reductions in corticosteroids during gestation on compliance in both unstressed pups, and in pups exposed to the acute postnatal stresses induced by HI. In Sham pups, gestational MET generally increased postnatal passive diameters and reduced compliance at the highest pressure (**Figure 6C vs. 6D**). In light of evidence that acute treatment with GCs can suppress expression of multiple ECM proteins (9), the present results hint that gestational reduction of corticosteroids also can influence postnatal expression of compliance-decreasing ECM proteins, such as collagens and possibly LOX, most probably through epigenetic mechanisms. By itself, HI significantly

increased passive diameters and decreased passive compliance, although these effects were largely absent in arteries transformed by gestational MET (**Figure 6**). Importantly, gestational MET reversed the effects of HI on neonatal compliance, revealing that the effects of gestational MET and HI were not simply additive. Indeed, these results offer another example of how gestational MET unmasked neonatal cerebrovascular effects of hypoxia, which in this case manifested as a modest ability of HI to increase compliance (**Figure 6D**). One mechanism through which HI possibly might increase compliance could be through contractile **de**-differentiation (**Figure 5B**) followed by arterial remodeling that increased expression of compliance-increasing ECM proteins such as MMPs or elastins (67). Conversely, hypoxia has been reported to increase expression of lysyl oxidase (68), and acute GCs can increase LOX activity (54), which would be expected to decrease compliance (67). How gestational MET shifts the postnatal effects of HI on compliance remains a topic for further investigation.

Gestational MET also significantly altered the contractile characteristics of MCAs from postnatal pups. Although MET had no consistent effects on changes in diameter or myofilament calcium sensitivity, it did enhance calcium mobilization responses in potassium-induced, but not pressure-induced, contractions in Sham arteries (**Figure 7B, 7E**). These results imply that gestational corticosteroids are important for development of postnatal calcium homeostasis, possibly through long-lasting (epigenetic) modulation of the expression or function of L-type and other membrane calcium channels that influence intracellular calcium responses to potassium-induced depolarization (24). Additional effects of gestational MET on calcium sequestration by SERCA pumps (15), release from

the sarcoplasmic reticulum (30), or extrusion into the extracellular space (57) cannot be excluded, but remain largely unexplored.

In parallel with the effects of gestational MET on neonatal MCA contractility, mild HI also had little influence on changes in diameter or myofilament calcium sensitivity, but elevated changes in wall calcium associated with both pressure- and potassium-induced contractions (**Figure 7**). These findings imply that HI altered mechanisms governing calcium mobilization associated with contraction, including calcium influx, release, extrusion or sequestration (23, 61). Given that other studies (61) have reported an ability of hypoxia to enhance influx and release in rat MCA, these mechanisms could potentially explain the observed results, although effects on sequestration or extrusion cannot be excluded. Gestational MET ablated these effects of HI in postnatal pups, inferring again that gestational corticosteroids play a critical developmental role in establishing calcium homeostasis in MCAs. In light of evidence that HI had no phenotypic effect on the fraction of arterial smooth muscle with high contractile efficiency (**Figure 5B**), it appears likely that the effects of HI on calcium mobilization were short-term and acute, and that these same effects underwent long-term modulation by gestational MET.

Measurements of neurobehavior revealed the composite consequences of global (**Figure 3**) and cellular (**Figure 4**) changes in the cerebral parenchyma, together with the changes in cerebrovascular structure (**Figures 5 and 6**) and function (**Figure 7**) attributable to the long-term effects of gestational transformation with MET, and the short-term effects of HI. In Sham animals, MET-induced gestational transformation significantly impaired the righting reflex, indicating a significant role for gestational

corticosteroids in the normal development of the sensorimotor functions required for the righting reflex. Conversely, mild HI alone significantly inhibited only open field exploration, and this effect was absent in pups transformed by gestational MET. In addition, gestational MET unmasked a significant effect of HI on negative geotaxis, such that MET-HI values were significantly greater, and thus worse, than MET-Sham values. This pattern of behavioral results implies that gestational corticosteroids are essential for reducing vulnerability of the negative geotaxis reflex to HI, and as such reinforce previous studies of the effects of cerebral ischemia on these behaviors (62). Although the present neurobehavioral assessments were limited by high variability, the results highlight the mild severity of our HI model and reveal that long-term effects of gestational MET, and the short-term effects of HI, exert differential effects on regional cell types and brain structure that ultimately influence discrete sensorimotor functions.

Overall, the present experiments demonstrate that reduction of corticosteroids during the latter half of gestation can induce mixed patterns of fetal vascular changes that include both beneficial and detrimental effects on neonatal cerebrovascular physiology. In Sham animals, gestational MET dampened HPA reactivity to stress secondary to anesthesia and surgical trauma in postnatal pups (**Figure 2A**). Gestational MET also decreased MCA compliance (**Figure 6C, 6D**), promoted contractile differentiation (**Figure 5**), and increased calcium mobilization during depolarization-induced contractions (**Figure 7B, 7E**). Gestational MET also enhanced basal activation of cerebral astrocytes and microglia (**Figure 4D, 4E**), promoted formation of cerebral edema (**Figure 3**), and ultimately impaired the righting reflex in P11 pups. As such, these findings support the main hypothesis that attenuation of corticosteroid levels during

the second half of gestation transforms the cerebrovasculature, and modulates the structure and function of postnatal cerebral arteries.

To assess the effects of MET-induced fetal vascular transformation on vulnerability to postnatal HI insults, the experimental design included development of a model of mild HI injury to test the corollary hypothesis that the neonatal cerebrovasculature is a key target of HI injury. This model revealed that mild HI initially caused a transient decrease in circulating GC levels (**Figure 2B**), and then subsequently decreased MCA compliance (**Figure 6C**), promoted **de**-differentiation of low-efficiency smooth muscle, preserved differentiation of high-efficiency smooth muscle (**Figure 5**), and increased MCA calcium mobilization during both myogenic and depolarization-induced contractions (**Figure 7B, 7E**), resulting in preserved post-HI contractility (**Figure 7A, 7D**). Our model of mild HI also increased neuronal injury in the territory of the MCA (**Figure 4B, 4C**) and a corresponding compromise in open-field exploration.

In studies of the interactions between MET-induced vascular transformation and mild HI, MET-induced transformation during late gestation abrogated HI-induced reactivity of the HPA axis (**Figure 2B**). Gestational MET also ablated HI-induced depression of MCA compliance (**Figure 6C, 6D**), enhanced the contractile **de**-differentiation of smooth muscle following mild HI (**Figure 5**), and attenuated the effects of HI on calcium mobilization responses during both myogenic and depolarization-induced contractions (**Figure 7B, 7E**). In addition, HI-induced neuronal degeneration was abolished in the territory of MCAs harvested from pups transformed by gestational MET (**Figure 4B, 4C**). In terms of neurobehavior, MET-induced fetal transformation suppressed the effects of HI on open field exploration but unmasked an effect of HI on

the negative geotaxis reflex. Together, these findings strongly support our corollary hypothesis that MET-induced fetal vascular transformation produces a mixture of beneficial and detrimental effects that significantly alters the cerebrovascular, parenchymal, and neurobehavioral responses to mild HI.

Perspectives and Significance

In the present study, MET was administered to the dam in the drinking water, which presumably reduced corticosterone and aldosterone availability to all maternal and fetal tissues and cells. Correspondingly, the effects of gestational MET potentially could include both direct and indirect, as well as genomic and non-genomic, effects on both the vasculature and other non-vascular tissues and organs. In addition, it is possible that MET-induced inhibition of 11- β hydroxylase increased tissue levels of corticosteroid precursors, such as progesterone or 11-deoxycorticosterone, that may have contributed to the observed spectrum of altered vascular physiology in maternal and neonatal tissues. Measurements of ACTH, aldosterone, and adrenal mass would be required to elucidate the organismal impact of gestational MET administration on the HPA axis. Similarly, studies of the effects of MET on the release of paracrine mediators and cytokines from multiple cell types of the brain parenchyma would be required to fully identify the indirect effects of MET on cerebrovascular and endothelial structure and function (55) (70). MET also may have modulated maternal and fetal fluid balance and cardiovascular homeostasis, which our model did not assess. Despite this broad potential range of direct and indirect effects, the present experiments offer novel evidence that MET administered during late gestation can induce some form of fetal cerebrovascular transformation that

persists through neonatal life and significantly influences how both vascular and non-vascular cerebral tissues function under basal conditions and after HI stress.

From a translational perspective, the present findings predict that neonates from pregnancies with low maternal corticosteroid levels, due possibly to a mutation or deficiency in CYP11 β or some form of adrenal insufficiency, are at greatly increased risk for developing mild cerebral edema and impairments in neurobehavioral function possibly mediated by persistent fetal vascular transformation that compromises structure-function relations in neonatal cerebral arteries. This type of fetal vascular transformation includes both beneficial and detrimental consequences for postnatal responses to HI insults. Without doubt, maintenance of corticosteroids within a normal range during pregnancy is critical; either too much or too little dramatically compromises both structural and functional cerebrovascular development.

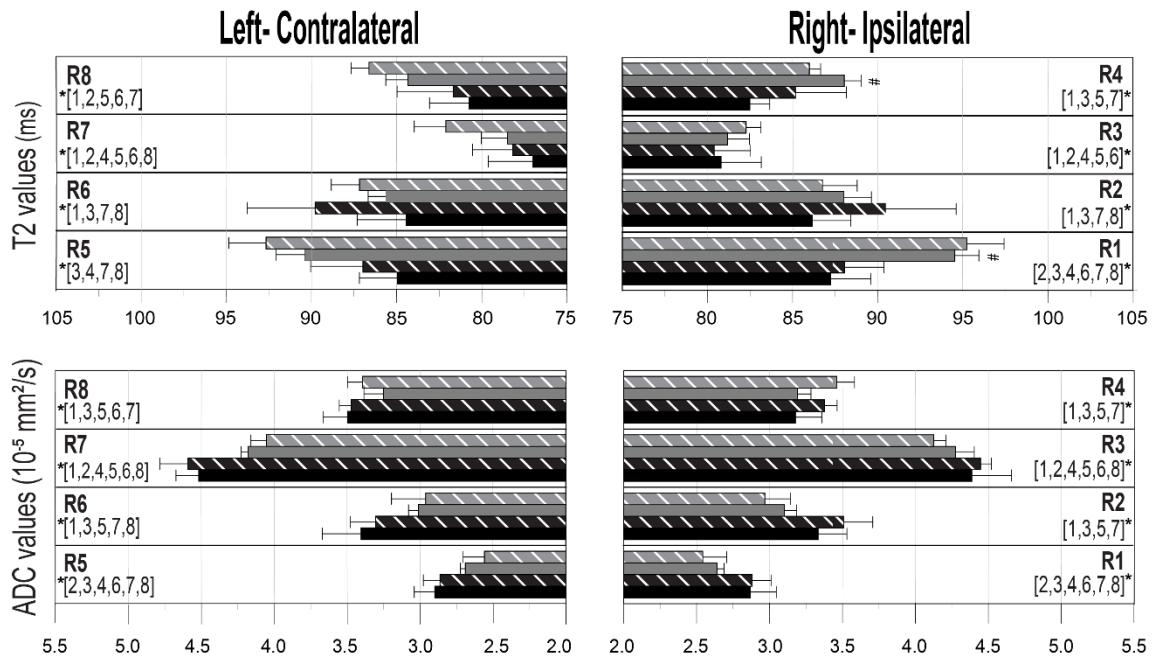
Acknowledgments

The authors greatly appreciate the contribution from Coleen Doan who performed some of the myography experiments. The authors also thank Mary Hamer for her assistance in the cardiac perfusion procedures. A portion of this research used resources in the Loma Linda University School of Medicine Advanced Imaging and Microscopy Core, a facility is supported in part by the National Science Foundation through the Major Research Instrumentation program of the Division of Biological Infrastructure Grant No. 0923559 and the Loma Linda University School of Medicine. The work reported in this manuscript was supported by National Institutes of Health Grants HD-

054920, HD-31266, HL-54120, HL-64867, NS-082184, NS-076945 and the Loma Linda University School of Medicine.

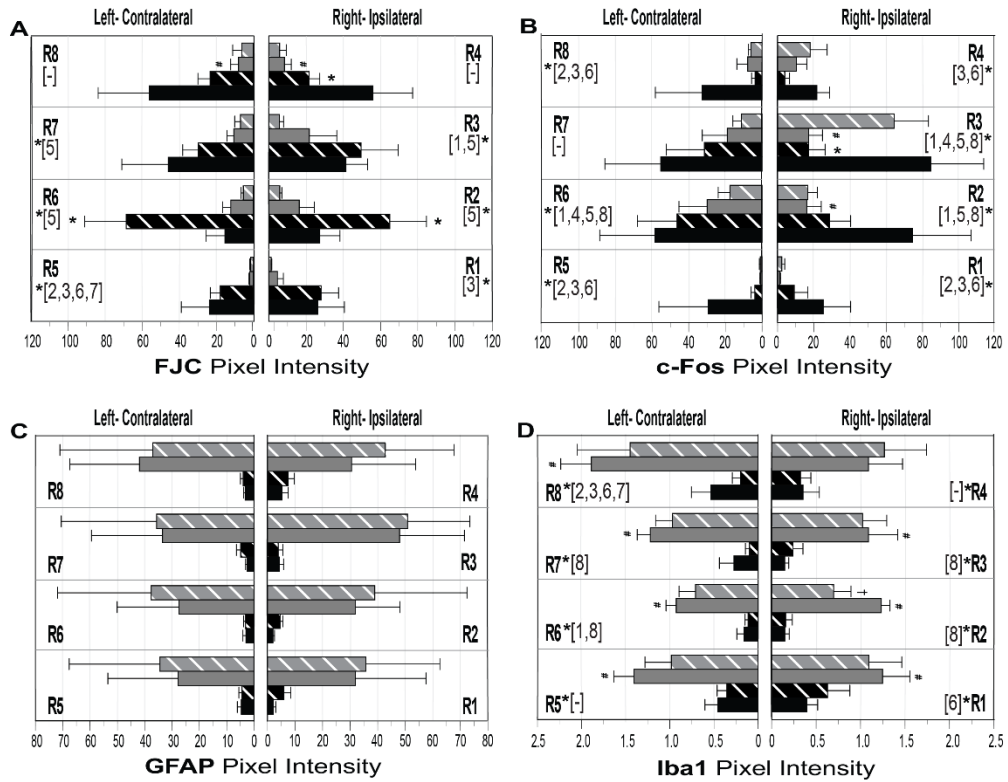
Supplemental Figures and Table

■ Sham-Control ▨ HI-Control ■ Sham-MET ▨ HI-MET P < 0.05 (#: Sham-Control vs Sham-MET)



Supplemental Figure 1. Effects of metyrapone-induced fetal transformation on brain injury in HI and Sham P11 pups. Region of interest sampling of MR images produced 8 separate values, designated with the letter R and corresponding region number as shown in Figure 4A. Each marker shows summarized group-group differences within region (R1-R8). Between region differences are indicated by bolded region numbers above brackets that list the regions that were significantly different (e.g. [1,3,5,7]*). Hash marks (#, P<0.05) denote significant group-group differences, as determined via ANOVA with a post-hoc Fischer's LSD analysis for Sham-Control vs. Sham-MET; no other group-group comparisons yielded significant differences. The columns and error bars indicate the mean \pm SEM for N=4 in Sham-Control and N=5 in all other groups.

Sham-Control
 HI-Control
 Sham-MET
 HI-MET
 P < 0.05 (#Sham-Control vs Sham-MET) (*Sham-Control vs HI-Control) († Sham-MET vs HI-MET)



Supplemental Figure 2. Effects of metyrapone-induced fetal transformation on brain injury. The panels above depict signal intensities for FJC (Figure 2A), c-Fos (Figure 2B), GFAP (Figure 2C) and Iba1 (Figure 2D) for the four experimental groups. Shown for each markers are group averages within each region (R1-R8). Within region differences ($P < 0.05$) determined via ANOVA with a post-hoc Fischer's LSD analysis are indicated by the following symbols: #=Sham-Control vs Sham-MET; *=Sham-Control vs. HI-Control; †= Sham-MET vs HI-MET. Between region differences are indicated by bolded region numbers above brackets that list the regions that were significantly different (e.g. [1,3,5,7] *). For all groups, $N=5$ except the HI-Control group where $N=6$ / Error bars indicate SEM.

Supplemental Table 1. Male-female analysis.

Endpoint	Aggregate Mean	Aggregate N	Male vs Female P-Value
GC Timecourse	5018±777 ng/mL corticosterone	41	0.301
T2 Left	84.7±0.7 ms	19	0.359
T2 Right	86.5±0.7 ms	19	0.092
ADC Left	3.40±.076*10 ⁻⁵ mm ² /s	19	0.897
ADC Right	3.39±.077*10 ⁻⁵ mm ² /s	19	0.881
FJC Left	21.5±3.5 Pixel Intensity	21	0.846
FJC Right	24.8±3.5 Pixel Intensity	21	0.132
GFAP Left	18.3±4.9 Pixel Intensity	21	0.855
GFAP Right	20.±4.4 Pixel Intensity	21	0.836
Iba1 Left	0.708±0.077 Pixel Intensity	21	0.506
Iba1 Right	0.678±0.072 Pixel Intensity	21	0.871
Righting Reflex	6.77±0.2 s	25	0.582
Openfield	32.5±2.1 boxes	25	0.941
Negative Geotaxis	10.7±1.4 s	25	0.329
Values from Aggregate P11 Rat Pup Population			
Passive Diameter at 20 mmHg	168±4 µm	64	0.561
Passive Diameter at 40 mmHg	172±4 µm	64	0.549
Passive Diameter at 60 mmHg	178±4 µm	64	0.504
Passive Diameter at 80 mmHg	183±4 µm	64	0.459
Pressure-Induced Δ Diameter	1250±108 µm*mmHg	63	0.103
Pressure-Induced Δ Wall Calcium	1453±163 %*mmHg	64	0.727
Pressure-Induced Δ Calcium Sensitivity	29.0±8.0 µm*mmHg	63	0.354
Potassium-Induced Δ Diameter	2573.0±202 µm*mmHg	64	0.648
Potassium-Induced Δ Wall Calcium	9444±546 %*mmHg	64	0.277
Potassium-Induced Δ Calcium Sensitivity	15.5±1.2 µm*mmHg	64	0.186

Descriptive statistics and corresponding P-values of rat pup male-female analysis obtained via ANOVA for the experimental endpoints listed below. Data are presented as mean ± SEM. Passive diameters and myography endpoints represent a subset selected from aggregate values pooled from a larger population of P11 rat pups used for multiple studies.

References

1. **Adeoye OO, Bouthors V, Hubbell MC, Williams JM, and Pearce WJ.** VEGF receptors mediate hypoxic remodeling of adult ovine carotid arteries. *Journal of applied physiology (Bethesda, Md : 1985)* 117: 777-787, 2014.
2. **Alcala DB, Haldeman BD, Brizendine RK, Krenc AK, Baker JE, Rock RS, and Cremo CR.** Myosin light chain kinase steady-state kinetics: comparison of smooth muscle myosin II and nonmuscle myosin IIB as substrates. *Cell biochemistry and function* 34: 469-474, 2016.
3. **Ashwal S, Tone B, Tian HR, Chong S, and Obenaus A.** Comparison of two neonatal ischemic injury models using magnetic resonance imaging. *Pediatric research* 61: 9-14, 2007.
4. **Briet M, and Schiffrin EL.** Vascular actions of aldosterone. *Journal of vascular research* 50: 89-99, 2013.
5. **Burchell SR, Dixon BJ, Tang JP, and Zhang JH.** Isoflurane Provides Neuroprotection in Neonatal Hypoxic Ischemic Brain Injury. *Journal of Investigative Medicine* 61: 1078-1083, 2013.
6. **Charles SM, Zhang L, Cipolla MJ, Buchholz JN, and Pearce WJ.** Roles of cytosolic Ca²⁺ concentration and myofilament Ca²⁺ sensitization in age-dependent cerebrovascular myogenic tone. *Am J Physiol Heart Circ Physiol* 299: H1034-1044, 2010.
7. **Chatelain A, Dupouy JP, and Allaupe P.** Fetal-maternal adrenocorticotropin and corticosterone relationships in the rat: effects of maternal adrenalectomy. *Endocrinology* 106: 1297-1303, 1980.
8. **Chen J, Wang J, Shao J, Gao Y, Xu J, Yu S, Liu Z, and Jia L.** The unique pharmacological characteristics of mifepristone (RU486): from terminating pregnancy to preventing cancer metastasis. *Medicinal research reviews* 34: 979-1000, 2014.
9. **Chuang TD, Pearce WJ, and Khorram O.** miR-29c induction contributes to downregulation of vascular extracellular matrix proteins by glucocorticoids. *Am J Physiol Cell Physiol* 309: C117-125, 2015.
10. **Chuang TD, Sakurai R, Gong M, Khorram O, and Rehan VK.** Role of miR-29 in Mediating Offspring Lung Phenotype in a Rodent Model of Intrauterine Growth Restriction. *Am J Physiol Regul Integr Comp Physiol* 2018.
11. **Collins RC, Dobkin BH, and Choi DW.** Selective vulnerability of the brain: new insights into the pathophysiology of stroke. *Annals of internal medicine* 110: 992-1000, 1989.

12. **Drouet JB, Michel V, Peinnequin A, Alonso A, Fidler N, Maury R, Buguet A, Cespuglio R, and Canini F.** Metyrapone blunts stress-induced hyperthermia and increased locomotor activity independently of glucocorticoids and neurosteroids. *Psychoneuroendocrinology* 35: 1299-1310, 2010.
13. **Durrant LM, Khorram O, Buchholz JN, and Pearce WJ.** Maternal food restriction modulates cerebrovascular structure and contractility in adult rat offspring: effects of metyrapone. *Am J Physiol Regul Integr Comp Physiol* 306: R401-410, 2014.
14. **Ferrero V, Ribichini F, Pesarini G, Brunelleschi S, and Vassanelli C.** Glucocorticoids in the prevention of restenosis after coronary angioplasty: therapeutic potential. *Drugs* 67: 1243-1255, 2007.
15. **Gayan-Ramirez G, Vanzeir L, Wuytack F, and Decramer M.** Corticosteroids decrease mRNA levels of SERCA pumps, whereas they increase sarcolipin mRNA in the rat diaphragm. *The Journal of physiology* 524 Pt 2: 387-397, 2000.
16. **Gerber AN.** Glucocorticoids and the Lung. *Adv Exp Med Biol* 872: 279-298, 2015.
17. **Goldman AS.** Experimental model of congenital adrenal cortical hyperplasia produced in utero with an inhibitor of 11-beta-steroid hydroxylase. *The Journal of clinical endocrinology and metabolism* 27: 1390-1394, 1967.
18. **Gonzalez-Orozco JC, and Camacho-Arroyo I.** Progesterone Actions During Central Nervous System Development. *Frontiers in neuroscience* 13: 503, 2019.
19. **Hai CM, Sadowska G, Francois L, and Stonestreet BS.** Maternal dexamethasone treatment alters myosin isoform expression and contractile dynamics in fetal arteries. *Am J Physiol Heart Circ Physiol* 283: H1743-1749, 2002.
20. **Hall ED.** The neuroprotective pharmacology of methylprednisolone. *Journal of neurosurgery* 76: 13-22, 1992.
21. **Hana V, Dokoupilova M, Marek J, and Plavka R.** Recurrent ACTH-independent Cushing's syndrome in multiple pregnancies and its treatment with metyrapone. *Clinical endocrinology* 54: 277-281, 2001.
22. **Herpers MJ, and Budka H.** Glial fibrillary acidic protein (GFAP) in oligodendroglial tumors: gliofibrillary oligodendroglioma and transitional oligoastrocytoma as subtypes of oligodendroglioma. *Acta neuropathologica* 64: 265-272, 1984.
23. **Hong H, Chen H, Gao W, Cai X, Sun Y, Yin M, and Liu J.** Hypoxia-induced cytosolic calcium decrease is mediated primarily by the forward mode of Na(+)/Ca(2+) exchanger in smooth muscle cells of fetal ductus arteriosus. *Pediatric cardiology* 30: 958-964, 2009.

24. **House SJ, Potier M, Bisailon J, Singer HA, and Trebak M.** The non-excitabile smooth muscle: calcium signaling and phenotypic switching during vascular disease. *Pflugers Archiv : European journal of physiology* 456: 769-785, 2008.
25. **Hubbell MC, Semotiuk AJ, Thorpe RB, Adeoye OO, Butler SM, Williams JM, Khorram O, and Pearce WJ.** Chronic hypoxia and VEGF differentially modulate abundance and organization of myosin heavy chain isoforms in fetal and adult ovine arteries. *Am J Physiol Cell Physiol* 303: C1090-1103, 2012.
26. **Ito D, Imai Y, Ohsawa K, Nakajima K, Fukuuchi Y, and Kohsaka S.** Microglia-specific localisation of a novel calcium binding protein, Iba1. *Brain research Molecular brain research* 57: 1-9, 1998.
27. **Jenkins JS, Meakin JW, Nelson DH, and Thorn GW.** Inhibition of adrenal steroid 11-oxygenation in the dog. *Science (New York, NY)* 128: 478-480, 1958.
28. **Khorram O, Chuang TD, and Pearce WJ.** Long-term effects of maternal undernutrition on offspring carotid artery remodeling: role of miR-29c. *Journal of developmental origins of health and disease* 6: 342-349, 2015.
29. **Khorram O, Ghazi R, Chuang TD, Han G, Naghi J, Ni Y, and Pearce WJ.** Excess maternal glucocorticoids in response to in utero undernutrition inhibit offspring angiogenesis. *Reprod Sci* 21: 601-611, 2014.
30. **Lee JH, Zhang J, Flores L, Rose JC, Massmann GA, and Figueroa JP.** Antenatal betamethasone has a sex-dependent effect on the in vivo response to endothelin in adult sheep. *Am J Physiol Regul Integr Comp Physiol* 304: R581-587, 2013.
31. **Leret ML, Rua C, Garcia-Montojo M, Lecumberri M, and Gonzalez JC.** Influence of metyrapone treatment during pregnancy on the development and maturation of brain monoaminergic systems in the rat. *Acta Physiol (Oxf)* 197: 333-340, 2009.
32. **Li JK.** A new description of arterial function: the compliance-pressure loop. *Angiology* 49: 543-548, 1998.
33. **Liu J, Pourcyrus M, Fedinec AL, Leffler CW, and Parfenova H.** Preventing harmful effects of epileptic seizures on cerebrovascular functions in newborn pigs: does sex matter? *Pediatric research* 82: 881-887, 2017.
34. **MacKenzie SM, van Kralingen JC, and Davies E.** Regulation of Aldosterone Secretion. *Vitamins and hormones* 109: 241-263, 2019.
35. **Moisiadis VG, and Matthews SG.** Glucocorticoids and fetal programming part 1: Outcomes. *Nature reviews Endocrinology* 10: 391-402, 2014.
36. **Ng PC.** Effect of stress on the hypothalamic-pituitary-adrenal axis in the fetus and newborn. *The Journal of pediatrics* 158: e41-43, 2011.

37. **Owens GK.** Molecular control of vascular smooth muscle cell differentiation and phenotypic plasticity. *Novartis Foundation symposium* 283: 174-191; discussion 191-173, 238-141, 2004.
38. **Owens GK, Kumar MS, and Wamhoff BR.** Molecular regulation of vascular smooth muscle cell differentiation in development and disease. *Physiological reviews* 84: 767-801, 2004.
39. **Patel SD, Pierce L, Ciardiello A, Hutton A, Paskewitz S, Aronowitz E, Voss HU, Moore H, and Vannucci SJ.** Therapeutic hypothermia and hypoxia-ischemia in the term-equivalent neonatal rat: characterization of a translational preclinical model. *Pediatric research* 78: 264-271, 2015.
40. **Pearce WJ, Doan C, Carreon D, Kim D, Durrant LM, Manaenko A, McCoy L, Obenaus A, Zhang JH, and Tang J.** Imatinib attenuates cerebrovascular injury and phenotypic transformation after intracerebral hemorrhage in rats. *Am J Physiol Regul Integr Comp Physiol* 311: R1093-r1104, 2016.
41. **Pearce WJ, Williams JM, White CR, and Lincoln TM.** Effects of chronic hypoxia on soluble guanylate cyclase activity in fetal and adult ovine cerebral arteries. *Journal of applied physiology (Bethesda, Md : 1985)* 107: 192-199, 2009.
42. **Poittevin M, Lozeron P, Hilal R, Levy BI, Merkulova-Rainon T, and Kubis N.** Smooth muscle cell phenotypic switching in stroke. *Translational stroke research* 5: 377-384, 2014.
43. **Reynolds RM.** Glucocorticoid excess and the developmental origins of disease: two decades of testing the hypothesis--2012 Curt Richter Award Winner. *Psychoneuroendocrinology* 38: 1-11, 2013.
44. **Rhen T, and Cidlowski JA.** Antiinflammatory action of glucocorticoids--new mechanisms for old drugs. *The New England journal of medicine* 353: 1711-1723, 2005.
45. **Rice JE, Vannucci RC, and Brierley JB.** The influence of immaturity on hypoxic-ischemic brain damage in the rat. *Annals of Neurology* 9: 131-141, 1981.
46. **Rigel DF, Fu F, Beil M, Hu CW, Liang G, and Jeng AY.** Pharmacodynamic and pharmacokinetic characterization of the aldosterone synthase inhibitor FAD286 in two rodent models of hyperaldosteronism: comparison with the 11beta-hydroxylase inhibitor metyrapone. *The Journal of pharmacology and experimental therapeutics* 334: 232-243, 2010.
47. **Romero DG, Zhou MY, Yanes LL, Plonczynski MW, Washington TR, Gomez-Sanchez CE, and Gomez-Sanchez EP.** Regulators of G-protein signaling 4 in adrenal gland: localization, regulation, and role in aldosterone secretion. *The Journal of endocrinology* 194: 429-440, 2007.

48. **Sapolsky RM, and Pulsinelli WA.** Glucocorticoids potentiate ischemic injury to neurons: therapeutic implications. *Science (New York, NY)* 229: 1397-1400, 1985.
49. **Schiffrin EL.** Effects of aldosterone on the vasculature. *Hypertension (Dallas, Tex : 1979)* 47: 312-318, 2006.
50. **Schillaci G, Bartoloni E, Pucci G, Pirro M, Settini L, Alunno A, Gerli R, and Mannarino E.** Aortic stiffness is increased in polymyalgia rheumatica and improves after steroid treatment. *Annals of the rheumatic diseases* 71: 1151-1156, 2012.
51. **Schmued LC, Stowers CC, Scallet AC, and Xu L.** Fluoro-Jade C results in ultra high resolution and contrast labeling of degenerating neurons. *Brain research* 1035: 24-31, 2005.
52. **Schneiderman M, Czuzoj-Shulman N, Spence AR, and Abenhaim HA.** Maternal and neonatal outcomes of pregnancies in women with Addison's disease: a population-based cohort study on 7.7 million births. *BJOG : an international journal of obstetrics and gynaecology* 124: 1772-1779, 2017.
53. **Sheng M, and Greenberg ME.** The regulation and function of c-fos and other immediate early genes in the nervous system. *Neuron* 4: 477-485, 1990.
54. **Shenoy RR, Sudheendra AT, Nayak PG, Paul P, Kutty NG, and Rao CM.** Normal and delayed wound healing is improved by sesamol, an active constituent of *Sesamum indicum* (L.) in albino rats. *Journal of ethnopharmacology* 133: 608-612, 2011.
55. **Silpanisong J, and Pearce WJ.** Vasotrophic regulation of age-dependent hypoxic cerebrovascular remodeling. *Current vascular pharmacology* 11: 544-563, 2013.
56. **Simko V, Takacova M, Debreova M, Laposova K, Ondriskova-Panisova E, Pastorekova S, Csaderova L, and Pastorek J.** Dexamethasone downregulates expression of carbonic anhydrase IX via HIF-1alpha and NF-kappaB-dependent mechanisms. *International journal of oncology* 49: 1277-1288, 2016.
57. **Smith L, and Smith JB.** Regulation of sodium-calcium exchanger by glucocorticoids and growth factors in vascular smooth muscle. *The Journal of biological chemistry* 269: 27527-27531, 1994.
58. **SmithSwintosky VL, Pettigrew LC, Sapolsky RM, Phares C, Craddock SD, Brooke SM, and Mattson MP.** Metyrapone, an inhibitor of glucocorticoid production, reduces brain injury induced by focal and global ischemia and seizures. *Journal of Cerebral Blood Flow and Metabolism* 16: 585-598, 1996.
59. **Stokum JA, Kurland DB, Gerzanich V, and Simard JM.** Mechanisms of astrocyte-mediated cerebral edema. *Neurochemical research* 40: 317-328, 2015.

60. **Stonestreet BS, Sadowska GB, McKnight AJ, Patlak C, and Petersson KH.** Exogenous and endogenous corticosteroids modulate blood-brain barrier development in the ovine fetus. *Am J Physiol Regul Integr Comp Physiol* 279: R468-477, 2000.
61. **Tang J, Li N, Chen X, Gao Q, Zhou X, Zhang Y, Liu B, Sun M, and Xu Z.** Prenatal Hypoxia Induced Dysfunction in Cerebral Arteries of Offspring Rats. *Journal of the American Heart Association* 6: 2017.
62. **Ten VS, Bradley-Moore M, Gingrich JA, Stark RI, and Pinsky DJ.** Brain injury and neurofunctional deficit in neonatal mice with hypoxic-ischemic encephalopathy. *Behavioural Brain Research* 145: 209-219, 2003.
63. **Thorpe RB, Hubbell MC, Silpanisong J, Williams JM, and Pearce WJ.** Chronic Hypoxia Attenuates the Vasodilator Efficacy of Protein Kinase G in Fetal and Adult Ovine Cerebral Arteries. *Am J Physiol Heart Circ Physiol* ajpheart.00480.02016, 2017.
64. **Tran ND, Kim S, Vincent HK, Rodriguez A, Hinton DR, Bullock MR, and Young HF.** Aquaporin-1-mediated cerebral edema following traumatic brain injury: effects of acidosis and corticosteroid administration. *Journal of neurosurgery* 112: 1095-1104, 2010.
65. **Vinukonda G, Dummula K, Malik S, Hu F, Thompson CI, Csiszar A, Ungvari Z, and Ballabh P.** Effect of prenatal glucocorticoids on cerebral vasculature of the developing brain. *Stroke; a journal of cerebral circulation* 41: 1766-1773, 2010.
66. **Volk KA, Roghair RD, Jung F, Scholz TD, Lamb FS, and Segar JL.** Coronary endothelial function and vascular smooth muscle proliferation are programmed by early-gestation dexamethasone exposure in sheep. *Am J Physiol Regul Integr Comp Physiol* 298: R1607-1614, 2010.
67. **Wagenseil JE, and Mecham RP.** Vascular extracellular matrix and arterial mechanics. *Physiological reviews* 89: 957-989, 2009.
68. **Xie Q, Xie J, Tian T, Ma Q, Zhang Q, Zhu B, and Cai X.** Hypoxia triggers angiogenesis by increasing expression of LOX genes in 3-D culture of ASCs and ECs. *Experimental cell research* 352: 157-163, 2017.
69. **Yehuda R, Engel SM, Brand SR, Seckl J, Marcus SM, and Berkowitz GS.** Transgenerational effects of posttraumatic stress disorder in babies of mothers exposed to the World Trade Center attacks during pregnancy. *The Journal of clinical endocrinology and metabolism* 90: 4115-4118, 2005.
70. **Zhang JH, Badaut J, Tang J, Obenaus A, Hartman R, and Pearce WJ.** The vascular neural network--a new paradigm in stroke pathophysiology. *Nat Rev Neurol* 8: 711-716, 2012.

71. **Zhang P, Fang L, Wu H, Ding P, Shen Q, and Liu R.** Down-regulation of GRalpha expression and inhibition of its nuclear translocation by hypoxia. *Life sciences* 146: 92-99, 2016.
72. **Zieman SJ, Melenovsky V, and Kass DA.** Mechanisms, pathophysiology, and therapy of arterial stiffness. *Arteriosclerosis, thrombosis, and vascular biology* 25: 932-943, 2005.

CHAPTER THREE

MATERNAL FOOD RESTRICTION MODULATES NEONATAL CEREBROVASCULAR STRUCTURE, FUNCTION AND VULNERABILITY TO MILD HYPOXIC-ISCHEMIC INJURY: EFFECTS OF METYRAPONE

By

Naomi Franco, Lara M. Durrant, Coleen Doan, Desirelys Carreon, Alejandra Beltran,

Amandine Jullienne, Elizabeth Haddad, Andre Obenaus, William J. Pearce

This chapter is unpublished as of December 2019.

Abstract

Prenatal undernutrition alters adult cerebrovasculature. How these effects are manifested in the neonatal cerebral circulation, however, remain unstudied. This study explored the hypothesis that prenatal maternal food restriction (MFR) programs the neonatal cerebrovasculature and thereby alters vulnerability to mild hypoxic-ischemic (HI) injury. This study also examined the corollary hypothesis that altered corticosteroids help mediate the effects of MFR on the immature cerebrovasculature.

At day 10 of gestation, pair-fed Sprague-Dawley rats experienced 50% caloric restriction. Metyrapone (MET), a corticosteroid synthesis inhibitor, was given via drinking water from prenatal day 11 to term to half of the MFR mothers. To test cerebrovascular function, we employed a model of mild HI injury in P9 MFR offspring. These pups underwent unilateral carotid ligation or sham surgery, followed 24h later by 8% or 21% O₂ for 90 min in a Bell jar. These procedures yielded 4 groups of MFR neonates: 1) MFR Untreated-Sham; 2) MFR MET-Sham; 3) MFR Untreated-HI; 4) MFR MET-HI where Untreated specifies pups who were not exposed to MET during gestation. Plasma corticosterone (GC) levels were measured just before surgery, 2h after surgery, and at 2h and 24h after Bell jar exposure. Behavioral measures of the Negative Geotaxis Reflex, Open Field assessment, and the Righting Reflex also were collected 24h after Bell jar exposure. At this time point, middle cerebral arteries (MCAs) were harvested for vessel myography studies that provided measurements of compliance and pressure-dependent contractility.

In MFR-Untreated pups 2h after hypoxia, HI increased GC levels in females only. In MFR-MET pups 2h after hypoxia, HI had no significant effect on GC levels in either

sex. MET increased passive diameters in both MFR Sham and MFR HI pups. In MFR-Untreated pups 24h after hypoxia, HI increased pressure-induced changes in diameter secondary to myofilament calcium sensitivity. In addition, in MFR-MET pups, HI significantly increased the magnitude of potassium-induced changes in diameter, possibly due to a parallel significant increase in myofilament calcium sensitivity. In MFR-Untreated pups 24h after hypoxia, HI had no significant effects on neurobehavior, but in MFR-MET pups, HI significantly worsened Negative Geotaxis times. In addition, relative to MFR Untreated-HI pups, MFR MET-HI pups exhibited worsened Negative Geotaxis times and Open Field Exploration.

In MFR neonates, mild HI increased GC levels only in females, and altered myogenic responses in both sexes. MET reduction of corticosteroid levels produced detrimental changes in MCA structure and function, along with worsened neurobehavior in MFR pups. These results show that corticosteroids are essential for homeostatic adaptation to mild HI, particularly in the immature cerebrovasculature. In addition, MFR values were compared to Ad libitum, or Control-Diet (CD), values from Chapter 2 to elucidate the effects of MFR programming; essentially MFR leads to HPA axis dysregulation, modulates cerebrovasculature structure, reveals HI-induced vulnerability in MCA function, and worsens neurobehavioral outcome.

Introduction

Epidemiological research revealed a link between low birth weight and increased risk of cardiovascular and metabolic diseases in adulthood (1). Born from this relationship, the fetal programming hypothesis states that gestational stressors, which may impair fetal growth, act on sensitive fetal tissues to permanently alter the course of development and result in increased risk of postnatal pathologies (44). As the global prevalence of undernourishment increases, maternal undernutrition, which can result in low birth weight, may be an important in utero stressor in the development of postnatal diseases (4, 5, 44).

Maternal undernutrition has been largely studied epidemiologically through the meticulously kept records of pregnant women during the Dutch Famine (41, 46, 47) and experimentally (15, 25, 53) in models of maternal food restriction (MFR) focusing on the kidney and heart (9). Numerous studies report MFR-induced changes to vasculature tissues (23, 24, 49), though studies on cerebral vessels are scarce. Novel cerebrovasculature studies from our lab demonstrate MFR-induced stiffening, vascular smooth muscle cell (vSMC) phenotype de-differentiation, and altered contractile function; some of these effects were attenuated by gestational corticosteroid reduction (10).

The significant increase in glucocorticoid levels in food restricted mothers supported a mechanistic role for glucocorticoids in programming (28), further supported by changes in both glucocorticoid hormone and its receptors in maternal, fetal, and postnatal tissues (27, 51). Glucocorticoids, a class of corticosteroid hormone, play an essential role in normal physiology and in pathophysiology, as their receptors are found

in nearly every cell. One such role is fetal development (3, 31). However, the role of glucocorticoids in MFR-induced fetal programming is controversial and other programming mechanisms, including placental, epigenetic, and microbiome alterations, are also likely involved (16, 19, 20, 38).

Using a rat model that reduced caloric intake by 50% during the latter half of gestation enabled the study of MFR on neonatal cerebrovasculature. The model also utilized metyrapone, a corticosteroid synthesis inhibitor, during the last 10 days of gestation to determine corticosteroid dependent and independent effects. Additionally, a mild model of neonatal hypoxic-ischemia (HI) was also employed to test structural and functional integrity of the middle cerebral artery between the groups following injury. The present study explored the hypothesis that late gestational maternal food restriction (MFR) and reduction of corticosteroids transform the cerebrovasculature, and modulate postnatal vulnerability to mild hypoxic-ischemic (HI) injury.

Methods

General Preparation

The Loma Linda University Institutional Animal Care and Use Committee approved all experimental procedures used in these studies. The Animal Care Facility housed first-time pregnant Sprague-Dawley rats (Charles River Laboratories, Hollister, CA; Envigo Laboratories, Placentia, CA) at constant temperature and humidity with a 12:12-h:light-dark cycle. At day 10 of gestation, non-food restricted rats were provided an ad libitum diet of standard laboratory chow (Lab Diet 5001, Brentwood, MO: protein

23%, fat 4.5%, metabolizable energy 3030 kcal/kg), while MFR and MFR-MET rats received a diet of the same chow restricted to 50% of the intake measured by weight in paired non-food restricted rats. From day 11 of gestation until term (21 days), approximately half of the rats' drinking water contained MET (cat# 14994 Cayman Chemical Company, Ann Arbor, MI), freshly dissolved each day at a final concentration of 0.5 mg/ml (**Figure 1**). Previous studies have demonstrated this concentration of MET to block maternal corticosterone synthesis and significantly reduce plasma corticosterone levels in both fetal and neonatal blood (23). All rats delivered spontaneously, and all MFR and MFR-MET pups were cross-fostered to rats fed ad libitum. The overall study design included four groups of MFR Sprague-Dawley rats: 1) Sham-operated animals that were gestationally exposed to MFR but not MET (MFR Untreated-Sham), 2) Animals that were gestationally exposed to MFR but not MET and that underwent unilateral carotid ligation surgery followed by hypoxia 24 hours later (MFR Untreated-HI), 3) MFR Sham animals that were administered MET during gestation (MFR MET-Sham), and 4) MFR HI animals that received MET during gestation (MFR MET-HI).

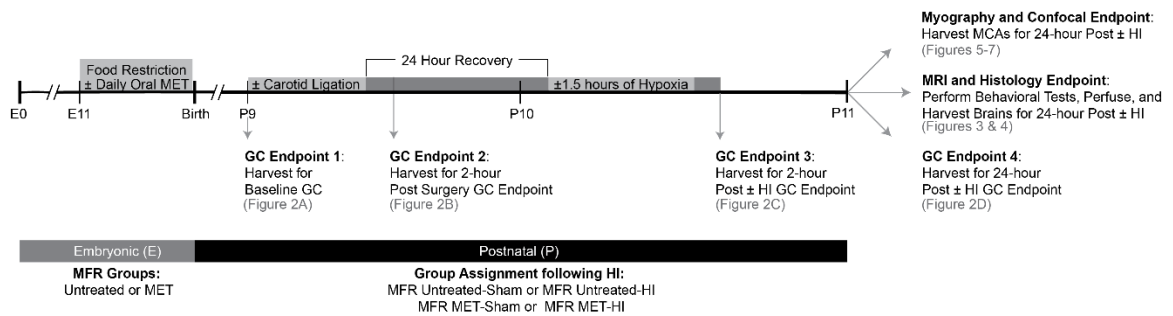


Figure 1. Experimental Overview of Embryonic and Postnatal Events. As indicated in the above diagram (not to scale), all pregnant Sprague-Dawley rats received a diet of 50% caloric reduction beginning at E10 until term and half received a daily oral dose of 0.5 mg/ml of metyrapone (MET) in the drinking water beginning at E11 through term, yielding two groups: the Untreated group (untreated water), and the MET group (MET-treated water). After birth, designated pups were euthanized at four specific timepoints after which trunk blood was collected to determine the plasma glucocorticoid (GC) levels. At P11, one cohort of rats was harvested for the final GC endpoint, a second was harvested to obtain arteries for myography and future confocal measurements, and a third cohort underwent behavioral testing followed by perfusion fixation, for future ex vivo MRI evaluation and histological analysis.

Blood Collection and Corticosterone Analysis

A time course study of corticosterone levels relative to the timing of the hypoxic insult quantified changes in corticosterone levels in each of the experimental groups (**Figure 1**). The collection of whole trunk blood into Lithium Heparin blood collection tubes (Greiner Bio-One, Kremsmunster, Austria) occurred at the time of sacrifice, according to four time course endpoints: immediately before surgery (pre-treatment baseline; **GC Endpoint 1**), 2 hours after unilateral carotid ligation (post-surgical baseline; **GC Endpoint 2**); 2 hours after HI injury (early ischemic endpoint; **GC Endpoint 3**); and 24 hours after HI injury (late ischemic endpoint; **GC Endpoint 4**). To reduce variability due to circadian oscillations in corticosterone levels, blood collection always occurred during a 4-hour block in the morning. Plasma samples then underwent centrifugation at 2000 RPM at 4 °C for 15 minutes to yield aliquots frozen at -20 °C.

In preparation for ELISA assays, the sample extraction procedure included treatment with perchloric acid followed by potassium hydroxide, which released any corticosterone bound by protein in thawed plasma samples. Twice repeated additions of ethyl acetate followed by centrifugation extracted corticosterone in the samples into the supernatant. A Savant SpeedVac Concentrator (ThermoFisher Scientific, Waltham, MA), then evaporated the supernatants. This step of the extraction concluded with capping and freezing the dried samples at -80 °C until the time of assay.

Corticosterone quantification employed an ELISA kit (cat#: ADI-900-097, ENZO Life Sciences, Farmingdale, NY) and a Gen5 1.11 BioTek microplate reader to read the samples (run in duplicate) at 405 nm. Known standards, provided and run with each kit, enabled construction of standard curves that determined the quantity of corticosterone in

each sample in picograms per milliliter. The kits detected a minimum concentration of 27 pg/ml and provided intra-assay variations no greater than 4%.

Carotid Ligation and Hypoxic Exposure: A Model of Mild Hypoxic-Ischemia

On postnatal days 9 and 10 (P9, P10), which correspond to the brain development of a full-term human infant (42), randomly selected pup littermates received surgical treatment (**Figure 1**). Following the induction of anesthesia with 3% isoflurane inhalation, the pups underwent right carotid ligation using 5-0 surgical silk (Ischemia surgery) or dissection without ligation (Shams). All surgeries typically lasted less than 15 minutes, which minimized the potential neuroprotective effects of isoflurane exposure (2). Post-surgical pups recovered with their dam for 24 hours, after which pups designated for hypoxia experienced exposure to a commercially prepared mixture containing 8% oxygen with balance nitrogen for 90 minutes in a sealed, humidified chamber maintained at 37 °C. An oxygen monitor continuously displayed oxygen levels in the chamber to assure consistency of the hypoxic exposure. After hypoxic exposure, the pups recovered 15 minutes under normoxic conditions (room air) in the chamber, and then continued recovery with their dam. Sham pups, which had no carotid ligation, were exposed to normoxia (room air) for 90 minutes at 37 °C.

Neurobehavior

Three neurobehavioral assessments (righting reflex, open field, and the negative geotaxis reflex) quantified behavioral responses 24 hours after hypoxic exposure in P11/P12 pups from each of the experimental groups. Each test consisted of three trials

that were averaged for analysis. To eliminate time of day differences in behavior, testing always occurred within the same 3-hour block in the morning. A heating pad set at 37 °C prevented loss of body heat and pups rested between trials on the heating pad. The time each pup was separated from its dam did not exceed 20 minutes. Wiping down all surfaces of the behavioral apparatus with 70% ethanol between trials helped remove pup scent and reduce bacterial transfer.

The righting reflex examined the ability of each pup to return to its four paws after being placed in a supine position. Observations of exploratory activity in the open field test enabled quantification of the number of times a rat's head (specifically, the point between the ears) moved into a new 2 cm by 2 cm square in an enclosed acrylic arena (38x40x40cm) during a 45-second interval. The negative geotaxis reflex tested the amount of time, up to 60 seconds, required for a pup placed head-downward on a 25° mesh incline to turn 180° (indicated by position of its head and front paws).

Perfusion-Fixation

Following behavioral testing, transcardial perfusion-fixation enabled subsequent measurement of HI injury via MRI and histology. After the induction of anesthesia with 3% isoflurane inhalation, the perfusion procedure began with exposure of the heart followed by the passage of a 25-gauge butterfly needle through the left ventricle and into the aorta. A peristaltic pump (Model EP-1 Econo Pump; Bio Rad, Hercules, CA) connected to the needle infused phosphate-buffered saline into the vasculature for the removal of blood through an incision in the right atrium. After this, perfusion with a solution containing 4% paraformaldehyde at 8 ml/min fixed the brain. The entire

procedure, not including induction time, lasted approximately 15 minutes. Following perfusion fixation, post-fixation of the extracted brains was accomplished overnight in 4% PFA in PBS at 4 °C.

Vessel Myography

To determine the contractile characteristics of MCAs, experiments with adjacent MCA artery segments included serial recordings of arterial diameter, first in physiological saline solution (PSS) and then in 120 mM K⁺ solution to determine maximum contractile capacity. Fura-2-AM (ThermoFisher Scientific) loaded at 1 μM, enabled simultaneous measurement of smooth muscle calcium concentration. The protocol included measurements in PSS and then 120 mM K⁺ at 20, 40, 60 and 80 mm Hg. After the final pressure step, addition of a zero calcium, 3 mM EGTA solution quenched cytosolic calcium to enable measurement of passive diameters at each pressure level used for contractility measurements. Previous publications detail all methods employed in these measurements (7, 10, 43).

Statistics

In all cases, N refers to the number of animals studied. For measurements of plasma corticosterone and all neurobehavioral assessments one-way ANOVA analyses with post-hoc comparisons using the Fisher Paired Least Significant Difference tested significance among experimental groups. Behren's-Fischer analysis with pooled variance compared values for passive diameter, compliance, and each vessel myography parameter (artery diameter, wall calcium, and calcium sensitivity). Pearson K2 test confirmed

normal distributions of all data sets, and within ANOVA analyses, Levene's test of equality verified homogeneity of variance.

Results

General findings

These protocols used 148 MFR animals from 19 litters in the following experiments: 1) corticosterone time course 2) behavior; and 3) myography. Each experimental endpoint included four experimental groups whose dams underwent 50% caloric restriction (~11.3 g of rat chow) during the final 11 days of gestation: 41 MFR Untreated-Sham and 40 MFR Untreated-HI pups from 9 litters whose mothers received normal drinking water during gestation, as well as 32 MFR MET-Sham and 35 MFR MET-HI pups from 10 litters that had undergone MET-induced fetal transformation produced by administration of MET in maternal drinking water during the latter half of gestation (**Figure 1**). In addition, the corticosterone time course cohort involved 10 additional groups from 11 MFR litters: nine Untreated Pre-Surgery (GC Endpoint 1), eight Untreated Sham-Ligated (GC Endpoint 2), eleven Untreated Ligated (GC Endpoint 2), nine 2-hour Untreated Post Normoxia (GC Endpoint 3), and eleven Untreated 2-hour Post Hypoxia pups (GC Endpoint 3), as well as ten MET Pre-Surgery (GC Endpoint 1), nine MET Sham-Ligated (GC Endpoint 2), nine MET Ligated (GC Endpoint 2), ten 2-hour MET Post Normoxia (GC Endpoint 3), and ten MET 2-hour Post Hypoxia pups (GC Endpoint 3). On average, each rat mother gave birth to 12 pups whose sex was determined by urogenital distance. From each litter, pups were paired by sex to undergo

either sham-surgery or HI-surgery for all experiments. ANOVA revealed sexual dimorphic differences for the corticosterone time course but not for behavior or myography, consistent with other studies of the neonatal cerebrovasculature (33).

In addition to assessing the effects of HI and MET within MFR groups, the comparisons of effects of MFR relative to ad libidum, or Control Diet (CD) offspring were made for all endpoints (See **Table 1**). Only CD results for the GC assay are included in a figure within the results, due to the pooling of sexes for this comparison. For more details on the CD group, please see Chapter 2.

Birth weight was significantly less (22%) in pups programmed by gestational MFR (5.2 ± 0.2 g) when compared to CD pups (6.7 ± 0.1 g), which demonstrated that our model of MFR induced intrauterine growth restriction in the rat. The presence of MET in MFR dams did not ablate this difference (5.2 ± 0.2 g). At P11/P12, MFR Untreated-Sham weighed significantly less (8.7%) than CD Untreated-Sham. Also, at this age, the MFR Untreated-Sham pups weighed significantly less (10%) than MFR MET-Sham pups. At 24-hours following the hypoxic insult, the weights of MFR Untreated-HI pups and MFR Untreated-Sham pups did not differ. Gestational MET, however, unmasked a significant difference between the MFR MET-Sham (20.3 ± 0.2 g) and MFR MET-HI pups (17.7 ± 0.4 g).

Blood Collection and Corticosterone Analysis

We first compared MFR offspring GC values to CD offspring (the cohort presented in Chapter 2) at each time point. No group-wise differences existed at pre-surgery measurements between MFR and CD plasma GC levels (**Figure 2**). In addition, baseline GC levels between CD Untreated and CD MET pups did not differ. However,

gestational MET significantly decreased baseline levels of plasma GCs between MFR MET and MFR Untreated pups (**Figure 2**).

Again, at 2h after surgery, no significant differences were found between MFR and CD GCs levels (**Figure 3A**). While ligation in CD offspring led to a significant increase in GC levels of CD Ligated-Untreated pups that was ablated by MET, MFR programming produced a contrasting pattern. GC levels did not vary between MFR Untreated-Ligated and MFR Untreated-Sham pups, but varied significantly between MFR MET-Ligated and MFR MET-Sham pups (**Figure 3A**).

At 2h post-bell jar exposure, HI resulted in an increase of plasma GCs in MFR Untreated-HI pups relative to CD Untreated-HI pups (**Figure 3B**). At this same time point, HI resulted in lowered plasma GC levels in CD Untreated pups and gestational MET ablated this effect. Once again, MFR produced a contrasting pattern whereby HI resulted in elevated plasma levels in MFR Untreated-HI pups relative to MFR Untreated-Sham. Similar to the CD cohort, gestational MET ablated this HI-induced difference in MFR MET-transformed pups (**Figure 3B**).

At 24h post-hypoxia, MFR resulted in higher levels of plasma GCs in MFR Untreated-Sham, MFR MET-Sham, and MFR MET-HI pups relative to plasma GCs in CD Untreated-Sham, CD MET-Sham pups, and CD MET-HI, respectively (**Figure 3C**). At this time point, no group-wise differences existed between CD pups. In MFR pups, HI did not yield significant differences between MFR Untreated-Sham and MFR Untreated-HI; however, MET-transformation resulted in a significant increase in MFR MET-HI relative to MFR MET-Sham plasma GC levels (**Figure 3C**).

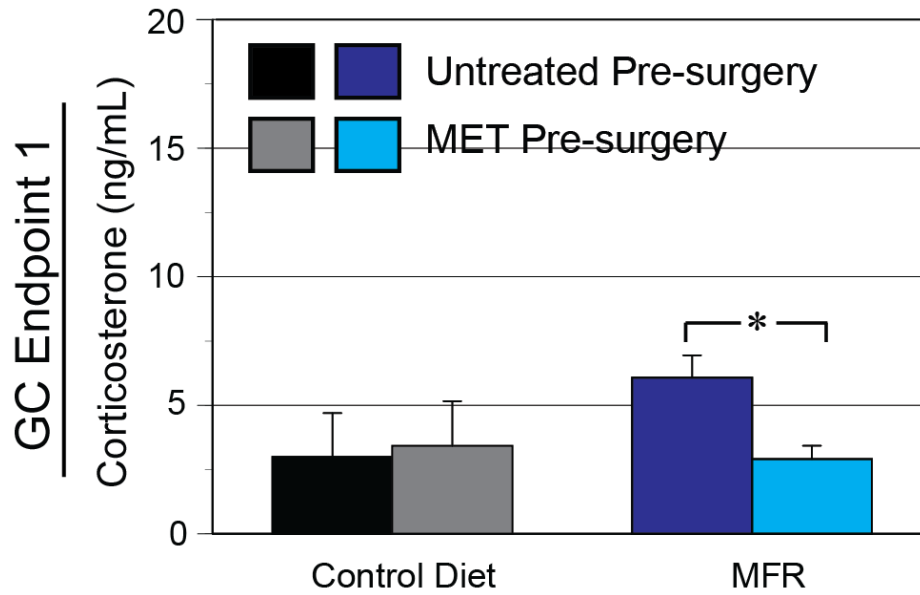


Figure 2. Effects of maternal food restriction and metyrapone-induced fetal programming on baseline (pre-surgical) plasma corticosterone in neonatal pups. Plasma corticosterone measurements were collected at the time of sacrifice in the four treatment groups immediately before surgery as a baseline value. CD values were previously reported in Chapter 2. N=3 for CD values. N=11 for MFR Untreated and N=8 for MFR MET. Data are presented as mean \pm SEM. Statistically significant differences ($P < 0.05$) determined by ANOVA are denoted by *.

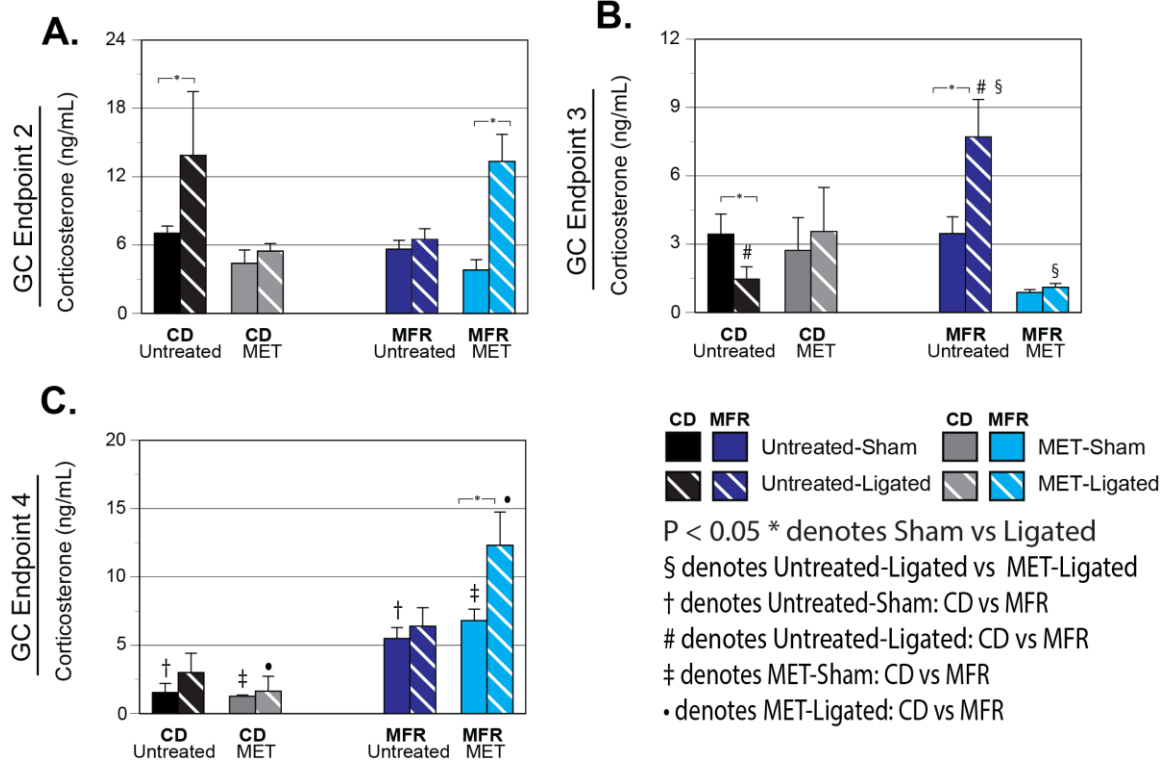


Figure 3. Effects of maternal food restriction and metyrapone-induced fetal programming on the time course of plasma corticosterone in a neonatal model of mild hypoxic-ischemic encephalopathy. Plasma corticosterone measurements were collected at the time of sacrifice in the eight treatment groups at three time points. CD values were previously reported in Chapter 2. Figure 3A: Corticosterone levels were determined 2 hours post-carotid ligation or Sham-surgery, which was also 24 hours pre-hypoxia. N values are listed left to right for each of the eight groups:4,4,4,3,8,11,9,9. Figure 3B: Corticosterone levels were assessed 2 hours post-hypoxia or normoxia in animals that were ligated or Sham-operated 24 hours prior, respectively. N values are listed left to right for each of the eight groups:4,4,4,4,9,9,9,9. Figure 3C: Plasma corticosterone was measured 24 hours post-hypoxia or normoxia in Ligated or Sham-operated pups. N values are listed left to right for each of the eight groups:4,7,4,4,13,11,12,10. Data are presented as mean \pm SEM. Statistically significant differences, denoted in the figure, were determined via ANOVA.

Statistical analysis using an ANOVA revealed sexual dimorphic differences ($p=0.02$) of MFR offspring within this experimental endpoint, prompting additional analysis of males and females within the MFR cohort (**Figure 4**). In MFR P9 pups prior to surgery (see **Figure 1, GC Endpoint 1**), baseline plasma corticosterone did not differ significantly between male Untreated pups (4.3 ± 1.1 ng/ml), and those transformed by gestational MET (2.7 ± 0.4 ng/ml). However, in females, corticosterone levels decreased significantly in MET-transformed MFR pups (3.1 ± 1.0 ng/ml) when compared to MFR Untreated pups (7.5 ± 1.0 ng/ml). In addition, MFR male Untreated plasma samples yielded a significantly lower corticosterone concentration when compared to MFR females. No other sex-based differences existed for this baseline time point (**Figure 4A**).

Two hours after surgery but 22 hours prior to hypoxic exposure in MFR Untreated pups (see **Figure 1, GC Endpoint 2**), unilateral carotid ligation produced no significant differences when compared to MFR Sham-Ligated Untreated pups for either males or females. However, in MFR female, but not MFR male, pups transformed by gestational MET, carotid ligation elevated plasma corticosterone levels to approximately 3.4-fold greater relative to MFR Untreated Sham-Ligated pups (**Figure 4B**). Additionally, MET-induced fetal transformation significantly increased corticosterone levels (17.5 ± 2.1 ng/ml) when compared to MFR Untreated Ligated in female pups (6.3 ± 1.3 ng/ml) and also when compared to MFR MET Ligated male pups ($8.2.5 \pm 3.2$ ng/ml).

At 2 hours post-hypoxia in MFR Untreated pups (see **Figure 1, GC Endpoint 3**), plasma corticosterone did not vary significantly between MFR Carotid-Ligated pups and MFR Sham pups. At this same time point in MFR Untreated females, hypoxia

significantly elevated corticosterone levels in pups that underwent carotid ligation when compared to MFR Sham pups, and gestational MET transformation ablated this effect.

No other differences existed for this time point. (**Figure 4C**).

At 24 hours post-hypoxia (see **Figure 1, GC Endpoint 4**), plasma corticosterone did not differ significantly among any of the MFR groups (**Figure 4D**). This pattern infers that transformation with MET during the last half of gestation differentially altered neonatal reactivity to stress in MFR females, and that sexual dimorphic differences were present.

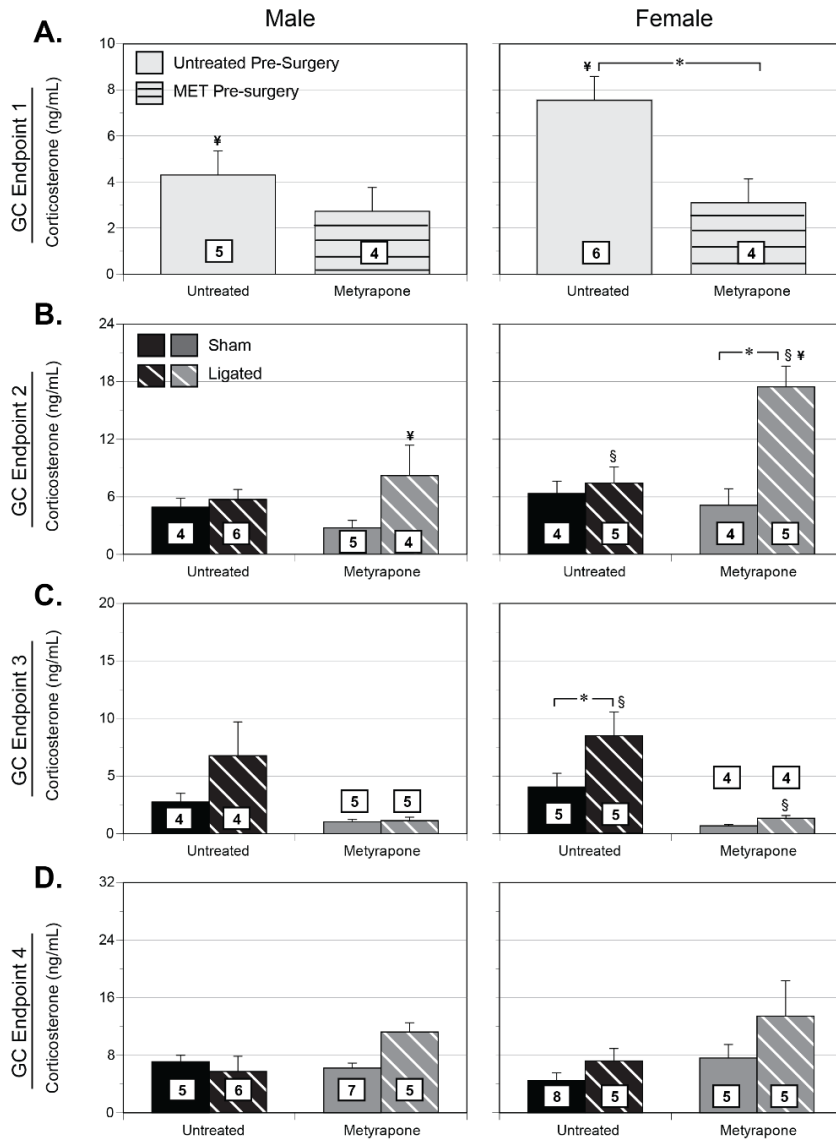


Figure 4. Effects of maternal food restriction, metyrapone-induced fetal programming, and sex on the time course of plasma corticosterone in a neonatal model of mild hypoxic-ischemic encephalopathy. Plasma corticosterone measurements were collected at the time of sacrifice in the four treatment groups at four time points in both male and female MFR pups. Figure 4A: Corticosterone concentrations were measured immediately before surgery as pre-treatment baseline. Figure 4B: Corticosterone levels were determined 2 hours post-carotid ligation or Sham-surgery, which was also 24 hours pre-hypoxia. Figure 4C: Corticosterone levels were assessed 2 hours post-hypoxia or normoxia in animals that were ligated or Sham-operated 24 hours prior, respectively. Figure 4D: Plasma corticosterone was measured 24 hours post-hypoxia or normoxia in Ligated or Sham-operated pups. The N number for each group is shown in a white box within or above each bar. Data are presented as mean \pm SEM. Statistically significant differences determined via ANOVA are indicated by: * = Untreated Pre-surgery vs MET Pre-surgery and for Sham vs Ligated and; # = Sham vs. MET-Sham; § = Ligated vs. MET Ligated; ¥ = Male vs. Female.

Passive Diameter and Arterial Compliance

Across all MFR groups, the average passive outer MCA diameter ranged from $152 \pm 9 \mu\text{m}$ at 20 mm Hg to $200 \pm 5 \mu\text{m}$ at 80 mm Hg (**Figure 5A, 5B**). Male and female pups were pooled due to lack of significant differences between them ($p=0.46$). Passive diameters between Sham and HI MCAs did not differ for either MFR Untreated or MFR MET groups. At all pressures passive diameters averaged to values that were significantly greater in MFR MET-Sham compared to MFR Untreated-Sham arteries. This was also true for MFR MET-HI relative to MFR Untreated-HI. Overall, MET-induced fetal transformation increased neonatal passive diameters in MFR MCAs.

Average values of arterial compliance (**Figure 5C, 5D**) calculated from the slopes of normalized pressure-diameter curves, ranged from $0.20 \pm .05\%$ diameter/mm Hg at 20 mm Hg to $0.05 \pm .01\%$ diameter/mm Hg at 80 mm Hg. HI did not produce changes between Untreated MCAs, but in MET-transformed MFR arteries, HI resulted in increased compliance at the highest pressures. Additionally, MET-transformation lowered compliance values in MFR MET-Sham MCAs relative to MFR Untreated-Sham MCAs at the highest pressures. MET-transformation also increased compliance in MFR MET-HI relative to MFR Untreated-HI at mid pressures. Comparisons between CD and MFR groups are in **Table 1**.

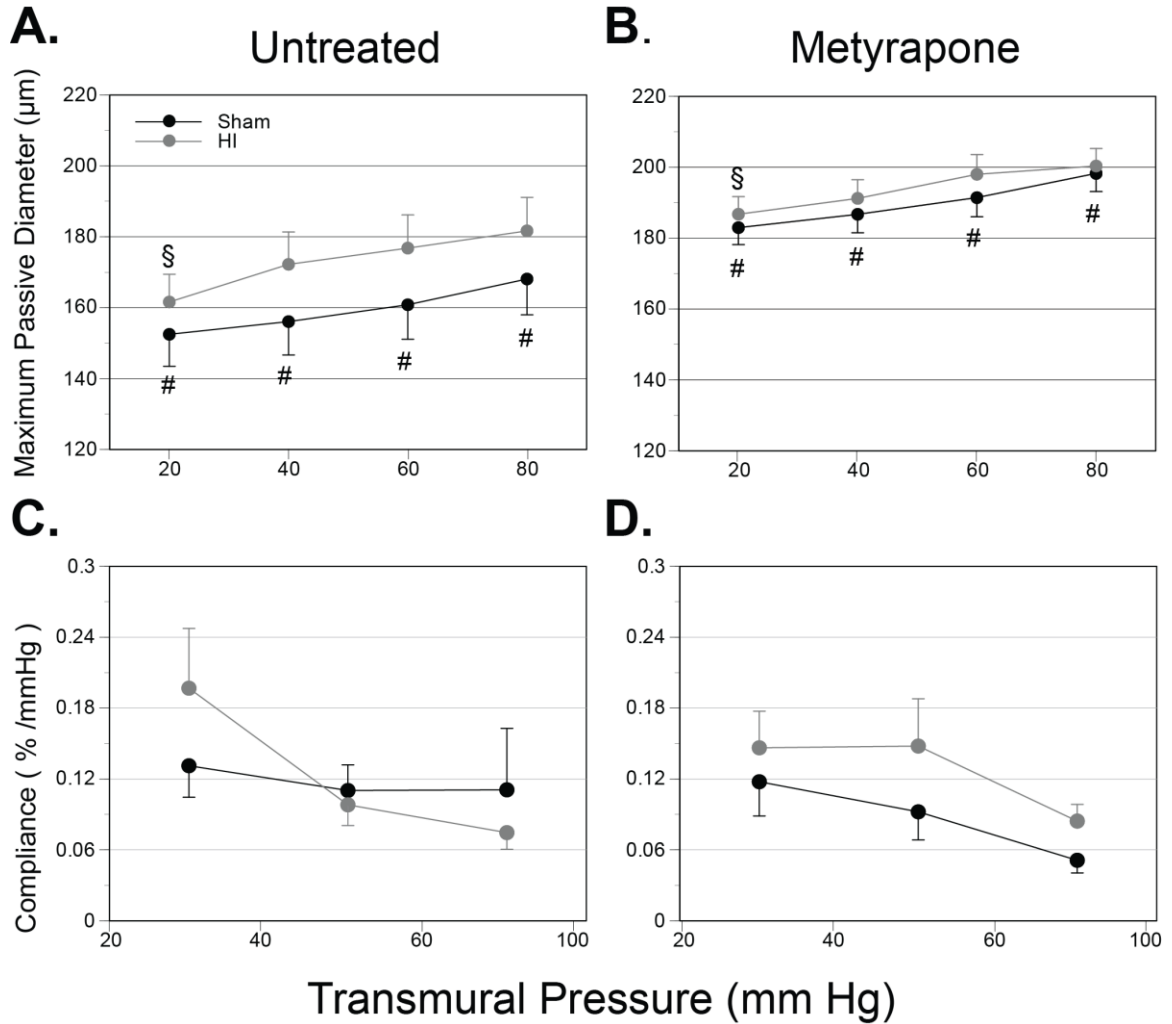


Figure 5. Effects of maternal food restriction and metyrapone-induced fetal programming on passive arterial diameter and compliance in MCAs from Sham and HI pups. Figure 5A and 5B: For middle cerebral arteries from P11 MFR pups, incubation in 3 mM EGTA buffer eliminated all active tone, and enabled measurement of passive vessel diameters as a function of transmural pressure. Figure 5C and 5D: Calculations from the slopes of passive diameter-pressure plots allowed for the determination of arterial compliance. Male and female pups were pooled due to the lack of significant differences between them. Error bars indicate SEM for N = 12 in all groups. The following symbols indicate statistical significance ($P < 0.05$) determined via Behren's-Fischer with pooled variance: *=MFR MET-Sham vs. MFR MET-HI; #=MFR Untreated-Sham vs. MFR MET-Sham; § =MFR Untreated-HI vs. MFR MET-HI.

Vessel Myography

Measurements of pressure-induced active changes in artery diameter (ΔD) enabled assessment of myogenic reactivity from 20 to 80 mm Hg also for intra MFR comparisons. Again, male and female pups were pooled due to lack of significant differences between them. Plots of these changes against intraluminal pressure allowed calculation of the areas beneath the ΔD -pressure curves (AUC), which in turn facilitated group-wise comparisons. Relative to MFR Untreated-Sham, mild HI significantly elevated pressure-induced ΔD and myofilament calcium sensitivity but depressed Δ Wall Calcium. (**Figure 6A-C**). In addition, mild HI also led to increased pressure-induced ΔD between MFR MET-Sham and MFR MET-HI. When examining the effects of gestational MET between MFR Untreated-Sham and MFR MET-Sham, no changes were observed for any pressure-induced parameter; however, gestational MET led depressed ΔD and myofilament calcium sensitivity in MFR MET-HI arteries relative to MFR Untreated-HI arteries.

To complement measurements of myogenic reactivity, which largely reflect physiological activation of smooth muscle contraction, the experimental approach included assessments of depolarization-induced contractile reactivity produced by 120 mM potassium, to indicate maximum receptor-independent contractile capacity. As for measurements of myogenic reactivity, AUC calculations facilitated statistical comparisons across groups (**Figure 6D-F**). For potassium-induced contractions, HI produced a significant increase ΔD values in when compared to MFR MET-Sham. No other group-wise differences existed. Regarding Δ Wall Calcium, group-wise comparisons yielded no significant differences in potassium-induced values. For estimates of

myofilament calcium sensitivity, values differed significantly only between MFR MET-Sham and MFR MET-HI groups. In aggregate, mild HI increased ΔD responses to physiological changes in transmural pressure in both MFR Untreated and MFR MET-transformed animals, and mildly reduced $\Delta \text{Wall Calcium}$ while increasing calcium sensitivity in MFR Untreated MCAs (**Figure 6A-C**). Additionally, mild HI significantly increased ΔD and myofilament sensitivity in response to potassium depolarization in MFR MET-transformed but not MFR Untreated arteries (**Figure 6D, 6F**). Comparisons between CD and MFR groups are in **Table 1**.

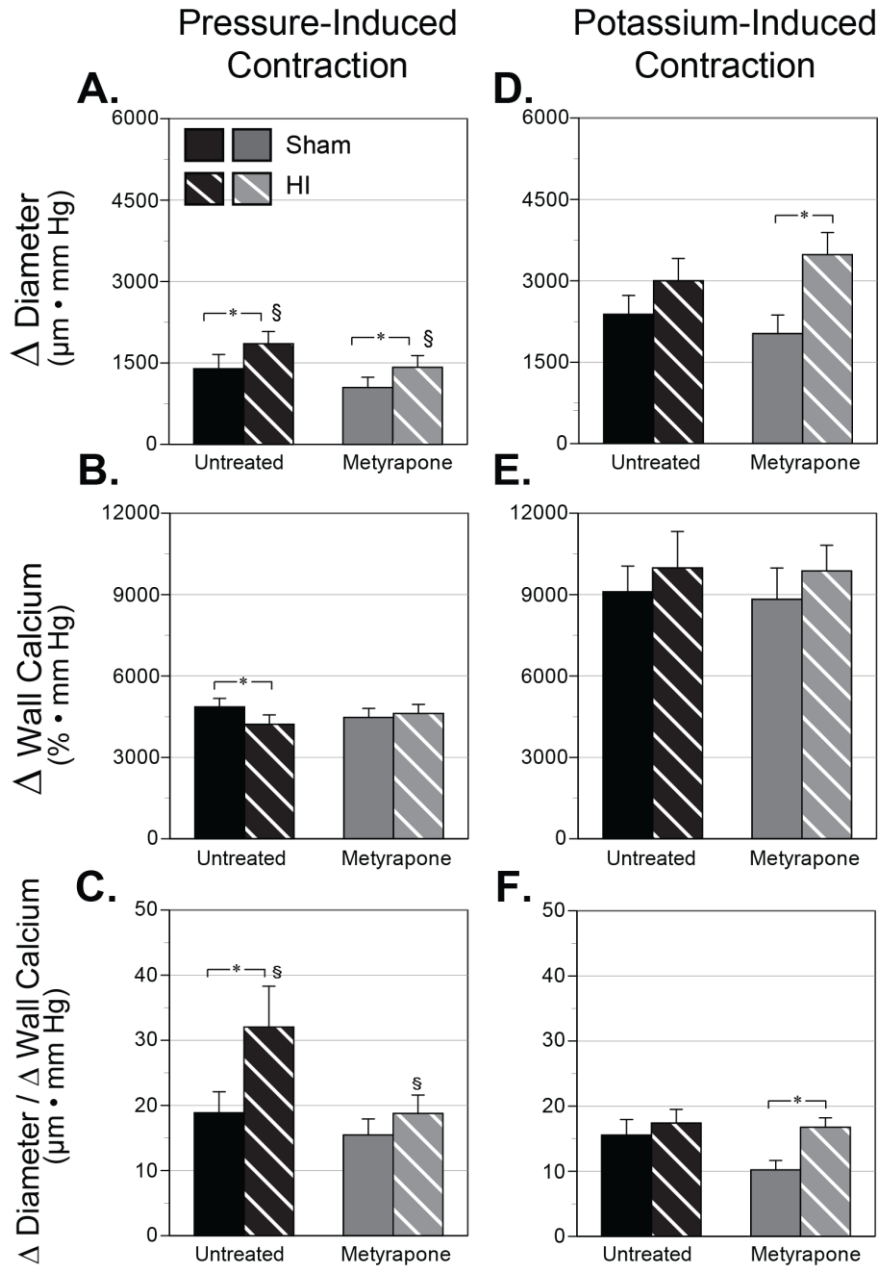


Figure 6. Effects of maternal food restriction and metyrapone-induced fetal programming on changes in diameter, wall calcium, and calcium sensitivity induced by pressure and K^+ in MCA of Sham and HI pups. MFR middle cerebral artery measurements of contractile responses to changes in intraluminal pressure enabled assessment of responses in PSS alone (Figure 6A-C) and in PSS with 120 mM K^+ (Figure 6D-F). Plots of these changes against intraluminal pressure on the abscissa allowed calculation of the areas beneath the curves for three different parameters on the ordinate: outside diameter (Δ Diameter), wall calcium concentration (Δ Wall Calcium), and calcium sensitivity (Δ Diameter / Δ Wall Calcium). Male and female pups were pooled due to the lack of significant differences between them. Error bars indicate SEM for $N = 12$ animals in all MFR groups. The following symbols indicate statistical significance ($P < 0.05$) determined via Behren's-Fischer with pooled variance: * = MFR Sham- vs. MFR HI; § = MFR Untreated-HI vs. MFR MET-HI.

Neurobehavior

With regards to comparisons within MFR-programmed pups, MFR MET-HI pups (18.4±1.7s) took significantly longer to turn 180° than MFR MET-Sham pups (13.6±1.7s) in the negative geotaxis test (**Figure 7**). Additionally, MET-induced fetal transformation delayed the negative geotaxis reflex when compared to MFR Untreated-HI pups. Negative geotaxis values did not differ significantly for any other group-wise comparisons. MFR MET-HI pups explored fewer boxes (31.4±1.9) than MFR MET-Sham pups (39.8±4.0), although this downward trend was not significantly different ($p=0.057$) (**Figure 7**). In MFR pups who had undergone MET-induced fetal transformation, mild HI significantly decreased the number of explored boxes between MFR MET-HI and MFR Untreated-HI groups. Field exploration values did not differ significantly for any other group-wise comparisons. Righting reflex results revealed no significant differences between any MFR groups (**Figure 7**).

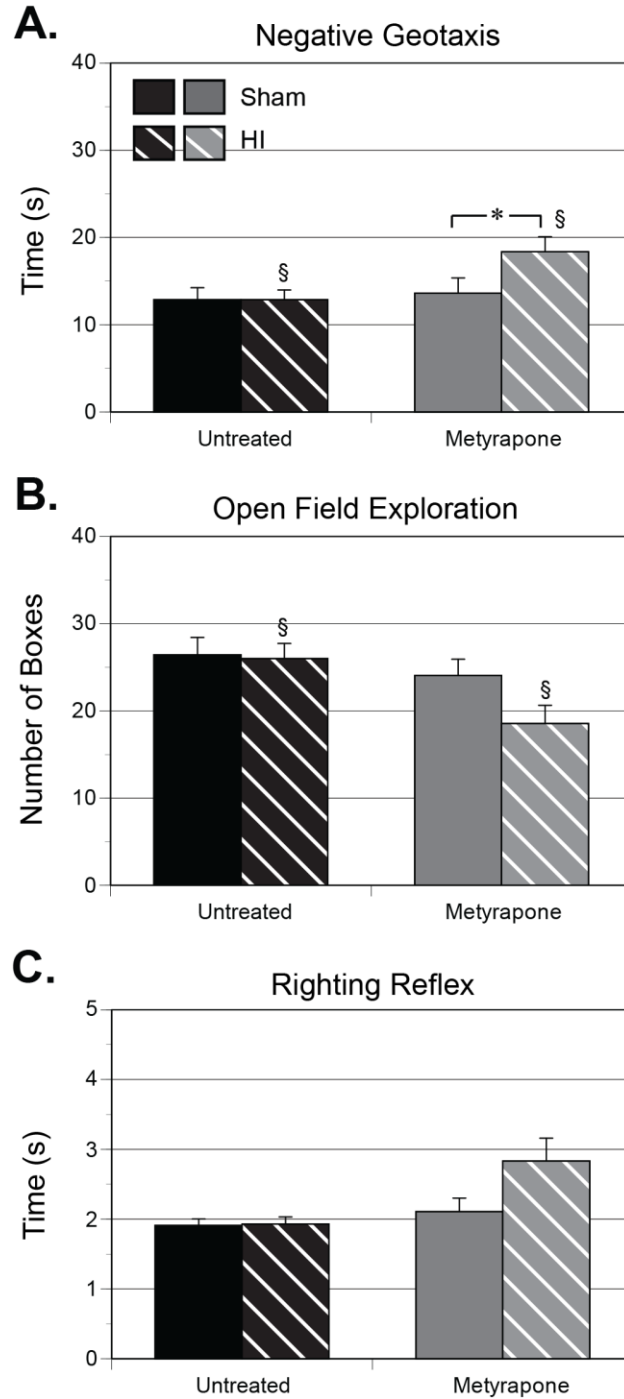


Figure 7. Effects of maternal food restriction and metyrapone-induced fetal programming on neurobehavior in Sham and HI pups. Neurobehavioral assessments conducted in neonatal MFR rats examined, negative geotaxis response, open field exploration, and righting ability. Lack of significant differences between males and females led to pooling of the two sexes. Error bars indicate SEM. N=20 in Untreated-Sham, N=19 in Untreated-HI and N = 12 animals in both MET groups. The following symbols indicate statistical significance (P<0.05) determined via ANOVA analyses: * =MET-Sham vs. MET-HI and § = Untreated-HI vs. MET-HI.

Table 1. The Relative Changes of Gestational Diet and Postnatal Mild HI in Neonatal Rats.

Endpoint	CD Untreated-HI		MFR Untreated-HI		MFR Untreated-MET		MFR Untreated-Sham		MFR Untreated-HI		MFR Untreated-Sham	
	Relative to Untreated-Sham	Relative to Untreated-Sham	Relative to Untreated-Sham	Relative to Untreated-Sham	Relative to Untreated-Sham	Relative to Untreated-Sham	Relative to Untreated-Sham	Relative to Untreated-Sham	Relative to Untreated-HI	Relative to Untreated-HI	Relative to Untreated-Sham	Relative to MFR MET-Sham
2h Post Hypoxia (Plasma GC Levels)	↓	↔	↑	↔	↔	↔	↔	↔	↔	↔	↔	↔
24h Post Hypoxia (Plasma GC Levels)	↔	↔	↔	↔	↔	↔	↔	↔	↔	↔	↔	↔
Passive Diameter at 20 mmHg	↑	↔	↔	↔	↔	↔	↔	↔	↔	↔	↔	↔
Passive Diameter at 40 mmHg	↑	↔	↔	↔	↔	↔	↔	↔	↔	↔	↔	↔
Passive Diameter at 60 mmHg	↑	↔	↔	↔	↔	↔	↔	↔	↔	↔	↔	↔
Passive Diameter at 80 mmHg	↑	↔	↔	↔	↔	↔	↔	↔	↔	↔	↔	↔
Compliance between 20-40 mmHg	↔	↔	↔	↔	↔	↔	↔	↔	↔	↔	↔	↔
Compliance between 40-60 mmHg	↓	↔	↔	↔	↔	↔	↔	↔	↔	↔	↔	↔
Compliance between 60-80 mmHg	↓	↔	↔	↔	↔	↔	↔	↔	↔	↔	↔	↔
Pressure-induced Δ Diameter	↔	↔	↔	↔	↔	↔	↔	↔	↔	↔	↔	↔
Pressure-induced Δ Wall Calcium	↑	↔	↔	↔	↔	↔	↔	↔	↔	↔	↔	↔
Pressure-induced Δ Calcium Sensitivity	↔	↔	↔	↔	↔	↔	↔	↔	↔	↔	↔	↔
Potassium-induced Δ Diameter	↔	↔	↔	↔	↔	↔	↔	↔	↔	↔	↔	↔
Potassium-induced Δ Wall Calcium	↑	↔	↔	↔	↔	↔	↔	↔	↔	↔	↔	↔
Potassium-induced Δ Calcium Sensitivity	↔	↔	↔	↔	↔	↔	↔	↔	↔	↔	↔	↔
Negative Geotaxis	↔	↔	↔	↔	↔	↔	↔	↔	↔	↔	↔	↔
Openfield	↓	↔	↔	↔	↔	↔	↔	↔	↔	↔	↔	↔
Righting Reflex	↔	↔	↔	↔	↔	↔	↔	↔	↔	↔	↔	↔

Significant changes (P<0.05) are indicated by ↑ as increases and ↓ as decreases. ↔ denotes no significant change.

Discussion

The present study explores the hypothesis that late gestational caloric restriction programs the long-term structure and function of the neonatal cerebrovasculature, thereby altering postnatal vulnerability to mild HI, through mechanisms mediated in part by reduction of gestational corticosteroids. The present studies demonstrate that in MFR Untreated pups 2h after hypoxia, HI increased GC levels in MFR females only. In MFR-MET pups 2h after hypoxia, HI had no significant effect on GC levels in either sex. MET increased passive diameters in both MFR Sham and MFR HI pups. In MFR-Untreated pups 24h after hypoxia, HI increased myogenic reactivity secondary to myofilament calcium sensitivity. In addition, in MFR MET pups, HI significantly increased the magnitude of K⁺-induced decreases in diameter, possibly due to a parallel significant increase in myofilament calcium sensitivity. In MFR Untreated pups 24h after hypoxia, HI had no significant effects on neurobehavior, but in MFR MET pups, HI significantly worsened Negative Geotaxis times. In addition, relative to MFR Untreated-HI pups, MFR MET-HI pups exhibited worsened Negative Geotaxis times and Open Field Exploration.

We also observed that MFR relative to CD: (1) reduced birth weights and (2) differentially altered HPA axis reactivity under basal and stressed conditions. As the CD data has already been presented separately in Chapter 2, additional comparisons for all other endpoints will be briefly referenced within this discussion and are documented in **Table 1**.

The Effects of MFR Programming on Neonatal Plasma GC Levels

Gestational glucocorticoids may mediate several programming effects of fetal undernutrition (45). Additionally, in utero dietary restriction alters the hypothalamic-pituitary-adrenal axis (HPA) during fetal and postnatal periods (14, 28, 32). In light of these findings, plasma GCs from MFR pups were compared to levels in CD pups to assess the effects of MFR programming. The CD measurements are obtained from Chapter 2. Baseline values of plasma GCs in P9 pups demonstrated that our model of 50% caloric restriction during the last half of gestation did not lead to altered levels of basal plasma GCs; however, MET treatment unmasked a decreased levels of plasma GCs in MFR pups that was not present in the CD group (**Figure 2**). This MET-induced alteration suggests that gestational corticosteroids are essential in maintaining baseline plasma GCs in P9 MFR pups. MFR also altered GC responses to carotid ligation. In CD pups, carotid ligation led to a MET-dependent elevation of plasma GCs (**Figure 3A**). In contrast, levels of plasma GC were not affected by this stressor in MFR Untreated, suggesting reduced sensitivity to carotid ligation. Additionally, gestational MET abolished this hyporeactivity in MFR pups, implying the involvement of a corticosteroid-dependent mechanism.

In response to the acute effects of HI in CD pups (**Figure 3B**), HI resulted in decreased levels of plasma GCs 2h after exposure, and this was abrogated by gestational MET. In MFR pups, acute HI resulted in increased levels of plasma GCs 2h after exposure and this was also abolished by gestational MET. These results suggest that MFR programs HPA hyperactivity following HI through mechanisms that are corticosteroid-dependent. At 24h following HI, neither CD or MFR Untreated had

altered GC levels (**Figure 3C**). However, gestational MET unmasked an HI-induced increase in plasma GC levels, which was not present in the CD MET group. This again suggests that corticosteroid-dependent mechanisms are likely involved in MFR programming of suppression of HI-induced changes to plasma GCs 24h after hypoxia. Also at this time point, all MFR groups, with the exception of MFR Untreated-HI, had significantly higher levels of plasma GCs relative to their CD counterparts, reinforcing the idea that MFR alters the postnatal HPA axis (29).

The Effects of Gestational MET on Neonatal Plasma GC Levels within MFR Pups

In addition, these first set of experiments sought to determine the effects of gestational MET on HPA axis function within MFR neonates before and after HI injury in a sex-based manner. In general, male and females followed similar trends in HPA responsiveness for all time points assayed (**Figure 4**), although the differences were only significant in females. Baseline plasma corticosterone levels decreased in MET-transformed pups when compared to Untreated pups. This trend was only significant in females (**Figure 4A**). This MET-induced drop in corticosterone levels may have resulted from increased degradation or decreased release of GC secondary to decreased release of, or sensitivity to, ACTH or CRF, possibly through epigenetic regulation (39, 40).

Two hours after surgery but 22 hours prior to HI exposure in Untreated pups, unilateral carotid ligation produced no significant differences when compared to Sham-Ligated Untreated pups for either males or females. However, in female, but not male, pups transformed by gestational MET, carotid ligation greatly elevated plasma corticosterone levels relative to Sham-Ligated Untreated pups (**Figure 4B**). This result

suggested that gestational MET led to an exaggerated HPA axis response following an acute stressor, hinting again at changes in inactivation of GCs, release, or sensitivity to, CRF or ACTH (8, 13, 18, 29).

At 2 hours post-hypoxia in Untreated pups, hypoxia elevated corticosterone levels in pups that underwent carotid ligation relative Sham pups. This result was only significant for females (**Figure 4C**). Whereas gestational MET produced a corticosterone-elevating response to carotid ligation, gestational MET transformation ablated the corticosterone-elevating response to HI. This suggests that gestational MET differentially transforms HPA reactivity based on stress type (ligation vs HI). At 24 hours post-hypoxia, plasma corticosterone did not differ significantly among any of the groups (**Figure 4D**), revealing: (1) that transient effects of carotid ligation and hypoxia primarily influenced HPA reactivity to acute stress; and (2) that these effects are likely mediated by transformation via gestational MET in a sex-dependent manner consistent with other findings, where males are less reactive (6, 21, 37). These changes may specifically involve 11-beta-hydroxysteroid dehydrogenase 2, which is an enzyme that converts GCs into its inactive form and has been reported to be altered by prenatal undernutrition in a sex-dependent manner (12). Additionally, MFR-induced epigenetic changes of this gene may account for these sexual dimorphic differences. While our data do not attempt to define a specific mechanism of HPA reactivity but rather focus on the endpoint of HPA axis activity, GC concentration, these results do demonstrate that MFR programs HPA axis alterations in a stress and sex-specific manner.

The Effects of MFR Programming on Passive Diameters and Arterial Compliance

To assess the structural consequences of MET transformation in MFR offspring MCAs in response to HI injury, the experimental design included measurements of passive arterial diameter as a function of increasing transmural pressure to enable calculation of arterial compliance ($\Delta\text{volume}/\Delta\text{pressure}$), a risk factor for cardiovascular disease (30) (54). Structurally, passive arterial compliance is determined by the net balance of: (1) compliance-decreasing extracellular matrix (ECM) proteins, including collagens and the collagen crosslinking enzyme, lysyl oxidase (LOX); and (2) compliance-increasing ECM proteins, such as elastin and collagenolytic matrix metalloproteinases (MMPs) (52). We have previously reported that MFR can depress cerebral artery compliance in adult offspring, mediated in part by mechanisms that increased expression of collagens in the ECM (10,22, 23). These effects of MFR on adult cerebral artery compliance were significantly reduced by gestational MET-transformation.

In light of findings that overexposure of the fetus to GCs can decrease cerebrovascular compliance in adult offspring, the present study examined the effects of corticosteroid reduction during gestation on compliance in MFR pups exposed to mild postnatal stresses induced by HI (**Figure 5**). No changes in compliance were observed between Untreated-Sham and Untreated-HI MFR groups; however, MET-transformation resulted in increased compliance in MFR MET-HI relative to MFR MET-Sham at the highest pressures. This was opposite to what was observed in CD pups where HI depressed compliance in MET-dependent manner (11). In addition, MFR Untreated-HI compliance values were significantly lower than CD Untreated-HI compliance values

(See **Table 1**). No differences existed between MFR Untreated-Sham and CD Untreated-Sham. This suggests that MFR programming reduced HI vulnerability to mild HI with regards to compliance. Given that MET that MFR MET-Sham and MFR MET-HI were only different at high pressures, it is likely that both MET-independent and MET-dependent epigenetic mechanisms were at play to alter the ECM in manner that was most evident under stress.

The Effects of MFR Programming on Contractile Function

We previously reported changes in contractile function of MCAs from MFR adult offspring (10); pressure-induced contractions were depressed secondary to myofilament calcium sensitivity in a manner that was glucocorticoid independent. In light of the ability of MFR to produce MCA contractile change in adults, we set out to assess MFR changes in neonates. Under pressure-induced contractions, mild HI significantly elevated ΔD secondary to increases in myofilament calcium sensitivity in MFR Untreated arteries (**Figure 6A-C**). Similarly, mild HI elevated ΔD in MET-transformed MCAs; however, this increase was not accompanied by significant changes in myofilament calcium sensitivity or Δ Wall Calcium. This suggests that MFR programming may cause epigenetic changes in proteins affecting myofilament calcium sensitivity, including myosin light-chain kinase, myosin light-chain phosphatase, and Rho-kinase (48). These data also suggest that, similar to adult MFR offspring, gestational GCs do not largely influence myogenic contraction in neonates, but may mildly, influence myofilament calcium sensitivity.

In contrast, CD Untreated pups only displayed hypoxia-induced elevations in Δ Wall Calcium (11) with no changes to Δ D. In addition, MFR Untreated-HI Δ Wall Calcium values were significantly lower when compared to CD Untreated-HI, but no differences existed between MFR Untreated-Sham and CD Untreated-Sham (See **Table 1**). This suggests that MFR programming inhibited this postnatal HI-induced increase of calcium mobilization through epigenetic mechanisms that mediate calcium mobilization, including calcium influx, release, extrusion and sequestration (17, 36, 50). It is unlikely that gestational corticosteroids influenced this effect as MFR MET-Sham and MFR MET-HI were not significantly different from each other. Given that these Δ Wall Calcium changes were unaccompanied by changes in contraction or myofilament calcium sensitivity, the exact functional significance remains in question. It may be possible that with a more severe form of HI, or even with an older animal, changes in contraction might be evident between MFR and CD arteries. However, MFR-programmed arteries are more vulnerable to HI, as seen by the increases in vasoconstriction following HI.

Under potassium induced contractions, HI did not influence any parameter within MFR Untreated pups (**Figure 6D-F**). Again, this contrasted from CD pups, in which HI increased calcium mobilization (11). Interestingly, both MFR Untreated-Sham and MFR Untreated-HI displayed significantly increased values of potassium-induced Δ Wall Calcium and depressed myofilament calcium sensitivity when compared to CD Untreated-Sham and CD Untreated-HI, respectively (See **Table 1**). This finding implies that MFR influenced mechanisms that mediate calcium mobilization, including calcium influx, release, extrusion and sequestration (35) and myofilament calcium sensitivity, including myosin light chain kinase or myosin light chain phosphatase (48). In addition,

the offsetting effects of increased Δ Wall Calcium with decreased myofilament calcium sensitivity may explain lack of changes in diameter between MFR and CD groups.

In MFR arteries transformed by MET, HI increased potassium-induced changes in diameter secondary to heightened myofilament calcium sensitivity in the MFR MET-HI group relative to MFR MET-Sham group (**Figure 6D and F**). This effect was absent in CD arteries and suggests that gestational MET transformation led to changes in myofilament calcium sensitivity specifically in MFR arteries. Generally, in response to hypoxia, cerebral arteries will vasodilate in order to promote oxygen delivery (34). This suggests that in MFR neonatal arteries, gestational corticosteroid transformation is essential in minimizing the potassium-induced vasoconstrictive responses in hypoxic conditions that allows for the maintenance of adequate tissue oxygenation. While this MET-induced response in MFR arteries under potassium-induced contractions would appear detrimental, more analysis is required to understand the significance of this change, including changes in vSMCs, neurons, and other cerebral cell types.

The Effects of MFR Programming on Neurobehavior

We also performed measurements of neurobehavior, which revealed the long-term consequences of MFR programming and gestational transformation with MET and the short-term effects of HI. Within group comparisons of MFR pups for the negative geotaxis assessment revealed that HI had no effect in MFR Untreated pups (**Figure 7A**). However, in MFR pups transformed by gestational MET, mild HI led to worsened negative geotaxis performance. This suggests an important role of gestational corticosteroids in the development of behavioral functions required for the negative

geotaxis performance. In addition, MFR Untreated-Sham and MFR Untreated-HI pups took significantly longer to complete the negative geotaxis assessment when compared to CD Untreated-Sham and CD Untreated-HI, respectively (See **Table 1**). This suggests that MFR worsened negative geotaxis performance.

Open field exploration within MFR groups revealed a subtle effect of mild HI injury between MFR Untreated-HI pups and MFR MET-HI, in which gestational MET transformation led to reduced exploratory behavior (**Figure 7B**). These results imply that within MFR programmed pups, gestational corticosteroids are important in preserving exploratory behavior following mild HI. In contrast, open field results in CD pups revealed that HI reduced exploration between CD Untreated-Sham and CD Untreated-HI in a corticosteroid-dependent manner (11). Additionally, both MFR Untreated-Sham and MFR Untreated-HI exhibited significantly less exploration than CD Untreated-Sham and CD Untreated-HI, respectively (See **Table 1**). Together these results imply that relative to CD pups, MFR programming altered the normal development of exploratory behavior in Sham and HI pup a manner that was likely glucocorticoid independent.

With regards to righting ability, no differences existed within MFR groups. We previously observed that within CD groups, righting reflex ability was also unchanged. In addition, gestational nutrition had no effect on righting reflex ability (See **Table 1**). The righting reflex does not appear sensitive enough to discern the programming effects of diet or of mild hypoxia in P11 rats.

Conclusion

Overall, the present experiments characterize the groupwise effects within MFR neonatal pups (**Figure 3-7**), focusing more on the long-term gestational role of MET and the short-term effects of acute HI, and the groupwise effects between MFR and CD neonatal pups (**Figure 1 and 2, Table 1**), emphasizing the role of gestational diet on cerebrovascular, neurobehavioral, and glucocorticoid responses.

Regarding the groupwise effects within MFR neonates, we observed a sexual dimorphic and acute effect of mild HI on HPA axis reactivity that was dependent on transformation by gestational corticosteroids; structural changes manifested as increased passive diameters in MET-transformed MFR arteries; general resistance to HI with regards to compliance; compromised myogenic contraction secondary to myofilament calcium sensitivity following HI; HI-induced vasoconstriction during potassium-induced contractions secondary to an increase in myofilament calcium sensitivity that appeared dependent on levels of gestational corticosteroids; and worsened neurobehavioral outcome, with regards to exploration and negative geotaxis performance, following HI in MET-transformed pups.

The effects of MFR relative to CD revealed that 50% caloric restriction during the latter half of gestation resulted in MFR-induced intrauterine growth restriction. MFR also altered GC levels in both basal and stress-induced (carotid ligation and mild HI) conditions that were largely dependent on gestational corticosteroid levels. In addition, MFR resulted in subtle, yet significant effects on MCA structure and function, suggesting that MFR influences neonatal compliance in response to mild HI while influencing

calcium mobilization and myofilament sensitivity under basal conditions. MFR also resulted in animals that performed worse neurobehaviorally.

There are limitations to this study and future work will need to determine the extent of HI injury, such as measuring changes in neurons, astrocytes, and microglia, as well changes in cerebral edema. In addition, changes in vascular phenotype may shed more light on how MFR affects neonatal cerebrovasculature and what role gestational corticosteroids play. Cerebrovascular changes involving the myogenic response and calcium homeostasis are evident in the neonatal period, and epigenetic mechanisms should be explored to explain some of the long-term effects of MFR on cerebral arteries.

From a translational perspective, the present findings predict that neonates born with intrauterine growth restriction secondary to prenatal stress, including maternal undernutrition, may be subject to heightened vulnerability to cerebrovascular diseases, such as hypoxic-ischemic encephalopathy and to an increased risk for developing neurobehavioral impairments.

References

1. **Barker DJ.** The fetal and infant origins of disease. *European journal of clinical investigation* 25: 457-463, 1995.
2. **Burchell SR, Dixon BJ, Tang JP, and Zhang JH.** Isoflurane Provides Neuroprotection in Neonatal Hypoxic Ischemic Brain Injury. *Journal of Investigative Medicine* 61: 1078-1083, 2013.
3. **Busada JT, and Cidlowski JA.** Mechanisms of Glucocorticoid Action During Development. *Current topics in developmental biology* 125: 147-170, 2017.
4. **Campbell DM, Hall MH, Barker DJP, Cross J, Shiell AW, and Godfrey KM.** Diet in pregnancy and the offspring's blood pressure 40 years later. *British journal of obstetrics and gynaecology* 103: 273-280, 1996.
5. **Ceesay SM, Prentice AM, Cole TJ, Foord F, Weaver LT, Poskitt EME, and Whitehead RG.** Effects on birth weight and perinatal mortality of maternal dietary supplements in rural Gambia: 5 year randomised controlled trial. *Bmj-British Medical Journal* 315: 786-790, 1997.
6. **Chadio SE, Kotsampasi B, Papadomichelakis G, Deligeorgis S, Kalogiannis D, Menegatos I, and Zervas G.** Impact of maternal undernutrition on the hypothalamic-pituitary-adrenal axis responsiveness in sheep at different ages postnatal. *J Endocrinol* 192: 495-503, 2007.
7. **Charles SM, Zhang L, Cipolla MJ, Buchholz JN, and Pearce WJ.** Roles of cytosolic Ca²⁺ concentration and myofilament Ca²⁺ sensitization in age-dependent cerebrovascular myogenic tone. *Am J Physiol Heart Circ Physiol* 299: H1034-1044, 2010.
8. **Dallman MF, Engeland WC, Rose JC, Wilkinson CW, Shinsako J, and Siedenburg F.** Nycthemeral rhythm in adrenal responsiveness to ACTH. *Am J Physiol* 235: R210-218, 1978.
9. **do Carmo Pinho Franco M, Nigro D, Fortes ZB, Tostes RC, Carvalho MH, Lucas SR, Gomes GN, Coimbra TM, and Gil FZ.** Intrauterine undernutrition--renal and vascular origin of hypertension. *Cardiovasc Res* 60: 228-234, 2003.
10. **Durrant LM, Khorram O, Buchholz JN, and Pearce WJ.** Maternal food restriction modulates cerebrovascular structure and contractility in adult rat offspring: effects of metyrapone. *Am J Physiol Regul Integr Comp Physiol* 306: R401-410, 2014.
11. **Franco PN, Durrant LM, Carreon D, Haddad E, Vergara A, Cascavita C, Obenaus A, and Pearce WJ.** Prenatal Metyrapone Treatment Modulates Neonatal Cerebrovascular Structure, Function and Vulnerability to Mild Hypoxic-Ischemic Injury. *Am J Physiol Regul Integr Comp Physiol* 2019.
12. **Guo C, Li C, Myatt L, Nathanielsz PW, and Sun K.** Cortisol metabolism in fetal baboon adipose and liver tissues. *Diabetes* 62: 1175-1185, 2013.
13. **Han ES, Evans TR, and Nelson JF.** Adrenocortical responsiveness to adrenocorticotropic hormone is enhanced in chronically food-restricted rats. *J Nutr* 128: 1415-1420, 1998.

14. **Hawkins P, Hanson MA, and Matthews SG.** Maternal undernutrition in early gestation alters molecular regulation of the hypothalamic-pituitary-adrenal axis in the ovine fetus. *J Neuroendocrinol* 13: 855-861, 2001.
15. **Holemans K, Aerts L, and Van Assche FA.** Fetal growth restriction and consequences for the offspring in animal models. *J Soc Gynecol Investig* 10: 392-399, 2003.
16. **Indrio F, Martini S, Francavilla R, Corvaglia L, Cristofori F, Mastrolia SA, Neu J, Rautava S, Russo Spena G, Raimondi F, and Loverro G.** Epigenetic Matters: The Link between Early Nutrition, Microbiome, and Long-term Health Development. *Frontiers in pediatrics* 5: 178, 2017.
17. **Jackson WF.** Ion channels and vascular tone. *Hypertension* 35: 173-178, 2000.
18. **Jacobson L, Zurakowski D, and Majzoub JA.** Protein malnutrition increases plasma adrenocorticotropin and anterior pituitary proopiomelanocortin messenger ribonucleic acid in the rat. *Endocrinology* 138: 1048-1057, 1997.
19. **Jansson T, and Powell TL.** Role of placental nutrient sensing in developmental programming. *Clin Obstet Gynecol* 56: 591-601, 2013.
20. **Jasarevic E, and Bale TL.** Prenatal and postnatal contributions of the maternal microbiome on offspring programming. *Front Neuroendocrinol* 100797, 2019.
21. **Jezova D, Skultetyova I, Makatsori A, Moncek F, and Duncko R.** Hypothalamo-pituitary-adrenocortical axis function and hedonic behavior in adult male and female rats prenatally stressed by maternal food restriction. *Stress* 5: 177-183, 2002.
22. **Khorram O, Chuang TD, and Pearce WJ.** Long-term effects of maternal undernutrition on offspring carotid artery remodeling: role of miR-29c. *Journal of developmental origins of health and disease* 6: 342-349, 2015.
23. **Khorram O, Ghazi R, Chuang TD, Han G, Naghi J, Ni Y, and Pearce WJ.** Excess maternal glucocorticoids in response to in utero undernutrition inhibit offspring angiogenesis. *Reprod Sci* 21: 601-611, 2014.
24. **Khorram O, Momeni M, Desai M, and Ross MG.** Nutrient restriction in utero induces remodeling of the vascular extracellular matrix in rat offspring. *Reprod Sci* 14: 73-80, 2007.
25. **Langley-Evans SC, and McMullen S.** Developmental origins of adult disease. *Med Princ Pract* 19: 87-98, 2010.
26. **Law CM, de Swiet M, Osmond C, Fayers PM, Barker DJ, Cruddas AM, and Fall CH.** Initiation of hypertension in utero and its amplification throughout life. *BMJ (Clinical research ed)* 306: 24-27, 1993.
27. **Leonhardt M, Lesage J, Dufourny L, Dickes-Coopman A, Montel V, and Dupouy JP.** Perinatal maternal food restriction induces alterations in hypothalamo-pituitary-adrenal axis activity and in plasma corticosterone-binding globulin capacity of weaning rat pups. *Neuroendocrinology* 75: 45-54, 2002.

28. **Lesage J, Blondeau B, Grino M, Breant B, and Dupouy JP.** Maternal undernutrition during late gestation induces fetal overexposure to glucocorticoids and intrauterine growth retardation, and disturbs the hypothalamopituitary adrenal axis in the newborn rat. *Endocrinology* 142: 1692-1702, 2001.
29. **Lesage J, Sebaai N, Leonhardt M, Dutriez-Casteloot I, Breton C, Deloof S, and Vieau D.** Perinatal maternal undernutrition programs the offspring hypothalamo-pituitary-adrenal (HPA) axis. *Stress* 9: 183-198, 2006.
30. **Li JK.** A new description of arterial function: the compliance-pressure loop. *Angiology* 49: 543-548, 1998.
31. **Liggins GC.** The role of cortisol in preparing the fetus for birth. *Reproduction, fertility, and development* 6: 141-150, 1994.
32. **Lingas R, Dean F, and Matthews SG.** Maternal nutrient restriction (48 h) modifies brain corticosteroid receptor expression and endocrine function in the fetal guinea pig. *Brain Res* 846: 236-242, 1999.
33. **Liu J, Pourcyrous M, Fedinec AL, Leffler CW, and Parfenova H.** Preventing harmful effects of epileptic seizures on cerebrovascular functions in newborn pigs: does sex matter? *Pediatr Res* 82: 881-887, 2017.
34. **Liu Y, Harder DR, and Lombard JH.** Interaction of myogenic mechanisms and hypoxic dilation in rat middle cerebral arteries. *Am J Physiol Heart Circ Physiol* 283: H2276-2281, 2002.
35. **Liu Z, and Khalil RA.** Evolving mechanisms of vascular smooth muscle contraction highlight key targets in vascular disease. *Biochem Pharmacol* 153: 91-122, 2018.
36. **Marin J, Encabo A, Briones A, Garcia-Cohen EC, and Alonso MJ.** Mechanisms involved in the cellular calcium homeostasis in vascular smooth muscle: calcium pumps. *Life Sci* 64: 279-303, 1999.
37. **McCormick CM, Smythe JW, Sharma S, and Meaney MJ.** Sex-specific effects of prenatal stress on hypothalamic-pituitary-adrenal responses to stress and brain glucocorticoid receptor density in adult rats. *Brain Res Dev Brain Res* 84: 55-61, 1995.
38. **Meaney MJ, Szyf M, and Seckl JR.** Epigenetic mechanisms of perinatal programming of hypothalamic-pituitary-adrenal function and health. *Trends in molecular medicine* 13: 269-277, 2007.
39. **Moisiadis VG, and Matthews SG.** Glucocorticoids and fetal programming part 1: Outcomes. *Nature reviews Endocrinology* 10: 391-402, 2014.
40. **Moisiadis VG, and Matthews SG.** Glucocorticoids and fetal programming part 2: Mechanisms. *Nature reviews Endocrinology* 10: 403-411, 2014.
41. **Painter RC, Roseboom TJ, and Bleker OP.** Prenatal exposure to the Dutch famine and disease in later life: an overview. *Reproductive toxicology (Elmsford, NY)* 20: 345-352, 2005.

42. **Patel SD, Pierce L, Ciardiello A, Hutton A, Paskewitz S, Aronowitz E, Voss HU, Moore H, and Vannucci SJ.** Therapeutic hypothermia and hypoxia-ischemia in the term-equivalent neonatal rat: characterization of a translational preclinical model. *Pediatr Res* 78: 264-271, 2015.
43. **Pearce WJ, Doan C, Carreon D, Kim D, Durrant LM, Manaenko A, McCoy L, Obenaus A, Zhang JH, and Tang J.** Imatinib attenuates cerebrovascular injury and phenotypic transformation after intracerebral hemorrhage in rats. *Am J Physiol Regul Integr Comp Physiol* 311: R1093-r1104, 2016.
44. **Rasmussen KM.** The "fetal origins" hypothesis: challenges and opportunities for maternal and child nutrition. *Annual review of nutrition* 21: 73-95, 2001.
45. **Reynolds RM.** Glucocorticoid excess and the developmental origins of disease: two decades of testing the hypothesis--2012 Curt Richter Award Winner. *Psychoneuroendocrinology* 38: 1-11, 2013.
46. **Roseboom T, de Rooij S, and Painter R.** The Dutch famine and its long-term consequences for adult health. *Early human development* 82: 485-491, 2006.
47. **Roseboom TJ, van der Meulen JH, Ravelli AC, Osmond C, Barker DJ, and Bleker OP.** Effects of prenatal exposure to the Dutch famine on adult disease in later life: an overview. *Twin research : the official journal of the International Society for Twin Studies* 4: 293-298, 2001.
48. **Somlyo AP, and Somlyo AV.** Ca²⁺ sensitivity of smooth muscle and nonmuscle myosin II: modulated by G proteins, kinases, and myosin phosphatase. *Physiological reviews* 83: 1325-1358, 2003.
49. **Szostak-Wegierek D.** Intrauterine nutrition: long-term consequences for vascular health. *Int J Womens Health* 6: 647-656, 2014.
50. **Thorneloe KS, and Nelson MT.** Ion channels in smooth muscle: regulators of intracellular calcium and contractility. *Canadian journal of physiology and pharmacology* 83: 215-242, 2005.
51. **Vieau D, Sebaai N, Leonhardt M, Dutriez-Casteloot I, Molendi-Coste O, Laborie C, Breton C, Deloof S, and Lesage J.** HPA axis programming by maternal undernutrition in the male rat offspring. *Psychoneuroendocrinology* 32 Suppl 1: S16-20, 2007.
52. **Wagenseil JE, and Mecham RP.** Vascular extracellular matrix and arterial mechanics. *Physiological reviews* 89: 957-989, 2009.
53. **Wu G, Bazer FW, Cudd TA, Meininger CJ, and Spencer TE.** Maternal nutrition and fetal development. *The Journal of nutrition* 134: 2169-2172, 2004.
54. **Zieman SJ, Melenovsky V, and Kass DA.** Mechanisms, pathophysiology, and therapy of arterial stiffness. *Arteriosclerosis, thrombosis, and vascular biology* 25: 932-943, 2005.

CHAPTER FOUR

**OPTIMIZATION OF CONFOCAL COLOCALIZATION OF CONTRACTILE
PROTEINS IN NEONATAL MIDDLE CEREBRAL ARTERIES**

By

Naomi Franco, Clarissa Do, Desirelys Carreon, Coleen Doan, William Pearce

This chapter remains unpublished as of December 2019.

Abstract

Cellular activity in both normal and pathological physiology are determined by protein interactions, which require proteins to be in close proximity to one another. Colocalization measures proximity between proteins, and requires labeling target proteins with antibody-fluorophore probes, and imaging via confocal microscopy. The methods used to quantify colocalization through image analysis, however, are vastly diverse and, to some extent, controversial. This project compares 36 different strategies of analysis. Three primary parameters were varied: 1) minimum acceptable intensity; 2) masking methods; and 3) image segmentation, to analyze images from P11,12 rat pup cerebral arteries exposed to either sham surgery (Sham), or to unilateral carotid ligation followed by 90 minutes of 8% O₂ (HI). The analysis quantified contractile protein colocalization between Smooth Muscle α Actin with two Myosin isoforms: SM-MHC and NM-MHC. Six methods of determining minimum acceptable intensity were employed, including 3 fixed and 3 variable methods, across all images. Fixed methods were applied manually, and variable methods were automated via software. Optimum statistical sensitivity was obtained by setting a fixed minimum intensity at 10% of maximum. High precision image masking, which set all pixels to an intensity of zero except those within the Region of Interest, did not increase statistical sensitivity, but reduced the false-positive rate. Analysis of segmented images revealed that maximum statistical sensitivity between Sham and HI groups was observed in the 20% of pixels with the highest intensity. Together, these results promote use of a fixed low level of minimum baseline (10% of maximum), application of high precision masking, followed by segmentation to restrict analysis to the 20% of pixels with the highest intensity. This study is the first

comprehensive and systematic comparison of methods used to quantify confocal colocalization, particularly for vascular contractile proteins.

Introduction

Proteins are an essential part of cellular biology. While a number of proteins function independently, most proteins interact with other proteins to perform cellular activity, and this interaction requires proximity. A common approach to measure protein proximity is through confocal colocalization (13). This requires imaging two or more fluorescently tagged proteins each with separate emission wavelengths. Once this image is captured an analysis method is used to quantify the proximity between the fluorescently labeled proteins. The high prevalence of confocal colocalization usage has also resulted in a high diversity of analysis methods (1). Some of these methods involve a degree of subjectivity, which has produced controversy in the field (5).

Quantification of protein colocalization involves a number of different parameters. One such parameter is minimum intensity of pixels, which aims to reduce noise by excluding low-intensity pixels. The minimum intensity can be set manually at a fixed value, consistent for each image, (i.e. 5%) or automatically through analysis software. Automatic selection of minimum intensity is based on analysis of pixel distributions of intensity and contrast and varies between each image. Another method of reducing noise is through the method of “masking,” which removes pixels outside of the region of interest. Common methods of masking include manual techniques to remove pixels in Photoshop or semiautomatic removal through imaging software such as FIJI. Segmentation is another important parameter, which requires restriction of analysis to either a region of interest or to a specific range of pixel intensities (i.e. only the brightest 20% of pixels).

The interaction of the vascular proteins smooth muscle α Actin and myosin enables smooth muscle contraction, which is important for regulation of blood pressure and blood flow (3). Both of these proteins express different isoforms dependent on developmental stage, cell type, and disease state (10). The pattern of isoform expression defines the phenotype of vascular smooth muscle. Significant shifts in phenotype occur following an ischemic event (9). We previously used a model of mild hypoxic-ischemic injury in neonatal rats to analyze the phenotype of the vascular smooth muscle cells through the colocalization of Smooth muscle α Actin with myosin isoforms and discovered dramatically different colocalization profiles following HI (7) (See also Chapter 2).

The goal of this study was to optimize the colocalization analysis of previously imaged middle cerebral arteries from neonatal rats exposed to HI injury. We sought to reduce noise and increase signal by enhancing selection of minimum pixel intensity, masking methods, and segmentation procedures.

Methods

Images

The confocal microscopy protocol used MCAs from separate cohorts of P11/12 pups from Sham or HI groups (described in Chapter 2). Overnight fixation of these MCA segments in 4% PFA preceded the embedding of arteries in paraffin and subsequent cutting into 5 μ m coronal sections. All IHC staining runs included a slide cut from a standard block of an adult cerebral artery, and the same standard block was used for all

runs for a given stain. Double-staining the sections with antibodies against smooth muscle α Actin (Sigma-Aldrich, A5228 @ 1:300 in PBS containing 2% NGS, 1% BSA at 4 °C for 18 hours) and either smooth muscle myosin heavy chain (Abcam, Ab53219 @ 1:400 in PBS containing 2% NGS, 1% BSA at 4 °C for 18 hours) or non-muscle myosin heavy chain (BioLegend, Poly19099 @ 1:300 in PBS containing 2% NGS, 1% BSA at 4 °C for 18 hours) allowed for identification of smooth muscle phenotype. The visualization procedure used secondary antibodies (Dylight-488 and Dylight-633 @ 1:300) in PBS containing 2% NGS, 1% BSA incubated at 22 °C for 2 hours. An Olympus FV1000 confocal microscope produced coronal images using a lens with a numerical aperture of 1.4 to yield lateral resolutions between 146 and 185 nm, and axial resolutions between 545 and 693 nm, depending on the wavelengths of illumination. For imaging, the standard section was imaged first, and used to set the key parameters for imaging including scan time, gain, illumination intensity, and photomultiplier voltage, as appropriate to provide between 1% and 5% saturation, which was confirmed off-line. All images were captured on the same day under identical conditions. Analyses of the confocal images of the artery sections employed CoLocalizer Pro (Version 2.6.1, CoLocalization Research Software) to calculate the extent of colocalization between the markers in each pair. Previous publications include detailed descriptions of all these methods (4, 6, 8) and validation by comparison to other established methods for quantitation of protein colocalization via confocal microscopy (11).

Masking

Artery images were masked to zero-out all pixels outside of the adventitial layer, or within the lumen using either manual methods in Photoshop (labeled as Before) or semi-automatic methods in FIJI (labeled as After). The purpose of this is to remove the background and define the region of interest. In addition, for each marker pair, six commonly used coefficients of colocalization were used to determine maximal statistical significance for each method of minimum pixel intensity. These include: Pearson's Correlation, Overlap Coefficient, Overlap k1, Overlap k2, Mander's M1, and Mander's M2 (12).

Minimum Pixel Intensity

To optimize the removal of low-intensity pixels, we assayed a total of six methods for images obtained from two marker pairs: SM-MHC & SM α Actin; and NM-MHC & SM α Actin. Manual methods included setting values to: 12-12, 25-25, and 75-75, which correspond to 5%, 10%, and 30% of the maximum intensity of 256. Automatic methods included setting values to: weak contrast, low average for both contrast and intensity, and distribution of intensity determined by FIJI. Again, six commonly used coefficients were used to assess maximal statistical significance between Sham and HI arteries

Segmentation

Histogram data from each FIJI-masked image was processed using custom-written software routines to identify the intensity that served as the border between the brightest 20% and all remaining pixels; this intensity was defined as the Threshold-20

(T20) intensity. Once determined, the T20 values were averaged across all images of each group. Similarly, the software determined average values for T25, T30, T35, and T40, which represent the upper 25, 30, 35, and 40% of pixels with the highest intensity for each protein, as determined by semi-automated analysis of the intensity distribution for each marker in each image. Analyses of the confocal images of the artery sections employed CoLocalizer Pro (Version 2.6.1, CoLocalization Research Software) to calculate the extent of colocalization between the markers in each pair. Again, six coefficients were used to assess maximal statistical significance between Sham and HI arteries

Statistics

For all images, the areas beneath the frequency-intensity curves were calculated from the maximum intensity to each threshold value (T20, T30, T40, etc.). The corresponding values for area beneath the curve were then compared via ANOVA among the experimental groups at each Threshold value (T20, T30, T40, etc.). The T-value used for the final statistical comparisons was that which produced the maximum statistical sensitivity for comparisons between Sham and Hypoxic-Ischemic groups.

Results and Discussion

Optimization of Minimum Intensity

With regards to SM-MHC and SM α Actin pairing, manual 12-12 settings yielded significant differences with Pearson's Correlation, Overlap, and Overlap k1 coefficients

between Sham and HI values of colocalization (**Figure 1**). At the 25-25 settings, only Pearson's Correlation revealed that Sham and HI groups were statistically different. The manual 75-75 settings did not discriminate between Sham and HI colocalization values for any coefficient. Both WC and AVG settings produced a significant difference only when using Pearson's correlation. When employing FJ parameters for optimizing minimum intensity, significant changes were present between Sham and HI groups with Overlap, Overlap k2, and Mander's M2. Significant differences were more prevalent with NM-MHC and SM α Actin pairing. All manual settings and the automatic setting AVG resulted in significant differences between Sham and HI groups for all six coefficients of colocalization, whereas WC and FJ parameters produced significant differences with all coefficients except Overlap k2. The results from minimum selection intensity revealed that the 25-25 setting yielded the best form of differentiation for the myosin isoforms under manual conditions, while AVG provided the best differentiation under automatic conditions.

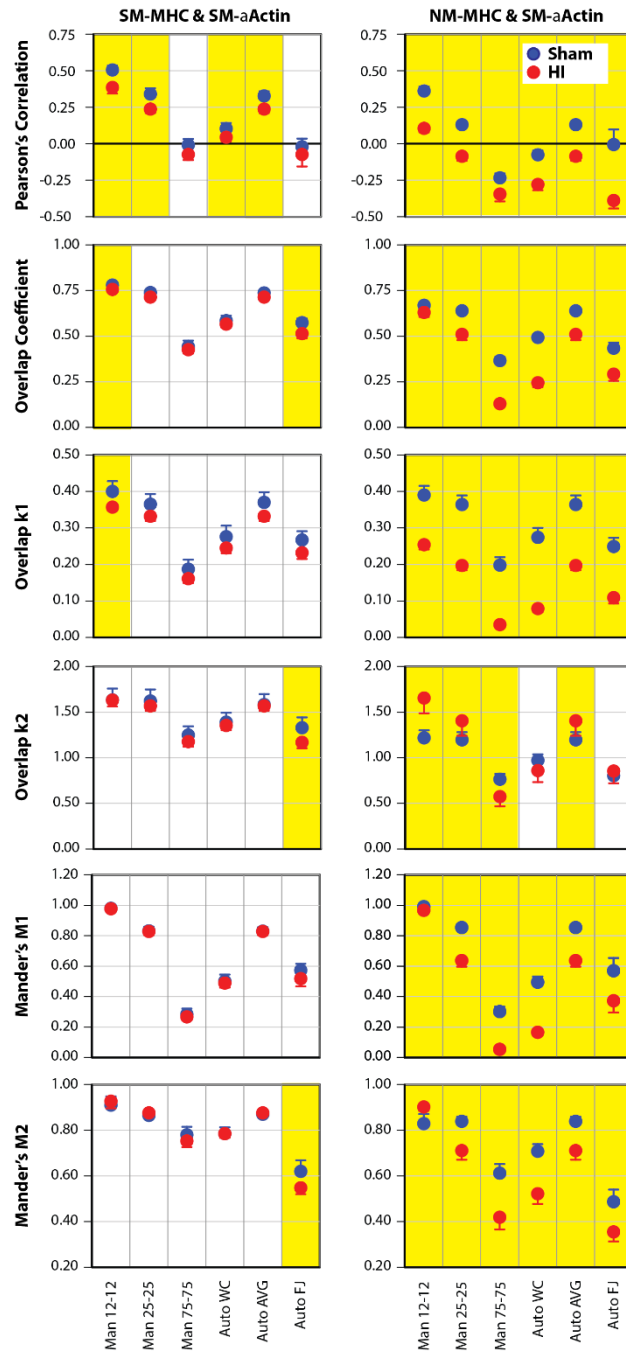


Figure 1. The Effects of Baseline Correction Method on Colocalization Coefficients. N=6 pups for both Sham and HI groups. Data are presented as mean \pm SEM for each of the six coefficients. Statistically significant differences are denoted by yellow background coloration.

Optimization of Masking

In SM-MHC and SM- α Actin pairing manual Photoshop masking revealed a significant change between Sham and HI values in the Overlap, Overlap k1, and Mander's M1 coefficients (**Figure 2**). After masking with FIJI, no statistical differences remained. In NM-MHC and SM- α Actin pairing, both manual and FIJI masking resulted in significant differences between Sham and HI for each coefficient. Additionally, FIJI masking generally increased values of all colocalization coefficients. The results from masking suggest that manual masking is susceptible to generating false-positives and that FIJI is more robust in noise removal.

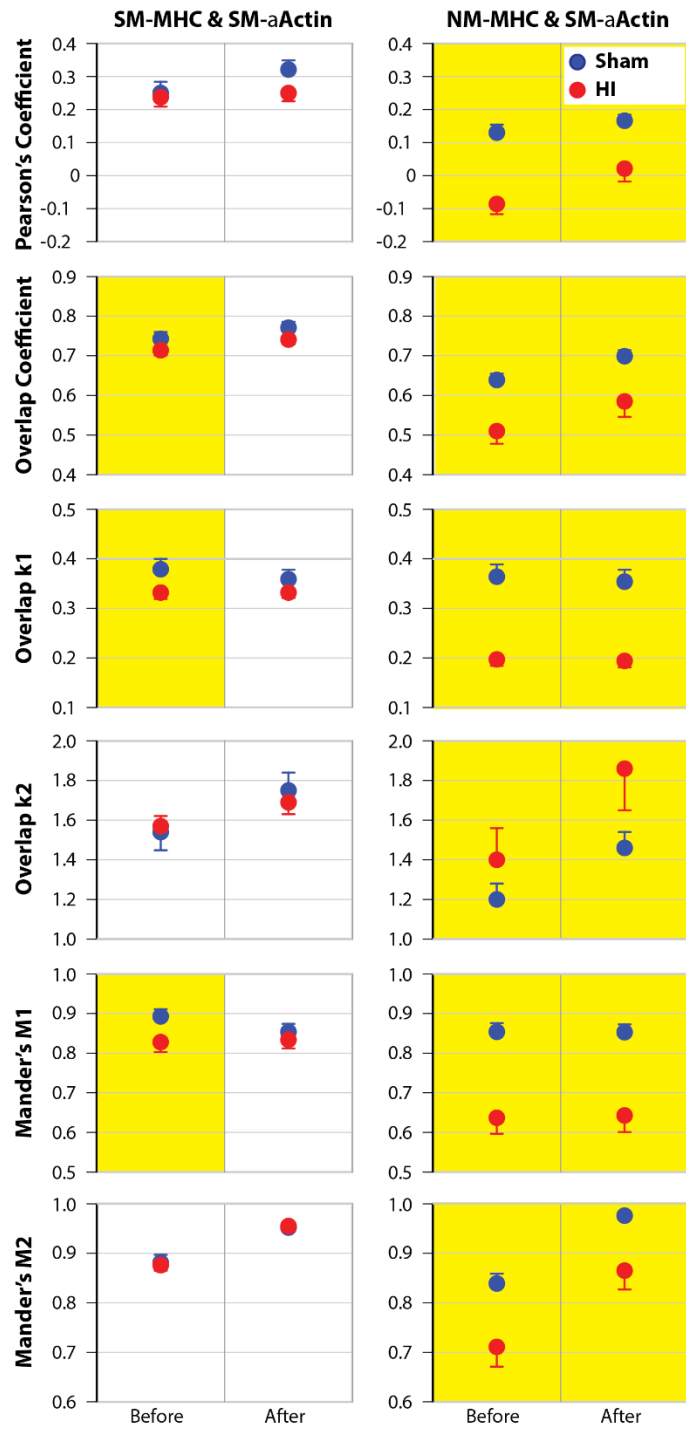


Figure 2. The Effects of Masking Method on Colocalization Coefficients. N=6 pups for both Sham and HI groups. Data are presented as mean \pm SEM for each of the six coefficients. Statistically significant differences are denoted by yellow background coloration.

Optimization of Segmentation

For SM-MHC and SM- α Actin pairing, significant differences were found at all thresholds sampled only with the Pearson's Coefficient (**Figure 3**). Between NM-MHC and SM- α Actin, both T20 and T30 showed significant differences between Sham and HI groups for all coefficients except Overlap k2. The T25 setting provided significance in all coefficients except Overlap k2 and Mander's M2. T35 and T40 produced significant differences for all coefficients. Segmentation through defining thresholds, show that Pearson's Coefficient and Overlap k2 were poor differentiators for SM-MHC and NM-MHC pairing.

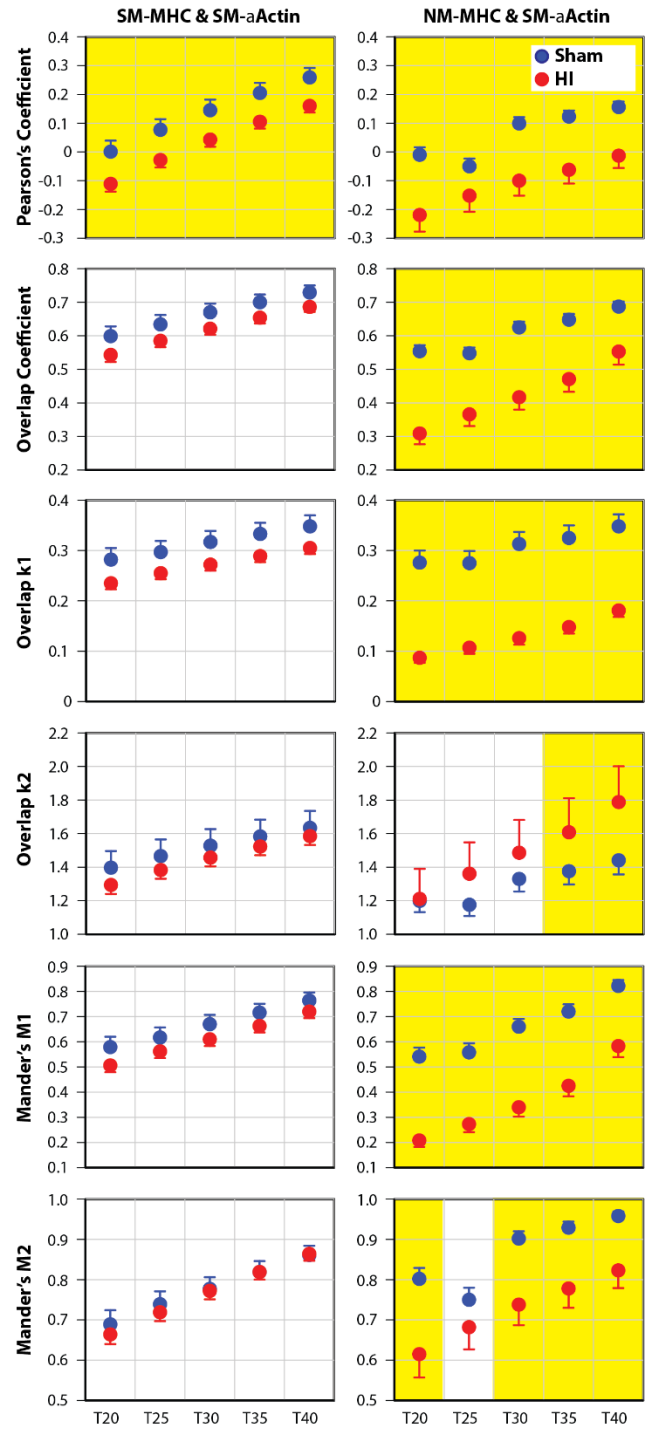


Figure 3. The Effects of Segmentation Method on Colocalization Coefficients. N=6 pups for both Sham and HI groups. Data are presented as mean \pm SEM for each of the six coefficients. Statistically significant differences are denoted by yellow background coloration.

Colocalization is an important application in the field of cell and molecular biology. This tool aids in better understanding structural and functional relationships. However, on its own, confocal colocalization should not be used to define function, as functional assays are necessary to provide certainty (12). The subjective nature often used in colocalization analysis (i.e. qualitatively observing yellow pixels, which represent colocalization) can render this application controversial. Through these experiments we sought to refine our analysis methods and increase objectivity in our study of neonatal HI. Mild HI significantly influences contractile protein colocalization in cerebral arteries of neonatal pups. In particular, NM-MHC is more vulnerable to HI injury when compared to SM-MHC. This may allude to an adaptive mechanism which confers protection to the less abundant, but more contractile-efficient SM-MHC isoform in neonatal arteries in order to maintain contractile ability following HI (2).

Conclusion

This study provides novel data on optimization of three parameters involved in colocalization analysis using six coefficients that describe the degree of overlap. Based on results presented herein for middle cerebral arteries in neonatal pups, we would recommend the use of: (1) masking via FIJI; (2) fixed manual intensities set at 10% of the maximum intensities, thereby using the 90% of pixels with the highest intensity for analysis; (3) pairing fixed minimum intensities of 25-25 with pixel segmentation at the T20 level (the 20% of pixels with the highest intensity); (4) the Mander's coefficients, which quantify colocalization as a measure of co-occurrence, rather than correlation, as in Pearson's correlation. More specifically, the Mander's coefficients quantify the fraction

of one probe relative to the other probe. The optimizations presented in this study introduced objective methods for analysis to characterize the overlap of fluorescently-labeled vascular proteins, and thus present a greater advantage by the reduction of subjective methods.

References

1. **Agnati LF, Fuxe K, Torvinen M, Genedani S, Franco R, Watson S, Nussdorfer GG, Leo G, and Guidolin D.** New methods to evaluate colocalization of fluorophores in immunocytochemical preparations as exemplified by a study on A2A and D2 receptors in Chinese hamster ovary cells. *The journal of histochemistry and cytochemistry : official journal of the Histochemistry Society* 53: 941-953, 2005.
2. **Alcala DB, Haldeman BD, Brizendine RK, Krenc AK, Baker JE, Rock RS, and Cremo CR.** Myosin light chain kinase steady-state kinetics: comparison of smooth muscle myosin II and nonmuscle myosin IIB as substrates. *Cell biochemistry and function* 34: 469-474, 2016.
3. **Brozovich FV, Nicholson CJ, Degen CV, Gao YZ, Aggarwal M, and Morgan KG.** Mechanisms of Vascular Smooth Muscle Contraction and the Basis for Pharmacologic Treatment of Smooth Muscle Disorders. *Pharmacological reviews* 68: 476-532, 2016.
4. **Charles SM, Zhang L, Cipolla MJ, Buchholz JN, and Pearce WJ.** Roles of cytosolic Ca²⁺ concentration and myofilament Ca²⁺ sensitization in age-dependent cerebrovascular myogenic tone. *Am J Physiol Heart Circ Physiol* 299: H1034-1044, 2010.
5. **Dunn KW, Kamocka MM, and McDonald JH.** A practical guide to evaluating colocalization in biological microscopy. *Am J Physiol Cell Physiol* 300: C723-742, 2011.
6. **Durrant LM, Khorram O, Buchholz JN, and Pearce WJ.** Maternal food restriction modulates cerebrovascular structure and contractility in adult rat offspring: effects of metyrapone. *Am J Physiol Regul Integr Comp Physiol* 306: R401-410, 2014.
7. **Franco PN, Durrant LM, Carreon D, Haddad E, Vergara A, Cascavita C, Obenaus A, and Pearce WJ.** Prenatal Metyrapone Treatment Modulates Neonatal Cerebrovascular Structure, Function and Vulnerability to Mild Hypoxic-Ischemic Injury. *Am J Physiol Regul Integr Comp Physiol* 2019.
8. **Pearce WJ, Doan C, Carreon D, Kim D, Durrant LM, Manaenko A, McCoy L, Obenaus A, Zhang JH, and Tang J.** Imatinib attenuates cerebrovascular injury and phenotypic transformation after intracerebral hemorrhage in rats. *Am J Physiol Regul Integr Comp Physiol* 311: R1093-r1104, 2016.
9. **Poittevin M, Lozeron P, Hilal R, Levy BI, Merkulova-Rainon T, and Kubis N.** Smooth muscle cell phenotypic switching in stroke. *Translational stroke research* 5: 377-384, 2014.
10. **Rensen SS, Doevendans PA, and van Eys GJ.** Regulation and characteristics of vascular smooth muscle cell phenotypic diversity. *Netherlands heart journal : monthly journal of the Netherlands Society of Cardiology and the Netherlands Heart Foundation* 15: 100-108, 2007.
11. **Thorpe RB, Hubbell MC, Silpanisong J, Williams JM, and Pearce WJ.** Chronic Hypoxia Attenuates the Vasodilator Efficacy of Protein Kinase G in Fetal and Adult Ovine Cerebral Arteries. *Am J Physiol Heart Circ Physiol* ajpheart.00480.02016, 2017.

12. **Zinchuk V, and Grossenbacher-Zinchuk O.** Recent advances in quantitative colocalization analysis: focus on neuroscience. *Progress in histochemistry and cytochemistry* 44: 125-172, 2009.
13. **Zinchuk V, Zinchuk O, and Okada T.** Quantitative colocalization analysis of multicolor confocal immunofluorescence microscopy images: pushing pixels to explore biological phenomena. *Acta histochemica et cytochemica* 40: 101-111, 2007.

CHAPTER FIVE

CONCLUSIONS AND FUTURE DIRECTIONS

Abundant evidence in both human and animal studies demonstrate that altered nutritional status during gestation, often associated with intrauterine growth restriction, programs increased incidence of postnatal disease and impairments. While the number of diverse models of gestational nutritional manipulation may produce subtle differences in offspring phenotype, each of these adverse conditions influence critical periods of fetal development in a manner that permanently alters its developmental trajectory. Collectively, these developmental changes define postnatal structures and function throughout the body. The work presented within these chapters demonstrate for the first time the effects of 50% caloric restriction during the last 10 days of gestation on cerebrovasculature changes and HI vulnerability in P11/12 rats.

Chapter One set the foundation of this study. It addressed the global rise in food insecurity. It also presented both epidemiological and experimental studies that detailed the consequences of MFR in the offspring, thus introducing the concepts of intrauterine growth restriction and fetal programming. Possible mechanisms of MFR were addressed, with a general focus on the glucocorticoid theory. Epigenetic mechanisms were also considered. In addition, this chapter highlighted the importance of studying cerebrovascular responses to MFR in neonates.

The work addressed in Chapter Two established the effects of gestational corticosteroid reduction on mild HI-induced vulnerability in the cerebrovasculature, as well as other cerebral tissues in neonatal offspring from ad libitum fed mothers. The results of that study demonstrated that corticosteroids during gestation play a key role in

normal cerebrovascular development and glial activation, induce persistent changes that in neonates manifest beneficially as preservation of post-ischemic contractile differentiation, but worsen cerebrovascular compliance following ischemia, and increase ischemic neuronal injury, and compromise neurobehavior. These data allowed us to characterize the responses of mild HI in CD pups; use of gestational MET enabled determination of corticosteroid dependent mechanisms in this population.

Chapter Three includes ongoing studies that focus on examining the role of maternal food restriction on the cerebrovascular, neurobehavioral, HPA axis responses to mild HI injury in neonatal rats. The role of corticosteroids, such as glucocorticoids, in MFR was also examined through gestational MET dosing. To date, it appears that cerebral vessels in MFR are more vulnerable to HI injury than CD groups. Additionally, marked changes appear in HPA reactivity and neurobehavioral outcome is worsened by MFR. These studies will be expanded to examine cerebral histology. We plan to survey changes in neuronal degeneration and astrocyte and glial activation. MRI will also be used to analyze cellular swelling and edema. In addition, vSMC phenotype (MHC isoforms colocalized with SM- α Actin) will be investigated.

Chapter Four presented the optimization of confocal colocalization of contractile proteins in neonatal middle cerebral arteries. The goal of this work primarily focused on refining a heavily-employed method of determining protein proximity from confocal imaging. The goal of this study was to standardize the methods used to determine colocalization to increase statistical sensitivity and efficiency. From our examination of three parameter analyses, we would recommend the use of: (1) fixed manual intensities set at 10% of the maximum intensities, thereby keeping 90% of pixels with the highest

intensity; (2) pairing fixed minimum intensities of 25-25 with pixel segmentation at the T20 level (the 20% of pixels with the highest intensity); (3) the use of the Mander's coefficients.

Ongoing and future studies involve elucidating the role of microRNA in HI injury in neonatal rats. Using RNA-Seq, we generated preliminary results of RNA expression profiles following mild hypoxic-ischemic brain injury to reveal how mild hypoxic-ischemia alters the transcriptome of neonatal middle cerebral arteries of CD rats. We surveyed over 29000 transcripts and found that more than 7000 transcripts increased or decreased by at least 1.5-fold 24h following mild HI injury. Among these changes were alterations to several microRNAs (miRs), and transcripts associated with ECM, cytoskeleton, and myosin families (**Figure 1**).

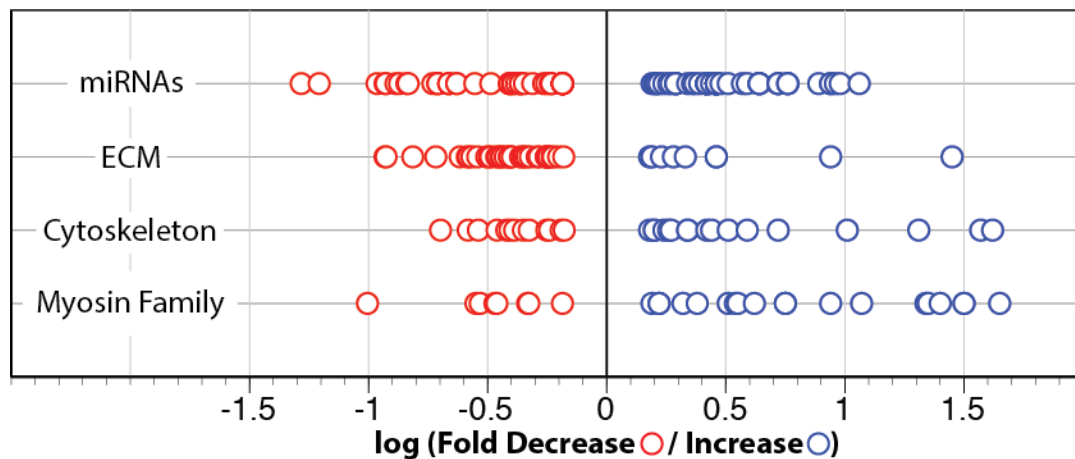


Figure 1. Transcriptomic changes in miRNAs, ECM, Cytoskeleton, and Myosin Families 24h following mild HI injury in P11 CD rats.

In addition, analysis of the 10 most affected miRs also revealed predicted targets associated with vascular smooth muscle cells, angiogenesis, the ECM, and glucocorticoid

activation (**Table 1**). We hope to repeat this analysis with more animals to better characterize transcriptome changes following mild HI and identify possible molecular and epigenetic targets. How miRs influence the neonatal cerebrovasculature is of great interest to our lab. RNA-Seq studies will allow us to determine target miRs, as well as non- miR targets that change in response to a number of perturbations, including neonatal HI, gestational MET, or MFR.

Through these studies we hope to advance the fields of fetal programming and neonatal vascular injuries with the translational goal of improving the health of offspring from abnormally stressed pregnancies, as in undernutrition, and also the health of neonates at risk for cerebrovasculature injuries secondary to HI.

Table 1. Predicted target miRs that are most affected by mild HI in CD neonates.

miRNA	Fold Change	Predicted Target Genes of Interest
Mir181a2	11.6	Smoothelin
Mir21	9.6	Wound healing;M-RIP
Mir6326	9.1	Cellular processes in over 169 genes
Mir325	8.7	Cellular processes in over 62 genes
Mir322-1	8.7	MLCK; VEGFA; MMP1; MMP17
Mir134	-8.4	COL17A1; COL2A1
Mir346	-8.5	COLGALT1
Mir6331	-9.2	COL1A1: MLC6
Mir758	-16.1	11b-HSD1
Mir431	-19.2	MMP16

Fold change [HI-Control/Sham-Control]. Positive numbers signify greater expression in HI-Control relative to Sham-Control and negative numbers signify the opposite.